Metabolic and Epigenetic Regulation in Development and in Embryonic Diapause

Abdiasis Mohamed Hussein

A dissertation

submitted in partial fulfillment of the requirements for the degree of

Doctor of Philosophy

University of Washington

2021

Reading Committee:

Hannele Ruohola-Baker, Chair
Carol B. Ware
David Hockenbery

Program Authorized to Offer Degree:

Biochemistry

University of Washington

Abstract

Metabolic and Epigenetic Regulation in Development and in Embryonic Diapause

Abdiasis Mohamed Hussein

Chair of the Supervisory Committee:
Hannele Ruohola-Baker, Ph.D., Professor
Department of Biochemistry

Embryonic diapause is a state of dormancy that interrupts the normally tight connection between developmental stage and time. Regulation of this dormant state, however, is poorly understood. To better understand the processes underlying diapause in mammals, we characterized the transcriptional and metabolite profiles of mouse pre-implantation, post-implantation and diapause embryos. We identified a unique cellular regulation signature placing diapause at a distinct developmental state with highly activated lipolysis, glycolysis and metabolic pathways regulated by AMPK. Significant enrichment of AMP further indicated activation of the cellular starvation-sensor, AMPK. We show that starvation in pre-implantation ICM derived mouse embryonic stem cells induce a reversible dormant state, transcriptionally mimicking the in vivo hormonally controlled diapause stage. During starvation, a splice variant of an upstream kinase of AMPK, Liver kinase b1 (Lkb1), induces a reversible, mTOR dependent glycolytic, H4K16Ac negative, diapause-like quiescence state in vitro through AMPK. We furthermore show that,

paradoxically, forced expression of a non- diapause Lkb1 splice variant results in a constitutive diapause-like state due to a phospho-AMPK dependent increase in glucose transporters and decrease in mTOR activation. Our analysis reveals increased lipolysis in diapause wherein triacylglycerol (TAG) and diacylglycerol (DAG) levels are highly reduced while their products, free fatty acids and phosphatidylcholine (PC) are enriched to support cell survival in diapause. Lipolysis is increased due to mTORC2 repression as both starvation-induced diapause-like state and knockout of *Rictor* show upregulation of lipolysis in mESC. Furthermore, glutamine transporters, SLC38A1/2 are highly enriched and essential for a H4K16Ac negative, diapause state. These data suggest that mTORC1/2 inhibition, regulated by amino acid levels is causal for diapause metabolism and epigenetic state.

In addition to studying embryonic diapause, we also investigated how pre-implantation (naïve) human embryonic stem cells transition to the post-implantation (primed) stage. These pluripotent stem cells are refractory to regenerative aging and have the capacity to remain in a pluripotent stage either by culture conditions *in vitro* or *in vivo* by entering a diapause state. We have previously identified metabolic differences that regulate the ESC epigenetic state. Here we define a novel epigenetic regulator during implantation stage, SUV420H2. A previous screen from this laboratory for early ESC regulators revealed SUV4020H2 as a critical component in naïve to primed transition. Using the CRISPR/Cas9 system, we generated a SUV420H2 knockout naïve hESC line to study its role in the pre- and post-implantation embryonic stages. We show that SUV420H2 mutants do not enter in vitro diapause, but instead continue dividing. By immunoblotting, we also show mutant cells have higher levels of H4K16ac as well as increased rates of proliferation. These data suggest that mechanistically, H4K20me3 repressive marks in key target genes are a pre-requisite for the diapause stage. Furthermore, our

functional metabolic assays show that SUV420H2 mutant cells have an increased levels of fatty acid β-oxidation, mitochondrial respiration and glycolysis compared to wildtype, suggesting SUV420H2 as a potential metabolic inhibitor. We conclude that increased OXPHOS and glycolytic metabolism might be due to blocking the inhibitory effect of SUV420H2 on PPAR-γ. The data reveal the mechanism for SUV420H2 requirement during naïve to primed embryonic transition. The epigenetic repression by H4K20me3 marks is a pre-requisite for the potential diapause and metabolic reprogramming that takes place during naïve to primed transition.

Finally, we studied the role of mitochondria in quiescence. Both normal and cancer stem cells can arrest cell division, avoid apoptosis, and then regenerate following acute genotoxic insult. This protective, reversible proliferative arrest is still poorly understood. We have shown that mitochondrial activity is reduced in mouse diapause embryos. We asked if mitophagy was critical for cells to enter and exit diapause state. Here, we show that mTOR-regulated mitophagy is required for mTOR-inhibition induced quiescence in human induced pluripotent stem cells (hiPSCs). Depletion of mitophagy by mutating PINK, an essential protein for mitophagy, eliminates entry into quiescence, whereas wildtype cells can enter a reversible quiescent state. Mitochondrial number significantly decreases as cells enter a diapause-like state. Our data suggest that mitochondrial number coordinates reversible quiescence. We further identify that the mechanism of quiescence in human induced pluripotent stem cells (iPSCs) relies on mitophagy to deplete the mitochondrial pool of CycE and limit cell cycle progression. This alternative method of G1/S regulation may present new opportunities for therapeutic purposes.

Table of Contents

List of Figures

List of Tables

Glossary

hESC: human embryonic stem cells
mESCs: Mouse embryonic stem cells
hiPSCs: Human induced pluripotent stem cells
SAM: S-adenosylmethionine
SAH: S-Adenosylhomocysteine
Trp: Tryptophan
PPP: Pentose phosphate pathway
SUV420H2: Suppressor of Variegation 4-20 Homolog 2
KMT5C: Lysine (K) methyltransferase 5 C
GREB1: Growth Regulating Estrogen Receptor Binding 1
FLCN: Folliculin
MAP2K7: Mitogen-Activated Protein Kinase Kinase 7
NELL2: Neural EGFL Like 2
EGFL: Epidermal growth factor-like
GPR161: G Protein-Coupled Receptor 161
GPI: Glucose phosphate isomerase (GPI)
CRISPR: clustered regularly interspaced short palindromic repeats
TCA: Tricarboxylic acid
ETC: Electron transport chain
ATP: Adenosine triphosphate
AMP: Adenosine monophosphate
ICM: Inner cell mass
Epi: epiblast
IF: Immunofluorescence
FACS: Fluorescence-Activated Cell Sorting
SLC38A1: Solute Carrier Family 38 Member 1
LKB1: Liver kinase B1
AMPK: adenosine monophosphate-activated protein kinase
mTORC1/2: mechanistic target of rapamycin complex 1/2
RICTOR: rapamycin-insensitive companion of mTOR
RAPTOR: regulatory-associated protein of mammalian target of rapamycin
PC: phosphatidylcholine
PE: phosphatidylethanolamine
LPC: lysophosphatidylcholine
LPE: lysophosphatidylethanolamine
FA: Fatty acids
TAG: Triacylglycerol
DAG: Diacylglycerol
FA: Fatty acids
SFA: saturated fatty acid
MUFA: mono-unsaturated fatty acid
PUFA: poly-unsaturated fatty acid
Cer: Ceradmide

AC: acylcarnitine
SM: Sphingomyelin
AICAR: 5-Aminoimidazole-4-carboxamide ribonucleotide
H4K16Ac: Histone 4 lysine 16 acetylation
H4K20me3: Histone 4 lysine 20 trimethylation
1-MNA: 1-methylnicotinamide
NF-kB: Nuclear factor kappa beta
ASAH1: N-acylsphingosine amidohydrolase 1
ACSS1: acyl-CoA synthetase short-chain family member 1
FASN: fatty acid synthase
AHCY: adenosylhomocysteinase
PMS: pregnant mare serum
hCG: human chorionic gonadotropin
CycE: Cyclin E
ATPSB: ATP synthase Beta subunit
PINK1: PTEN-induced kinase 1 (PINK1)
PTEN: Phosphatase and tensin homolog
EGR1: Early growth response 1
MBD2: Methyl-CpG Binding Domain Protein 2
Pitx1: Pituitary homeobox 1
Tfe3: Transcription Factor E3
Stard4: StAR Related Lipid Transfer Domain Containing 4
Pfkfb2: phosphofructo-2-kinase/fructose-2,6-biphosphatase 2
F2,6P2: Fructose 2,6-bisphosphate
PFK-1: phosphofructokinase-1
ATF3/5: Activating Transcription Factor 3/5
KLF4: Kruppel Like Factor 4
PCNA: Proliferating cell nuclear antigen
Asns: Asparagine Synthetase
Gpnmb: glycoprotein nonmetastatic B

Acknowledgements

I would like to express my sincere gratitude to my supervisor, Professor Hannele Ruohola-Baker for accepting me as a graduate student in the lab and for her invaluable advice, continuous support and for giving me the opportunity to work with her and learn from her. Thank you so much Hannele for helping me to become the scientist I am. Your thoughtful guidance helped me gain a deeper understanding and appreciation for stem cell biology and metabolism. I also like to thank my thesis committee (Professors Jim Hurley, Carol Ware, David Hockenbery, and Dana Miller). Thank you so much for great discussions and for all your suggestions and experimental ideas when things were not working and thank you for helping me get to where I am.

I would also like to thank Biochemistry faculty that I had an opportunity to work with as a teaching assistant in biochemistry 440, 442 and 406 (Professors Susan Brockerhoff, Justin Kollman, Peter Brzovic, Michael Ailion, David Kimelman, and Hannele Ruohola-Baker). Thanks for your wisdom and thank you for helping me become a better teacher. I would also like to thank Erin Kirschner and everyone in the Biochemistry for everything you do for the trainees.

I would also like to thank my fellow lab mates and all the members of the Ruohola-Baker lab, past and present. It has been a pleasure to get to know you and work with in the last five years. To all the collaborators that I have had the pleasure to work with, thank you for helping me with my Ph.D. projects. To my colleagues in Tom and Sue Ellison Stem Cell Core: Carol Ware, Julie Mathieu, Jennifer Hesson and Chris Cavanaugh thanks for your help. To Professor Julie Mathieu, I am truly grateful for your mentorship and that I had the chance to work with you and learn from you over past five years. To the friends that I have made in the Biochemistry department and ISCRM at South Lake Union, thank you for valuable discussions and support during my time in graduate school. I am grateful to ISCRM Fellows Program and Biological Mechanisms of Healthy Aging Training Grant for funding.

Finally, I would like to express my gratitude to my family: my parents, siblings, uncles, aunts, grandma, my wife, and children. Without their tremendous understanding and encouragement in the past five years, it would be impossible for me to complete my PhD. To my wife, Samira, and my children – Aisha, Ibrahim, and Naima – thank you for always being there for me.

Dedication

To the strong women in my life –
my grandma, my mom, my aunt and my wife -
I attribute my success to all of you.

Chapter 1

INTRODUCTION

1.1 Cellular Quiescence

Cellular quiescence is a dormant state at the Gap 0 (G_0) phase of the cell cycle. This cell cycle block is temporary and reversible (Daignan-Fornier and Sagot, 2011). Quiescent cells have the capacity to re-enter the cell cycle unlike terminally differentiated and senescent cells that are also in the G_0 phase. Senescent cells are dysfunctional cells that stop proliferation and permanently remain in the G_0 phase of the cell cycle (Campisi, 2011). Senescent cells secrete inflammatory factors that trigger chronic activation of inflammatory signaling, contribute to tissue aging (Baker et al., 2016) and establishment of aging-associated diseases (Campisi et al., 2011). Quiescent stem cell populations can be found in several stem cell types such as hematopoietic stem cells (HSCs), hair follicle stem cells (HFSCs), muscle stem cells (MuSCs), and neural stem cells (NSCs) (Cheshier et al., 1999; Blanpain et al., 2004; Cheung and Rando, 2013; Codega et al., 2014).

Quiescent cells are distinct from other Gap 1 (G1) phase cells because they delay progress through G1 and S phase and can remain in G_0 anywhere from hours to years until they receive external signals to become activated and re-enter the cell cycle. Quiescent cells at G_0 have a different transcriptional profile compared to cells at G1 (Coller et al., 2006). Changes that result when mammalian cells arrest their cell cycles in G1, such as terminally differentiated and senescent cells, were found to have different gene expression profiles compared to changes that happen in response to quiescence signal (Coller et al., 2006; Sang et al., 2008). Genes that are involved in DNA replication and cell cycle progression are decreased in quiescent stem cells

compared to G1 cells. This emphasizes that the G_0 quiescence state does not mirror a prolonged G1 phase, but rather it is a very distinctive state from G1 arrested cells, regardless of the cause of arrest.

1.2 Cell Cycle Regulation

Cell division cycle is a tightly regulated series of events that are required for cell growth. The cell cycle can be divided into five phases: G1, S, G2, mitosis and cytokinesis. G1 is the primary growth phase where the cell increases in size. The S phase is where the cell synthesizes its genome. G2 is the second growth phase and a preparatory phase for cell division. The fourth phase is mitosis where the cell divides and the replicated chromosomes are separated into two identical genomes. The fifth and final phase is cytokinesis where the cytoplasm divides creating two identical daughter cells.

There are three checkpoints that tightly control the cell cycle process in eukaryotes. These checkpoints serve as internal control to regulate cell cycle events and allow progression of a cell to the next stage upon DNA repair (Hartwell and Weinert, 1989). The first checkpoint is in the G1 phase, in which cell growth and DNA damage is assessed before entry into the S phase. The G1 checkpoint is thought to be the only checkpoint in which cells can enter a reversible quiescence state (Matson and Cook, 2017). The second checkpoint occurs at the end of G2 in which the accuracy of DNA replication and DNA damage is assessed. The third and final checkpoint occurs at the M phase in which mitosis is assessed at the end of the metaphase stage of mitosis.

Multiple internal and external cues signal what decisions are taken at each checkpoint before cells transition to the next phase. Activation of transcription factor p53 transiently arrests cell cycle to allow DNA repair. However, if repair does not take place, p53 induces apoptosis in

response to DNA damage (Kohn, 1999; Amundson et al., 1998). p53-mediated cell cycle arrest is critical for cell cycle checkpoint functions during DNA damage. This cell cycle arrest is mediated by the activation of p21, a cyclin-dependent protein kinase inhibitor (CDKI) and a target of p53 (el-Deiry et al., 1993; Harper et al., 1993). p53 improves survival of damaged cells by arresting cells at the G1 phase and allowing more time for the repair of DNA double-stranded breaks (Chen, 2016). However, if DNA repair cannot be completed successfully, apoptotic pathway is induced by p53 (Aubrey et al., 2018). p53 function has also been implicated in quiescence. Quiescent cells have elevated levels of p53 (Itihana et al., 2002) and many of them also express high levels of p21 (Noda et al., 1994; Itihana et al., 2002) and p63 (Forster and Ellisen, 2011). Abolishing p53 function pauses entry into G_0 upon withdrawal of growth factors (Itihana et al., 2002) and loss of p21 function causes quiescent cells to exit G_0 and re-renter the cell cycle (Nakanishi et al., 1995). Interestingly, proliferating, quiescent and senescent cells have differential p53 phosphorylation patterns (Webley et al., 2000), indicating p53 might function differently in these three growth states. Furthermore, although p53 can activate apoptosis, apoptotic pathway was found to be downregulated in diapause (Bulut-Karslioglu et al., 2016; Hussein et al., 2020; Arena et al., 2021). Overall, these data suggest p53 plays an important role for quiescent cells to enter and remain in G_0.

Different factors can affect how long cells can remain in a non-dividing state during checkpoints. These factors include molecular signals, DNA integrity and cell size, and timing can also vary between these factors. Although duration of arrest in response to DNA damage correlates to extent of the damage (Chao et al., 2017), if DNA damage repair is successful, cells will pass the checkpoint. However, if DNA cannot be repaired prior to the cell cycle transition checkpoint, the cell will undergo p53-mediated apoptosis. On the other hand, cells can remain in

a quiescent state potentially longer than the normal checkpoint. Cells kept under quiescence-inducing conditions for a long period of time transitioned deeper into quiescence (Coller et al., 2006). These G_0 quiescent cells remained viable but took longer to re-enter the cell cycle (Yanez and O'Farrell, 1989; Owen et al., 1989; Lemons et al., 2010). Based on these findings, we propose that the main difference between G1 arrested cells and quiescent cells in G_0 is regulation of the apoptotic pathway. Quiescent cells remain at G_0 and downregulate the apoptotic pathway; whereas, unsuccessful p53-induced DNA damage repair stimulates apoptosis.

1.3 Defects in Quiescence

Loss of quiescence or its dysregulation can disrupt the balance of the progenitor cell populations and deplete the progenitor stem cell population (Orford and Scadden, 2008) resulting in a failure to regenerate in response to injury. In HSCs, a depleted progenitor cell population can lead to diminished adaptive immune function and myeloproliferative disease (Orford and Scadden, 2008; Jacob and Osato, 2009) and in NSCs, it can result in failure to regenerate new neurons and cognitive deficits (Farioli-Vecchioli et al., 2012; Jones et al., 2015). These show how critical stem cell quiescence is for tissue homeostasis and regenerative medicine.

1.4 Embryonic Diapause

Embryonic diapause is a unique example of quiescence. Diapause is a reversible state of suspended embryonic development that is associated with delayed blastocyst implantation. Embryos from over 130 mammalian species can enter a dormant state called embryonic diapause, in which the blastocysts survive unimplanted in the uterus for a prolonged period of time (Fenelon et al., 2014). Two types of diapause, obligate and facultative, have been described in vertebrates (reviewed by Lopes et al., 2004). Obligate diapause occurs in each gestation of a species and serves to ensure that offspring is born in a favorable environmental condition.

Facultative diapause is a delayed implantation commonly due to lactational stress. In mice, the blastocyst remains in a diapause state as the newly born pups nurse, because the suckling stimulus promotes an increased secretion of prolactin which downregulates ovarian estrogen release (McLaren, 1968; Yoshinaga, 2013). Elimination of the stimulus induced by suckling through removal of pubs results ovarian estrogen increase and initiates embryonic reactivation and implantation of the embryo. Facultative diapause is therefore believed to be used as a reproductive strategy to avoid metabolic stress due to nursing overlapping litters (Mantalenakis and Ketchel, 1966; Cha et al., 2020

During embryonic development, fertilization and zygote formation take place, followed by cleavage, mitotic divisions with no significant growth, and formation of the early blastocyst and finally implantation (Figure 1.1). However, in embryonic diapause, the embryo will be arrested at the blastocyst stage and there will be no implantation (Figure 1.1). In many vertebrates, lactation or unfavorable environmental conditions can lead to a complete block of embryonic development at the blastocyst stage (McLaren, 1968; Nichols et al., 2001; Rose-John, 2002). Development and implantation resume after stress is removed (McLaren, 1968) and this can take several days or months depending on the species.

Mouse is one of the best studied models of diapause. Facultative delayed blastocyst implantation or diapause occurs naturally in rodents and can be experimentally induced in mice by ovariectomy (Yoshinaga and Adams, 1966) or a non-surgical castration method by using the drug tamoxifen in combination with Depo-Provera to reduce estrogen but maintain progesterone levels, a known hormonal inducer of diapause (Hunter and Evans, 1999; Paria et al., 1993). Mouse embryos in diapause, have an inner cell mass (ICM) surrounded by trophoblasts (Figure 1), and it occurs in blastocysts on day 3.5 when the embryo contains about 30-40 cells. The

diapause embryo then enlarges and hatches from the zona pellucida and continues to grow in the first few days to approximately 130 cells followed by dormancy during the diapause (Fenelon et al., 2014; McLaren, 1968).

1.5 Naïve (pre-implantation) and Primed (post-implantation) Pluripotent Stem Cells

Embryonic diapause disrupts the naïve-to-primed transition of embryonic stem cells before implantation. Embryonic and induced pluripotent stem cells are both pluripotent stem cells because of two distinct features: the capacity to self-renew and the potential to regenerate all tissues in the body. Multiple pluripotent states have been isolated and stabilized in vitro in mouse and in humans. Two of these are the pre-implantation (naïve) and post-implantation (primed) embryonic stem cell (ESC) states (Brons et al., 2007; Tesar et al., 2007; Nichols and Smith, 2009; Ware et al, 2014; Gafni et al., 2013; Chan et al., 2013; Takashima et al., 2014; Ware, 2017; Theunissen et al., 2014; Valamehr et al., 2014; Wu et al., 2016; Weinberger et al., 2016). Human ESCs are isolated from the inner cell mass (ICM) of the pre-implantation blastocyst (Thomson et al., 1998). The blastocyst contains an inner cell layer termed the inner cell mass (ICM), and an outer cell layer called the trophectoderm (TE). Naïve and primed pluripotent cells display important metabolic, epigenetic and gene expression differences (Sperber et al., 2015; Takashima et al., 2014; Zhou et al., 2012; Sone et al., 2017; Moody et al., 2017).

1.6 Metabolism of Naïve and Primed Pluripotent Stem Cells

One of the major energy-producing pathways in living cells is glycolysis, converting a molecule of glucose to pyruvate, ATP and NADH. Glucose can be metabolized in two ways to generate ATP, either aerobically in the presence of oxygen or anaerobically in the absence of oxygen. Complete oxidation of glucose yields the most ATP (36) in a process called oxidative

phosphorylation in the electron transport chain (ETC) compared to glycolysis (2 ATP) (see Figure 1.2). The pentose phosphate pathway (PPP) is another important pathway in which glycolytic intermediates can be shunted into the PPP for cell growth and proliferation. The PPP is an essential pathway for pluripotent stem cells (Filosa et al., 2003; Varun et al., 2011). In addition, products of the PPP include NADPH which is used in the reduction of glutathione.

One of the main differences between naïve and primed pluripotent stem cells is their metabolism. For example, naïve ESCs both in mouse and human utilize both oxidative phosphorylation (OXSPHOS) and glycolysis for their energy demands, whereas primed cells depend solely on glycolysis (Zhou et al., 2012, Takashima et al., 2014; Sperber et al., 2015; Mathieu and Ruohola-Baker, 2017). Amino acids are also differentially expressed between naïve and primed hESCs. For example, the amino acid tryptophan (Trp) is critical for the growth of hESCs at the primed stage (Shiraki et al., 2014; Sperber et al., 2015) and the Trp degradation product kynurenine is highly enriched in primed hESCs (Sperber et al., 2015). In contrast, methionine as well as its product S-adenosylmethionine (SAM) are downregulated in naïve hESCs (Sperber et al., 2015).

Naïve and primed hESCs also differ in their lipid metabolism (Sperber et al., 2015). Lipids are a major source of energy in cells which can be generated from breakdown of lipids through fatty acid β-oxidation, generating acetyl-CoA (see Figure 1.3). Acetyl-CoA can further be oxidized in the tricarboxylic acid (TCA) cycle generating the energy rich molecule, GTP, and the electron carriers NADH and FADH2 to deliver the electrons to the ETC. Both mouse and human naïve ESCs do not accumulate lipids whereas both mouse and human primed ESCs accumulate lipids (Sperber et al., 2015). In addition, using functional analysis of live cells, it was

shown thar naïve ESCs can use palmitate as an energy source whereas primed ESCs are not able to utilize palmitate (Sperber et al., 2015).

Naïve and primed pluripotent cells differ in many other aspects. It is not fully understood how pluripotent states transition between pre-implantation naïve to post-implantation primed stage and how they exit from pluripotent states. To resolve this and to better understand the differences between human ESCs states, we performed a whole genome CRISPR screen to identify genes that are essential in the naïve-to-primed hESC transition (Mathieu et al., 2019). Based on this functional screen, we discovered novel regulators of naïve-to-primed transitions and we validated genes in secondary screens from different classes that are required for the transition. The whole genome CRISPR screen also identified multiple genes that regulate human primed pluripotent stem cells (Mathieu et al., 2019; Chia et al., 2010) and revealed many regulators not previously known to participate in stability of pluripotent states, including GREB1, FLCN, MAP2K7, NELL2, GPR161, GPI, and SUV420H2. From this screen, we chose to further study the role SUV420H2 - a histone methyltransferase implicated in aging and in senescence - in early development and in quiescence

1.7 FIGURES

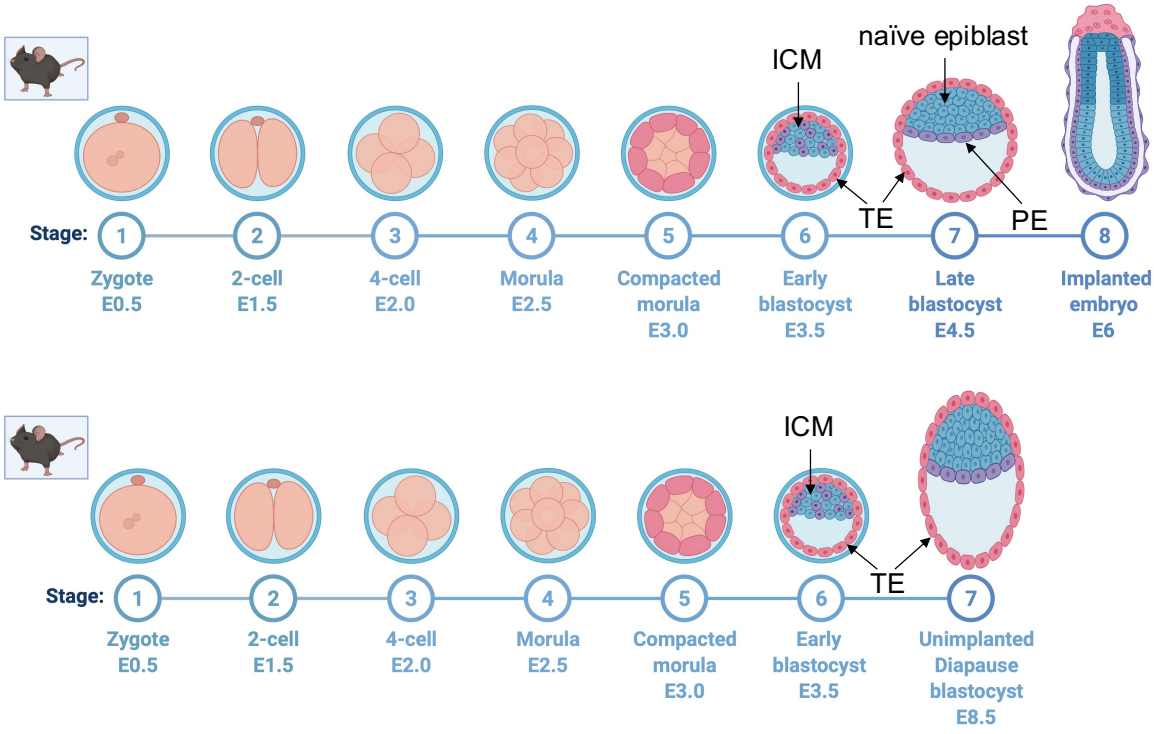

Figure 1.1: Mouse embryonic development progress and induction of diapause.

A: A simplified version of mouse development showing formation of zygote, 2-cell, 4-cell and morula formation followed by early blastocyst on embryonic day 3.5. In normal development, this is followed by formation of the late blastocyst on embryonic day 4.5 and implantation of the embryo on day 6. B. This process can be halted in embryonic diapause at the blastocyst stage on day 3.5. The embryo hatches from the zona pellucida, remains viable without implanting but remains loosely attached to the uterine wall. The figure was created with Biorender.com.

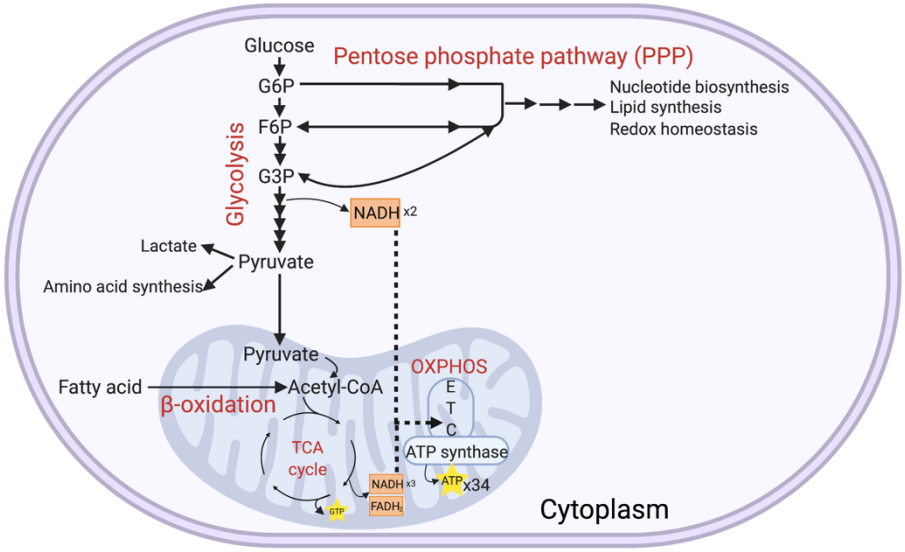

Figure 1.2: Overview of major cellular metabolic pathways.

Metabolic pathways (indicated in red): Glycolysis, pentose phosphate pathway (PPP), β-oxidation, TCA (Krebs) cycle and oxidative phosphorylation (OXPHOS). Intermediate metabolites from glycolysis can be shuttled to PPP to generate NADPH and precursors for nucleotide and lipid biosynthesis. In addition to making ATP, glycolysis generates pyruvate which is further oxidized in the TCA cycle. Pyruvate can also be used to make lactate or converted to amino acids. OXPHOS yields the most ATP in the electron transport chain (ETC). Both pluripotent and adult stem cells can utilize these metabolic pathways (see text for details). G6P, glucose 6 phosphate; F6P, fructose 6 phosphate; G3P, glyceraldehyde- 3-phosphate; TCA, tricarboxylic acid; GTP, guanosine triphosphate; ATP, adenosine triphosphate; ATPase, ATP

synthase; ETC, electron transport chain; FAD, Flavin adenine dinucleotide; NAD, Nicotinamide adenine dinucleotide. The figure was created with Biorender.com.

Chapter 2

METABOLIC CONTROL OVER THE MTOR-DEPENDENT DIAPAUSE-LIKE STATE

Parts of this chapter are in the following manuscripts:

Metabolic Control over mTOR-Dependent Diapause- like State

Abdiasis M. Hussein, Yuliang Wang, Julie Mathieu, Lilyana Margaretha, Chaozhong Song, Daniel C. Jones, Christopher Cavanaugh, Jason W. Miklas, Elisabeth Mahen, Megan R. Showalter, Walter L. Ruzzo, Oliver Fiehn, Carol B. Ware, C. Anthony Blau, Hannele Ruohola-Baker

2.1 ABSTRACT

Regulation of embryonic diapause, dormancy that interrupts the tight connection between developmental stage and time, is still poorly understood. Here, we characterize the transcriptional and metabolite profiles of mouse diapause embryos and identify unique gene expression and metabolic signatures with activated lipolysis, glycolysis, and metabolic pathways regulated by AMPK. Lipolysis is increased due to mTORC2 repression, increasing fatty acids to support cell survival. We further show that starvation in pre-implantation ICM-derived mouse ESCs induces a reversible dormant state, transcriptionally mimicking the in vivo diapause stage. During starvation, Lkb1, an upstream kinase of AMPK, represses mTOR, which induces a reversible glycolytic and epigenetically H4K16Ac-negative, diapause-like state. Diapause furthermore activates expression of glutamine transporters SLC38A1/2. We show by genetic and small molecule inhibitors that glutamine transporters are essential for the H4K16Ac-negative, diapause state. These data suggest that mTORC1/2 inhibition, regulated by amino acid levels, is causal for diapause metabolism and epigenetic state.

2.2 INTRODUCTION

The term diapause describes a reversible, environmentally inducible state of suspended embryonic development that is associated with delayed blastocyst implantation. Diapause has been described in more than 130 mammalian species, indicating an exceptional degree of evolutionary conservation in the coordination between birth and favorable environmental conditions (Fenelon et al., 2014). However, the molecular controls of the entry and exit of this reversible dormant stage are poorly understood.

Diapause can be triggered experimentally in mice through ovariectomy (Yoshinaga and Adams, 1966) or estrogen deprivation (Hunter and Evans, 1999; Paria et al., 1993) and occurs at day 3.5 (E3.5) of embryonic development. The pre-implantation, diapause blastocyst, comprised of inner cell mass (ICM) surrounded by trophectoderm, remains developmentally arrested until implantation is triggered (Fenelon et al., 2014; McLaren, 1968). While some studies have been performed to understand the cellular and molecular changes that occur when embryos enter diapause, a comprehensive analysis of metabolites is required to dissect the metabolic regulation of a diapause state. It has been shown that some metabolic activities including protein and DNA synthesis as well as carbohydrate metabolism are reduced in diapause (Fenelon et al., 2014; Menke and McLaren, 1970; Pike, 1981; Van Blerkom et al., 1978; Hamatani et al., 2004; Liu et al., 2012; Martin and Sutherland, 2001; Fu et al., 2014). Furthermore, amino acids in the uterine fluids have been shown to affect diapause (Renfree and Fenelon, 2017; Gardner and Lane, 1993; Van Winkle et al., 2006), although the downstream targets for this regulation have not been dissected.

Autophagy, a metabolic pathway that generates nutrients required for cellular survival during starvation, has been shown to be activated during diapause (Lee et al., 2011).

Furthermore, autophagy can be regulated by mTOR (Kim and Guan, 2015; Nicklin et al., 2009). Accordingly, recent work has revealed that inhibition of the mTOR pathway or depletion of transcription factor, Myc, can induce a diapause-like state (Bulut-Karslioglu et al., 2016; Scognamiglio et al., 2016). However, how mTOR is downregulated in diapause and the signals that reactivate mTOR in blastocyst development are not well understood in any mammal (Fenelon et al., 2014; Van Blerkom et al., 1978; Scognamiglio et al., 2016; Shaw and Renfree, 1986; Renfree and Shaw, 2014; Murphy, 2012; He et al., 2019).

Our study shows a key molecular mechanism and metabolic and epigenetic regulation for entry and exit of diapause. We found that both diapause and diapause-like cells have highly reduced H4K16Ac epigenetic marks, an upregulated glycolytic signature, reduced mitochondrial activity and reduced fatty acid β-oxidation. We further show that mTOR-dependent H4K16Ac epigenetic marks are inhibited by nutrient-starvation-dependent LKB1-induced AMPK activation, as well as diapause-enriched glutamine transporter activity (*Slc38A1/2*).

2.3 MATERIALS AND METHODS

2.3.1 Isolation of mouse embryos

All embryos were recovered from superovulated (Day -2 injection with Pregnant Mare Serum Gonadotropin (PMS), Day 0 injection with human Chorionic Gonadotropin (hCG)) C57BL/6 females (Charles River). The day of the vaginal plug was considered day 0.5. The third day following detection of a vaginal plug was referred to as day 3.5. Embryonic diapause was induced by intraperitoneal injection of tamoxifen and subcutaneous administration of 0.5 mg of Depo Provera on day 2.5 (Hunter and Evans, 1999). Diapause blastocysts were harvested 6 days later. Day 3.5 and diapause blastocysts were flushed from the uterus of superovulated pregnant females. For the isolation of ICM, the zona pellucida was first removed from day 3.5 embryos by

incubation in acid Tyrode's solution. To remove the trophoectoderm through immuno-surgery, blastocysts were placed in a rabbit anti-mouse polyclonal antibody (Rockland Immunochemicals) for 20 min at 37 ^{o}C, followed by guinea pig serum complement for 20–30 min at 37 ^{o}C. The lysed trophectoderm cells were removed and the isolated ICM was placed in lysis buffer to isolate RNA. The derivation of epiblast (Epi) from day 6.5 post-implantation embryos has been described previously (Brons et al., 2007). Briefly, they dissected the late epiblast layer completely from mouse at the pre-gastrula stage and fully separated the epiblast layer from the extraembryonic tissues (Brons et al., 2007). Each biological triplicate for ICM and dICM and duplicate for samples contained lysates from approximately 50 embryos. Our work has been performed in compliance with ethical regulations, IACUC protocol # 4152-02.

2.3.2 Generation of LKB1 isoforms in mouse ESC lines using TALEN-based gene editing

Two mESC lines were created using Talen-based gene editing: 1. A heterozygous line in which one allele was modified to only express the short isoform of LKB1 (SL) and 2. A homozygous line in which both alleles were modified to express only the short isoform of *LKB1* (SS). A schematic diagram illustrating the donor construct, the wild-type (wt) *LKB1* locus and the targeted allele is shown in Figure Appendix A 3A. Exon 8 is the last common exon of the long and short forms of *LKB1*. The short form of *LKB1* has exon 9A while the long form of *LKB1* has exons 9B/10. The modified *LKB1* locus will express only the short form of LKB1 since the short form-specific exon 9A is fused directly in frame with exon 8 followed by the 2A peptide and the *neomycin/puromycin* resistance cassette followed by a poly A site. mESCs were transfected with the TALEN pairs and donor plasmid. *Neo* resistant clones were analyzed for homologous recombination using PCR (Figure Appendix A 3B). We have also analyzed the expression of both LKB1 long and LKB1 short using primers that are specific to each form using

RT-PCR (Figure Appendix A 3C). LKB1 long is 55-kDa on a western blot and LKB1 short form is 48-kDa (Figure Appendix A 3D). The control mESC line, R1(LL; wildtype for both alleles) expresses predominantly the LKB1 long form while short form is expressed at a very low level. In the m/m mESC line, both alleles are modified to express LKB1 short form only (SS). Because the modified LKB1 short form is expressed with an additional 22 amino acids (2A peptide) as compared to the endogenous short form, its size on the western blot is the same as the LKB1 long form. Because the modified alleles express only the LKB1 short form with the 2A peptide, the wild-type short form is not present and disappears in the m/m lane of the western blot (Figure Appendix A 3D).

2.3.3 Generation of mESCs expressing LKB1 short isoform only

TALEN-mediated gene editing of the endogenous *LKB1* locus was employed. Exon 8 is the last common exon of the long and short forms of *LKB1*. Exons 9A and 9B are short form- and long form-specific exons, respectively. The wild-type *LKB1* locus was modified using a donor construct that expresses exon 9 plus the 2A peptide by homologous recombination. The modified *LKB1* locus expressed only the short form of LKB1 since the short form-specific exon 9A is fused directly in-frame with exon 8 followed by the 2A peptide and *Neo* followed by a poly A site. mESCs were transfected with the TALEN pairs and donor plasmid. *Neo* resistant clones were analyzed for homologous recombination using PCR. Primer pairs were used to amplify specifically either the wild-type or the modified locus (Figure Appendix A3).

2.3.4 mESC culture

R1 mESCs from A. Nagy (Samuel Lunenfeld Research Institute, Toronto, Canada) were cultured on feeder free plates coated with 0.1% (w/v) gelatin (Sigma) 37^{o}C for 10 min. Medium for mESCs contained high glucose DMEM supplemented with 20% ESC-qualified fetal bovine

serum, 1mM sodium pyruvate, 1mM non-essential amino acids (NEAA), 1mM penicillin/streptomycin (all from Invitrogen, Carlsbad), 0.1mM 2- β-mercaptoethanol (Sigma Aldrich, St. Louis, MO), with addition of 10ng/mL mouse LIF (EMD Millipore), 1 mM GSK inhibitor (CHIR99021, Selleckchem) and 1 mM MEK inhibitor (PD0325901, Selleckchem). mESCs were passaged every 2–3 days as a single-cell suspension using 0.05% trypsin/EDTA (Invitrogen, Carlsbad).

2.3.5 RNA-seq

Total RNA was extracted using Qiagen Micro RNeasy kit and amplified following protocols of WT-Ovation Pico kit (Nugen). The quality and quantity of RNAs were determined on an Agilent 2100 Bioanalyzer (Agilent Technologies). Cluster generation of the cDNA library was performed on a cBot Cluster Station (Illumina) and the samples were sequenced on a Genome Analyzer IIx (Illumina). Transcripts expressed in ICM, dICM or Epi with >1.4-fold change and a p value < 0.05 (adjusted for multiple testing with the Benjamini-Hochberg procedure) were considered to be differentially expressed. The UCSC genome browser tracks of RNA-Seq reads are available at: http://www.cs.washington.edu/homes/ruzzo/papers/Margaretha/.

2.3.6 Data analysis

RNA-seq samples were aligned to NCBIM37 using TopHat (Trapnell et al., 2009) (version 2.0.13). Gene-level read counts were quantified using htseq-count (Anders et al., 2015) using Ensembl GRCh37 gene annotations. Genes with total expression above 2 normalized read counts in at least 2 RNA-seq samples were kept for further analysis. *prcomp* function from R was used to for principal component analysis. DeSeq (Anders and Huber, 2010) was used for differential gene expression analysis. Genes with fold change >1.5 and FDR <0.1 were

considered differentially expressed. topGO R package (Alexa et al., 2006) was used for Gene Ontology enrichment analysis. Hallmark gene sets were used for pathway enrichment analysis (Liberzon et al., 2015). Combat (Johnson et al., 2007) was used to correct batch effects between RNA-seq samples of this study (Boroviak et al., 2015). *In vitro* starvation RNA-seq samples were projected onto the PCA using eigenvectors calculated from the combined *in vivo* RNA-seq samples of this study and Boroviak et al. (2015).

2.3.7 Metabolomics

2.3.7-1 Mouse embryos

Mouse embryos were isolated as mentioned above. Briefly, embryonic diapause was induced by the injection of tamoxifen with Depo Provera on day 2.5 and diapause blastocysts were harvested 5 days later. Triplicate samples for diapause (n=134) and duplicate for pre-implantation blastocysts (n=114) were collected and washed with M2 media (Millipore Sigma) at room temperature. Embryos were flash frozen in liquid nitrogen before performing metabolite analysis (HILIC, GC-MS and lipidomics).

2.3.7-2 Mouse ESCs

Mouse ESC lines [R1(LL) and R1(SS) and *Rictor* knockout – generated from R1(LL) line] were plated ($1x10^5$ cells/35 mm plate, minimum triplicate plates for each group) and starved overnight on day 2. Cells were harvested on day 3 and flash frozen in liquid nitrogen before performing metabolite analysis (HILIC, GC-MS and lipidomics).

2.3.8 Sample preparation for LC-QTOFMS analysis

A total of 134 and 114 pre-implantation and diapause mouse embryos respectively were extracted with 225 ml of methanol at -20 ^oC containing an internal standard mixture of PE(17:0/17:0), PG(17:0/17:0), PC(17:0/0:0), C17 sphingosine, ceramide (d18:1/17:0), SM

(d18:0/17:0), palmitic acid-d3, PC (12:0/13:0), cholesterol-d7, TG (17:0/17:1/17:0)-d5, DG (12:0/12:0/0:0), DG (18:1/2:0/0:0), MG (17:0/0:0/0:0), PE (17:1/0:0), LPC (17:0), LPE (17:1), and 750 mL of MTBE (methyl tertiary butyl ether) (Sigma Aldrich) at -20 ^{o}C containing the internal standard cholesteryl ester 22:1. Samples were shaken for 6 min at 4 ^{o}C with an Orbital Mixing Chilling/Heating Plate (Torrey Pines Scientific Instruments). After shaking, 188 ml of LC-MS grade water (Fisher) was added. Samples were vortexed, centrifuged and the upper (non-polar) and bottom (polar) layers were collected (350 mL and 125 mL, respectively in two aliquots) and evaporated to dryness. One dried 350-mL aliquot of the non-polar layer was re-suspended in 100 mL of methanol:toluene (9:1, v/v) mixture containing 50 ng/ml Cuda (12-[[(cyclohexylamino)carbonyl]amino]-dodecanoic acid), Cayman Chemical). One dried 125-mL aliquot of the polar layer was resuspended in an acetonitrile:water (4:1, v/v) mixture with 5 mg/ml Val-Try-Val (Sigma). Samples were then vortexed then centrifuged and prepared for lipidomic or polar metabolite analysis. Method blanks and pooled human plasma (BioreclamationIVT) were included as quality control samples.

2.3.9 Chromatographic and mass spectrometric conditions for lipidomic LC-QTOF analysis

For analysis of the non-polar phase, re-suspended samples were injected at 3 mL and 5 mL for ESI positive and negative modes respectively, onto a Waters Acquity UPLC CSH C18 (100-mm length 3 2.1 mm id; 1.7-mm particle size) with an additional Waters Acquity VanGuard CSH C18 pre-column (5 mm 3 2.1 mm id; 1.7-mm particle size) maintained at 65 ^{o}C was coupled to a Vanquish Horizon UHPLC (Thermo Fisher Scientific). To improve lipid coverage, different mobile phase modifiers were used for positive and negative mode analysis (Cajka, 2016). For positive mode 10 mM ammonium formate and 0.1% formic acid were used

and 10 mM ammonium acetate (Sigma–Aldrich) was used for negative mode. Both positive and negative modes used the same mobile phase composition of (A) 60:40 v/v acetonitrile:water (LC-MS grade) and (B) 90:10 v/v isopropanol:acetonitrile. The gradient started at 0 min with 15% (B), 0–2 min 30% (B), 2–2.5 min 48% (B), 2.5–11 min 82% (B), 11–11.5 min 99% (B), 11.5–12 min 99% (B), 12– 12.1 min 15% (B), and 12.1–15 min 15% (B). A flow rate of 0.6 mL/min was used. For data acquisition a quadrupole/orbital ion trap mass spectrometer Q Exactive HF with a HESI-II ion source (Thermo Fisher Scientific). Simultaneous MS^1 and MS/MS (data- dependent MS/MS) acquisition was used. The parameters were ESI polarity, positive or negative; sheath gas pressure, 60 psi; aux gas flow, 25 arbitrary units; sweep gas flow, 2 arbitrary units; spray voltage, ±3.6 kV; capillary temperature, 300 ^{o}C; aux gas heater temperature, 370 ^{o}C; MS^1 mass range m/*z* 60–900; MS^1 resolving power, 30,000 FWHM (*m*/*z* 200); number of data-dependent scans per cycle: 3; MS^2 resolving power, 15,000 FWHM; acquisition speed: 2 MS^1 spectra/s; normalized collision energy, 20, 30, 40%.

2.3.10 Chromatographic and mass spectrometric conditions for polar metabolite HILIC-QTOFMS analysis

Hydrophilic interaction liquid chromatography (HILIC) method was used for analysis of the polar phase. Five microliters of re-suspended sample were injected onto a Waters Acquity UPLC BEH amide column (150-mm length 3 2.1 mm id; 1.7-mm particle size) with an additional Waters Acquity VanGuard BEH amide pre-column (5 mm 3 2.1 mm id; 1.7-mm particle size) maintained at 45 ^{o}C coupled to a Vanquish Horizon UHPLC (Thermo Fisher Scientific). The mobile phases were prepared with 10 mM ammonium formate and 0.125% formic acid (Sigma–Aldrich) in either 100% LC-MS grade water for mobile phase (A) or 95:5 v/v acetonitrile:water for mobile phase (B). Gradient elution was performed from 100% (B) at 0–

2 min to 70% (B) at 7.7 min, 40% (B) at 9.5 min, 30% (B) at 10.25 min, 100% (B) at 12.75 min, isocratic until 16.75 min with a column flow of 0.4 mL/min. Spectra were collected using a quadrupole/orbital ion trap mass spectrometer Q Exactive HF with a HESI-II ion source (Thermo Fisher Scientific). Simultaneous MS^1 and MS/MS (data-dependent MS/MS) acquisition was used. The parameters were ESI polarity, positive or negative; sheath gas pressure, 60 psi; aux gas flow, 25 arbitrary units; sweep gas flow, 2 arbitrary units; spray voltage, ±3.6 kV; capillary temperature, 300 °C; aux gas heater temperature, 370 °C; MS^1 mass range m/*z* 120–1200; MS^1 resolving power, 30,000 FWHM (*m*/*z* 200); number of data-dependent scans per cycle: 3; MS^2 resolving power, 15,000 FWHM; acquisition speed: 2 MS^1 spectra/s; normalized collision energy, 20, 30, 40%.

2.3.11 LC-MS data processing using MS-DIAL

Both lipidomic and HILIC data processing was performed using MS-DIAL (Tsugawa et al., 2015) for peak picking, alignment, and identification. For both lipidomic and polar metabolite analysis, in house *m*/*z* and retention time libraries were used in addition to MS/MS spectra databases in msp format (Kind et al., 2013).

2.3.12 LKB1 splice variant analysis

We used Isolator Software to identify alternative splicing events. Isolator uses a Bayesian hierarchical model to boost signal in small sample number settings (Jones, 2016). Isolator has been previously used to find differential alternative splicing in cardiomyocyte maturation (Kuppusamy et al., 2015). Reads were aligned to mouse GRCm38 using HISAT2 (Kim et al., 2015). Ensembl gene 38, release 92 were used for annotation.

2.3.13 Starvation studies

mESCs were serum (fetal bovine serum) and glucose starved for 24 h. Cells were

cultured only with DMEM (0 g/L D-glucose, Invitrogen) with addition of 10ng/mL mouse LIF (EMD Millipore), 1 mM GSK inhibitor (CHIR99021, Selleckchem) and 1 mM MEK inhibitor (PD0325901, Selleckchem). To reverse starvation-induced effects, starvation media was removed from the culture after 24 h and mESCs were cultured with DMEM (4.5 g/L D-glucose, Invitrogen), supplemented with 20% ESC-qualified fetal bovine serum, 1mM sodium pyruvate, 1mM non-essential amino acids (NEAA), 1mM penicillin/streptomycin (all from Invitrogen), 0.1mM 2- β-mercaptoethanol (Sigma Aldrich), with addition of 10ng/mL mouse LIF (EMD Millipore), 1 mM GSK inhibitor (CHIR99021, Selleckchem) and 1 mM MEK inhibitor (PD0325901, Selleckchem).

2.3.14 mTORC1/2 inhibition

mTORC1/2 activity was inhibited in mESCs (LKB1 long and LKB1 short) by treatment with INK-128 for 24 h (200nM, Medchem).

2.3.15 Generation of rictor KO mESCs

One million of R1 mESCs were electroporated with SpCas9 (0.3mM, Sigma) and gRNA (1.5mM, Synthego) as RNP complex (assembled 15min at room temperature) using Amaxa Nucleofector (mouse ESC kit, Lonza) in the presence of ROCK inhibitor. Individual colonies were hand-picked and plated into 96-well plates. After passaging onto 24-well plates, proteins were extracted from the clones and *RICTOR* protein expression was assessed by western blot analysis. DNA of the clones was extracted using Quick Extract DNA extraction solution (Epicentre#QE09050) and nested PCR was performed around the *RictoR* gRNA targeting site. The PCR products were purified using EXO-SAP enzyme (ThermoFisher) and sent for Sanger sequencing analysis (through Genewiz).

2.3.16 OCR and ECAR measurement using Seahorse Cellular Flux Assays

Mouse ESCs were seeded onto 96-well Seahorse plates at $2x10^4$ cells/well. Cells were cultured in DMEM with or without glucose, depending on starvation criteria, overnight. For mTORC1/2 inhibition, cells were treated with INK-128 overnight (200 nM, Medchem). Culture media were exchanged for base media (unbuffered DMEM (Sigma D5030) supplemented with sodium pyruvate (Gibco, 1mM) and with 25-mM glucose (for Mitostress assay), or 25mM glucose and 50mM carnitine (for palmitate assay), 1 h prior to the assay. Substrates and selective inhibitors were injected during the measurements to achieve final concentrations of glucose (2.5mM), 4-(tri- fluoromethoxy) phenylhydrazone (FCCP, 300nM–500nM), oligomycin (2.5 mM), antimycin (2.5mM), rotenone (2.5mM), palmitate (50mM in BSA), BSA and ETO (50mM). The OCR and ECAR values were normalized to the number of cells present in each well, quantified by Hoechst staining (HO33342; Sigma-Aldrich). Changes in OCR and ECAR in response to substrate and inhibitor addition were defined as the maximal change after the chemical injection compared to the last OCR or ECAR value before the injection. Glycolytic capacity is a measure of the maximum rate of conversion of glucose to lactate after using oligomycin to inhibit ATP synthase in the electron transport chain (ETC) and thus block the generation of ATP. Measurements of ECAR before and after 2-DG addition is a readout of the maximum glycolytic capacity of the cell. Glycolytic reserve is a measure of ECAR differences before and after oligomycin and indicates the ability of a cell to respond to an energetic demand.

2.3.17 Glutamine transporter inhibition in diapause embryos

Embryonic diapause was induced by intraperitoneal injection of tamoxifen and subcutaneous administration of 0.5 mg of Depo Provera on day 2.5 of embryonic development in 4 to 7-week-old mice for various strains (C57BL/6, B6C3 and B6D2). The diapause blastocysts were harvested 6 days later in M2 solution (Millipore Sigma) supplemented with INK128

(200nM). The embryos were cultured in KSOM media (Zenith Biotech) with or without 10 mM of the glutamine transporter inhibitor L-γ-Glutamyl-p-nitroanilide (GPNA, MP Biomedicals) for 1h. Embryo were then stained with H4K16Ac.

2.3.18 CRISPR KO of glutamine transporters in mouse zygotes

Female mice from various strains were superovulated by intraperitoneal injection of 5 IU (for 4 week old C57BL/6 mice) or 7.5IU (for 7 week old B6C3 mice) of PMSG, followed by intraperitoneal injection of 5 IU hCG (for 4 week old C57BL/6 mice) or 7.5IU (for 7 week old B6C3 mice) 48 h later. Superovulated females were mated with adult males and euthanatized the next morning. Zygotes were harvested from the oviducts in M2 solution (Millipore Sigma). RNP complexes were prepared with 4mM SpCas9 (Sigma) and 4mM of gRNA against *Slc38a1* (Synthego) and gRNA against *Slc38a2* (Synthego), and incubated for 15min at room temperature. 2 batches of 40 embryos were electroporated with RNP complex in electroporation buffer (Chen et al, 2016) using a BioRad electroporator (GenePulser Xcell: 30V, 10ms, 4pulses) and cultured in KSOM media for 4 days and supplemented with INK128 (200nM) for an additional 24h before imaging and DNA extraction. DNA was extracted using Quick Extract DNA extraction solution (Epicentre#QE09050) and nested PCR were performed for around *Slc38a1* and *Slc38a2* gRNA target sites. The PCR products were purified using EXO-SAP enzyme (ThermoFisher) or gel extraction (Qiagen) and sent for Sanger sequencing analysis (through Genewiz) to validate the genotype of the embryos.

2.3.19 Design of guide RNA (gRNA) targeting exons 3 and 4 of *Slc38a1/2*

We designed gRNAs that target exons 3 and 4 of *Slc38a1*and *Slc38a2*, respectively. Non-Homology End Joining (NHEJ) repair created indels at the gRNA cutting site. In *Slc38a1*, the deletions generated a frameshift that led to the creation of a premature stop codon in exon 4,

resulting in a truncated protein in the first transmembrane domain which renders the transporter non-functional. In *Slc38a2*, there was a deletion of 2 amino acids (alanine and isoleucine) at residues 83 and 84. Previous studies have shown that mutations in the residue 82 of SLC38A2 reduce the affinity of the transporter for sodium (Na^+) and therefore the transport of glutamine, suggesting that the first transmembrane domain is crucial for the function of SLC38 transporters (Zhang et al., 2008, 2009).

2.3.20 Measurement of mitochondrial mass and mitochondrial DNA amount

Mitochondrial mass was measured using flow cytometry after MitoTracker Green staining of R1(LL) and R1(SS) mESCs before or after overnight starvation. Briefly, cells were washed with PBS and incubated in 50 nM of MitoTracker green for 30 min before analysis on a Canto I flow cytometer (BD Biosciences). Data analysis was performed using the FlowJo software (Tree Star, Ashland, OR, USA).

Mitochondrial DNA amount was evaluated by measuring the ratio of mitochondrial DNA (mtDNA) versus nuclear DNA (nDNA) by qPCR analysis. Briefly, the DNA of R1(LL) and R1(SS) mESCs after overnight starvation was isolated using DNAzol (Invitrogen) following manufacturer's protocol. mtDNA was measured using mt-Co1 primers mt-Co1-F 5'-CAGTCTAATGCTTACTCAGC-3' and mt-Co1-R 5' -GGGCAGTTACGATAACATTG-3', and nDNA was measured using Gapdh primers Gapdh-F 5 GGGAA GCCCATCACCATCTTC-3' and Gapdh-R 5'AGAGGGGCCATCCACAGTCT-3'. Each reaction contained 10ng of DNA extract, 13 SYBR Green Master Mix, and 300nM of each primer. qPCR was performed using a 7300 real-time PCR system (Applied Bio- systems) and the ratios mtDNA/nDNA were measured.

2.3.21 Protein extraction and western blot analysis

For protein analysis, $1x10^5$ cells were plated on 35 mm plates. Cells were lysed directly on the plate with lysis buffer containing 20mM Tris-HCl pH 7.5, 150mM NaCl, 15% glycerol, 1% Triton X-100, 1M b-glycerolphosphate, 0.5M NaF, 0.1M sodium pyrophos- phate, orthovanadate, PMSF and 2% SDS. 25 U of BenzonaseÒ nuclease (EMD Chemicals, Gibbstown, NJ) was added to the lysis buffer right before use. Proteins were quantified by Bradford assay (Bio-Rad), using BSA (bovine serum albumin) as the standard using the EnWallac Vision. The protein samples were combined with the 43 Laemli sample buffer with 10% β-mercaptoethanol (Bio-Rad #1610747), heated (95 ^oC, 5mins) and run on SDS-PAGE (protean TGX pre-casted gradient gel, 4%–20%, Bio-Rad) and transferred to the nitrocellulose membrane (Bio-Rad) by semi-dry transfer (Bio-Rad). Membranes were blocked for 1 h with 5% milk or 5% BSA (for antibodies detecting for phosphorylated proteins), and incubated in the primary antibodies overnight in 4 ^oC. The antibodies used for western blot were β-actin (Cell Signaling 4970 (1:10000), pAkt (Ser 473) (Cell Signaling 9271, 1:1000), Akt (Cell Signaling 9272, 1:1000), phospho-mTOR (Ser 2448) (Cell Signaling 5536, 1:1000), mTOR (Cell Signaling 2972, 1:1000), pS6 (Cell Signaling 2215, 1:1000), S6 (Cell Signaling 2117, 1:1000), p4EBP1 (Cell Signaling 236B4, 1:1000), 4EBP1 (Santa Cruz, sc-9977, 1:1000), p-p70 S6 kinase (T389 Cell Signaling 108D2, 1:1000), p70 S6 kinase (Cell Signaling 49D7, 1:1000), pULK1 (S757 Cell Signaling D7O6U, 1:1000), Rictor (cell Signaling 53A2, 1:1000), histone 4 (Lys16) acetylation (H4K16Ac) (Millipore Sigma 07-329, 1:1000), AMPKα (Cell Signaling 2532, 1:1000), and pAMPKa (Thr172 Cell Signaling 40H9, 1:1000). The membranes were then incubated with secondary antibodies (1:10000, goat anti-rabbit or goat anti-mouse IgG HRP conjugate (Bio-Rad) for 1 h and detection was performed using the Immobilon-luminol reagent assay (EMP Millipore).

2.3.22 Immunofluorescence staining

Mouse ESC cells were fixed in 4% paraformaldehyde in PBS for 5 min, permeabilized for 10 min in 0.1% Triton X-100 and blocked for 1 h in 5% serum in PBS. The cells were then incubated in primary antibody overnight at 4 ^{o}C, washed with PBS (2x10 min), incubated with the secondary antibody and stained with 1mg/ml DAPI in 1% serum in PBS for 1 h at 37 ^{o}C, washed (3x5min). Mounting media was composed of 2% of n-propyl gallate in 90% glycerol and 10% PBS. Analysis was done on a Leica TCS-SPE Confocal microscope using a 403 objective and Leica Software. The antibodies used for immunostaining were anti-OCT-4 (Santa Cruz, 1:100), anti-pAMPKα (Thr172 Cell Signaling 40H9, 1:100), anti-ATP synthase β-subunit (Abcam, Ab14730, 1:100) and Alexa 488- or 647-conjugated secondary antibody (Molecular Probes).

2.3.23 Whole-mount immunofluorescence

The zona pellucida was removed from day 3.5 embryos by incubation in acid Tyrode's solution. Embryos were fixed in 4% paraformaldehyde in phosphate-buffered saline (PBS) for 15–20 min at room temperature, rinsed in PBS+0.1% Triton X-100, permeabilized in 0.25% Triton X-100 for 15–20 min, rinsed in PBS+0.1% Triton X-100 and blocked in blocking buffer for at least 1 h at room temperature or overnight at 4 ^{o}C. Blocking buffer was made of PBS supplemented with 10% FBS and 0.1% Triton X-100. The primary antibodies used for immunostaining were anti-RUNX1 (OriGene, TA307515), anti-Oct-4 (Santa Cruz, sc-5279), anti-pAMPKα (Thr172 Cell Signaling 40H9) and anti-LKB1 (Santa Cruz, sc-5638). Primary antibodies were diluted 1:100 in blocking buffer, and embryos were incubated with the appropriate antibodies at 4 ^{o}C overnight. They were rinsed (3x10 min) in blocking buffer and incubated with secondary antibodies for 1 h at room temperature. Alexa Fluor secondary

antibodies (Invitrogen) were used at 1:500 dilution in blocking buffer. Embryos were then incubated in Hoechst 33342 (Invitrogen, 1 mg/mL) for 10 min at room temperature, rinsed (3x10 min) in blocking buffer, and mounted on a 35 mm glass-bottom dish (Mat Tek Corporation, P35G-1.5-14-C) in a PBS droplet overlaid with mineral oil (Sigma). Images were taken with a Nikon A1R confocal microscope (603 water immersion objective) or with a Zeiss LSM 510 Meta confocal microscope (403 water immersion objective). ImageJ 1.44 and NIS-Elements Viewer 3.20 software was used to visualize the data. All embryo images are individual laser confocal sections.

2.3.24 Quantification and statistical analysis

R was used to perform statistical analysis between groups. Transcripts expressed in ICM, dICM or Epi with >1.4-fold change and a p value < 0.05 (adjusted for multiple testing with the Benjamini-Hochberg procedure) were considered to be differentially expressed. Genes with fold change >1.5 and FDR<0.1 were considered differentially expressed. p values < 0.05 were considered significant. PCA plots were generated using the *prcomp* function from R with a $\log_{10}$ transformation of the data and 95% confidence intervals were generated using the Euclidian method. Graphical abstract was created with Biorender.com. ns: $p > 0.05$; *: = $p < 0.05$; **= $p < 0.01$; ***: $p < 0.001$; ****: $p < 0.0001$.

All the statistical details of the experiments and the figures they correspond to can be found in this section. Data are represented as mean + SEM, and Student's t test was used unless specified otherwise. *n* represents number of replicate experiments used in the experiment unless otherwise specified as number of animals in the experiment.

2.3.25 Data and code availability

The accession number for the sequencing data reported in this chapter (and published in

Developmental Cell **52**, 236-250) is NCBI GEO: GSE143494.

2.4 RESULTS

2.4.1 Diapause is associated with a unique transcriptional state

To understand the processes underlying embryonic diapause, we characterized the transcriptional profiles of the cells contributing to the future embryo in pre-implantation (ICM, day 3.5 post- fertilization), post-implantation (Epi, day 6.5), and diapause (dICM, day 8.5– induced on day 2.5 and harvested on day 8.5) mouse embryos using RNA sequencing (RNA-seq) (Figures 2.2A–1C). We identified 12 hallmark pathways significantly enriched in genes upregulated in the diapause state (Figure Appendix A1A), including: TNFα signaling via NF-κB, the p53 pathway, hypoxia, and cholesterol homeostasis (FDR < 0.1). Significantly downregulated pathways in diapause included the late estrogen response pathway (reflecting experimentally induced diapause by estrogen depletion). We further analyzed the transcriptomes by using principal component analysis (PCA) and found three distinct clusters: pre-implantation, post-implantation, and diapause. This defines a robust diapause gene expression signature (Boroviak et al., 2015) (Figures 2.2B and 1C).

Metabolic genes contributed significantly to the 2nd principal component (Figure 2.2B), corresponding to differences between diapause and pre- and post-implantation (Figure 1C). The gluconeogenesis gene, fructose bisphosphatase 2 (*Fbp2*) was significantly downregulated in diapause, and its downregulation is known to promote glycolysis (Li et al., 2013). In contrast, phosphofructo-2-kinase/fructose-2,6-biphosphatase 2 (*Pfkfb2*), which catalyzes the formation of fructose 2,6-bisphosphate (F2,6P$_2$), is upregulated in diapause (Figure 2.2C). F2,6P2 strongly activates glycolysis by activating the key glycolytic enzyme phosphofructokinase-1 (PFK-1) (Hue and Rider, 1987). The significant changes observed in

these rate-limiting enzymes suggest a major change in the regulation of glycolysis as a blastocyst transitions from the pre-implantation to the diapause stage. Furthermore, genes associated with lipid transfer (e.g., cholesterol transfer protein *Stard4*) are also upregulated in diapause. Interestingly, it was recently shown that cholesterol biosynthesis affects intestinal stem cell proliferation (Wang et al., 2018). However, it is not yet understood how cholesterol affects cellular quiescence versus cell division. We further used a hypergeometric test to identify the enrichment of up- and downregulated genes in 64 metabolic pathways of the human metabolic network and found that diapause is characterized by its unique metabolism, including upregulation of glycolysis, upregulation of cholesterol synthesis and uptake (Figure 2.2D), as discussed above.

Another metabolic pathway regulator, solute carrier family 38, member 1 (*Slc38a1*), a sodium-dependent glutamine transporter that affects the mTORC1 pathway (Liu et al., 2017), was significantly upregulated during diapause (Figure 2.2C).

2.4.2 Diapause is associated with a unique transcript splice variant state

In addition to its specific gene expression, we found that diapause has distinct transcript splicing variants (Figure 2.2E). PCA based on transcript splicing rate across RNA-seq samples separated the diapause stage from pre- and post- implantation stages. The fact that both differential splicing and differential gene expression analysis cluster diapause samples separate from pre- and post-implantation samples clearly strengthens the finding that diapause is characterized by a unique transcriptomic state.

Specific examples of alternative splicing events that may be beneficial for diapause can be observed with many transcripts, including *Pitx1*, *Mbd2*, *Tfe3*, and *Lkb1* (Figures 2.2F and Appendix A1A–D). In particular, the short isoform of *Pitx1* (644 bp, 123 amino acids) is expressed in diapause (dICM), while the longer isoform (2,451 bp, 315 amino acids) is only

expressed in pre-implantation ICM. *Pitx1* is a homeobox transcription factor that regulates multiple genes involved in early development and prolactin expression (Quentien et al., 2002). Interestingly, the diapause-specific splice variant is missing the DNA-binding domain possibly rendering the transcription factor unable to activate development. It is therefore plausible that the specific, dominant isoforms play a role in pluripotency during diapause.

2.4.3 Diapause is associated with a LKB1 isoform switch

RNA-seq results identified a dramatic difference in splice variants for the key metabolic kinase, *Lkb1*, between the three developmental stages. A sashimi plot, which visualizes raw RNA-seq reads along splice junctions, was used to examine *Lkb1*-alternative splicing in more detail (Figure 2.2F). We found that exon 9a is expressed in ICM and Epi, but not in dICM. Multiple reads span exon 8 and 9a in pre-implantation ICM supporting the expression of *Lkb1* short (*Lkb1s*) isoform in that stage. On the other hand, in ICM, dICM, and Epi, multiple reads span the junctions between exon 8 to 9b and 9b to 10, supporting the expression of *Lkb1* long (*Lkb1L*) isoform in all these stages (Figure 2.2F). Therefore, the *Lkb1* short isoform is expressed in pre-implantation ICM and post-implantation epiblast (Epi) but not in diapause (dICM). We validated the RNA-seq data with quantitative PCR (qPCR) and found that the *Lkb1L* isoform was present in all stages whereas the *Lkb1s* isoform was present in pre-implantation ICM and post-implantation Epi, but not in diapause (dICM) (Figure 2.2G). We show that LKB1 protein can be detected in mouse blastocyst ICM, both in the pre-implantation and diapause stages (Figure 2.2H).

2.4.4 Starvation induces a diapause-like transcriptional program in pre-implantation ICM-derived mESCs

Since nutritional deprivation is one of the ways embryonic facultative diapause is induced in some animals, we tested the outcome of starvation in mouse pre-implantation ICM-derived

embryonic stem cells (mESCs). We performed RNA-seq on mESCs that were cultured under pre-implantation naïve conditions, with and without overnight starvation (using DMEM that lacks glucose and FBS). Results were analyzed in the context of the transcriptional profiles of ICM, dICM, and Epiblast. We calculated eigenvectors from the PCA in Figure 2.2B and projected the *in vitro* starvation data into the resulting space (Figure 2.3A). Importantly, the RNA-seq analysis revealed that our *in vitro* starvation condition of mESCs produced a gene expression signature, which highly mimics the diapause state and thus can be regarded as an *in vitro* model of the diapause-like state.

To dissect the similarity between diapause and starvation models, we identified all downregulated and upregulated overlapping genes between starved versus non-starved ESCs and diapause versus ICM and analyzed their biological connectivity by STRING- and GO-analysis (Figure Appendix A2A–D). This analysis revealed similar changes in cell-cycle controllers, epigenetic modifiers, metabolic remodeling (e.g., phosphocholine lipases and amino acid transport), and stress response genes both in *in vivo* diapause and starvation models. One of the major differences between the two models, however, is that the *in vivo* diapause ensures efficient free fatty acid accumulation in cells, not only with transporters but also the triglyceride lysis process, while the starvation model expresses fewer genes in these pathways, presumably affecting fatty acid (FA) levels with fewer parallel mechanisms. In summary, using PCA, our transcriptomic data of both diapause and starved pre-implantation mESCs suggest that starved mouse ESCs mimic diapause.

We hypothesized that nutrient starvation might induce this diapause-like state through the LKB1 pathway (Figure 2.3B). We therefore tested whether any known components in the LKB1 pathway affect this diapause-like state. LKB1 is an upstream activating kinase for AMP-

activated protein kinase (AMPK) (Figure Appendix A3). In response to energetic stress, LKB1 can negatively regulate mTOR signaling through LKB1-dependent phosphorylation of AMPK (Shaw et al., 2004). By immunofluorescence we confirmed that phospho-AMPK was observed in diapause ICM (Figure 2.3C). To test the action of phospho-AMPK, phospho-mTOR, and phospho-S6 in starved or stressed pre-implantation ICM-derived ESCs, we cultured mESCs in starvation medium (1h), in 2-Deoxy-D-glucose (2-DG) (10 min), or 5-Aminoimidazole-4-carboxamide ribonucleotide (AICAR) (1h), an analog of adenosine monophosphate (AMP) that stimulates AMPK activity (Figure 2.3D). 2-DG is a synthetic glucose analog that inhibits glycolysis. Upon entering the cell, 2-DG is phosphorylated by hexokinase (HK) and 2-DG-6-P cannot be further metabolized through glycolysis. It accumulates and noncompetitively inhibits HK and competitively inhibits phosphoglucose isomerase (PGI) (Ralser et al., 2008; Kurtoglu et al., 2007; Urakami et al., 2013). We identified significant AMPK activation upon starvation and exposure to AICAR or 2-DG, as indicated by increased AMPK phosphorylation compared to untreated cells (Figure 2.3D). Total AMPK levels were the same across all samples, regardless of culture conditions. The presence of 2-DG resulted in the complete loss of mTOR (Ser^{2448}) phosphorylation but not phosphorylation of S6. Total mTOR and S6 levels remained the same. However, 24 h of starvation resulted in the complete absence of both mTOR and S6 phosphorylation, and lack of the epigenetic mark of transcriptionally active cells, H4K16Ac, as seen previously in the diapause state (Shogren-Knaak et al., 2006; Deng et al., 2013; Bulut-Karslioglu et al., 2016) (Figure 2.3E).

Phosphorylation of Akt(S473) and ULK1(S757) also decreased in starvation compared to control, whereas phosphorylation of 4EBP1 did not change (Figure 2.3E). Immunostaining analysis revealed that starved mESCs maintain the expression of the pluripotency factor OCT4

(Figure 2.3F). These results suggest that under extended nutrient starvation, AMPK is activated, and mTOR and its targets are inactivated in mESCs.

Next, we wanted to address the role of LKB1 in starvation-dependent mTOR inactivation through AMPK. To do this, we determined whether the transient depletion of *Lkb1* in wild- type mESCs would attenuate mTOR dephosphorylation in response to AMPK activation through starvation. *Lkb1*-siRNA was used to transiently knockdown (KD) the expression of *Lkb1* (Figures 2.3G, 2H, and Appendix A2E–H). When the *Lkb1* KD and control cells, transfected with a siRNA targeting luciferase, were starved, control cells showed a significantly larger reduction of mTOR phosphorylation compared to *Lkb1* KD samples (Figure 2.3H). These data suggest that LKB1 is required for starvation-induced mTOR inhibition.

2.4.5 The dormant ESC diapause-like state *in vitro* is reversible

mTOR is a key nutrient sensor and regulator of cell growth and proliferation (Zoncu et al., 2011). Inhibition of mTOR using INK- 128, an inhibitor of both mTOR complexes (Hsieh et al., 2012), induces a diapause-like pluripotent state (Bulut-Karslioglu et al., 2016). Since diapause is a natural process that can be reversed (implantation takes place after exit from diapause), we wanted to determine if the dormancy was also reversible in our *in vitro* models. Using naïve mESCs, we showed that INK-128 inhibits phosphorylation of the downstream substrates of mTORC1/2 (S6 and 4EBP1, Akt Ser^{473}) after 24 h in culture, and it also decreased the epigenetic mark of transcriptionally active cells, H4K16Ac (Figures 2.3I,J). We further showed INK-128 and the starvation-induced diapause-like state are both reversible (Figures 2.4B–D). These two reversible treatments were used as surrogate *in vitro* models to induce the diapause- like state by reversible inactivation of mTOR in naïve mESCs.

2.4.6 LKB1 lacking a regulatory c-terminal domain is constitutively active

We hypothesized that the *Lkb1* isoform switch that we observed in diapause embryos might contribute to the diapause-like metabolic state. We therefore created two mESC lines using Talen-based gene editing: 1. A heterozygous line in which one allele was modified to only express the short isoform of *Lkb1* (SL) and 2. A homozygous line in which both alleles were modified to express only the short isoform of *Lkb1* (SS) (Figures 2.4A and Appendix A3). Like R1(LL), R1(SS) can be used to induce the reversible diapause-like state *in vitro* using both starvation and INK-128 (Figures 2.4B–D).

Interestingly, the phospho-mTOR protein levels in the un- treated and the reversed samples of R1(SS) were reduced 35% and 40%, respectively, when compared to their respective control samples of R1(LL) (Figures 2.4C and D). To test this further, we investigated the phosphorylation state of the LKB1 downstream target, AMPK, using cell lines R1(LL) and R1(SS). We found AMPK was phosphorylated in the presence of 2-DG with either splice variant (Figure 2.4E). However, R1(SS) phosphorylates AMPK even in the absence of 2-DG. This suggests that R1(SS) constitutively activates AMPK. The two corresponding LKB1 proteins have different C-terminal sequences generating a 50 kDa form (*Lkb1L*) and a 48 kDa form (*Lkb1s*) (Denison et al., 2009) (Figure 2.4F). The C-terminal region is proposed to be a site of regulation of this protein (Towler et al., 2008). A previous study suggested that *Lkb1* short has an essential role in spermiogenesis and fertility and that males lacking *Lkb1* short were sterile (Towler et al., 2008). We concluded that in ESCs the differences in mTOR and AMPK activities between *Lkb1* splice variants are due to the fact that the LKB1 kinase without the C-terminal regulatory domain (R1(SS)) was partially constitutively active, even without external cues such as starvation.

2.4.7 LKB1 regulatory c-terminal domain is required for dynamic changes in mitochondrial respiratory activity during the diapause-like state

As described above, our gene expression analysis identified a diapause associated upregulation of glycolytic, pyruvate, and cholesterol metabolic pathways *in vivo* and *in vitro* (Figure 2.2D). Thus, we sought to assess the functional metabolic profile of mESCs cultured in a diapause-like state.

Measurement of oxygen consumption rate (OCR) determines the level of mitochondrial respiration. No differences in OCR in response to FCCP, an uncoupling agent that disrupts mitochondrial membrane potential, were detected in the cell lines with different *Lkb1* splice variants after a 3-h starvation (Figures 2.5A and B). However, after overnight starvation, there was a reduced OCR after FCCP injection in the starved mESC lines with short *Lkb1* R1(SS), compared to R1(LL) (Figures 2.5C and D). These data indicate that mouse ESCs expressing the *Lkb1* long isoform, which is the only isoform that is present in the diapause state, can withstand stress better than mouse ESCs bearing either one or two copies of the *Lkb1* short form and that the stress response is biologically linked to *Lkb1* isoform composition of different cell types.

Using palmitate as a substrate, the level of fatty acid β-oxidation in *Lkb1* splice variants R1(LL), R1(SS), and R1(SL) were tested by performing a palmitate-oxidation assay with the Sea- horse metabolic flux analyzer. Without starvation, the R1(SS) and R1(SL) mESC lines showed higher FA oxidation compared to the wild-type line (Figure 2.5E). However, after overnight starvation, both SS and SL lines exhibited decreased OCR compared to the wild-type R1(LL) (Figure 2.5F). These results indicate that after starvation, mouse ESC lines, R1(SS) and R1(SL), have a lower mitochondrial respiration capacity than R1(LL) and suggests that mouse ESCs with the *Lkb1* short isoform have a compromised stress response.

To better understand the reduced mitochondrial response to starvation (diapause-like state) in the ESC line that was lacking the long form of *Lkb1*, normally seen in diapause, we tested if *Lkb1* short isoform alters mitochondrial mass, with or without starvation. Using FACS analysis after Mitotracker Green stains and qPCR analysis to determine the amount of mitochondrial DNA, we observed no significant changes in mitochondrial mass and amount due to forced expression of the *Lkb1* short isoform (Figures 2.5G and Appendix A4A). These experiments show that the changes we see in Figures 2.5C–F are due to functional and not structural defects. We therefore analyzed the gene expression data under different conditions, and we observed dramatic defects in nutrient-transporters in samples with short form *Lkb1* (SS and SL) compared to controls (R1(LL)) (Figures Appendix A4B–D). The long isoform of *Lkb1* elicited a dynamic increase in nutrient-transporter expression after challenge (starvation), whereas the *Lkb1* short isoform lacked this response (Figure Appendix A4D). These data support and give a mechanistic explanation as to why mESCs with the *Lkb1* short form, R1(SS) do not have the same dynamic mitochondrial activity as control ESCs with a long *Lkb1* form, R1(LL), that can be regulated by multiple signaling pathways.

2.4.8 Diapause-like state *in vitro* has high glycolytic activity, as seen *in vivo*

Based on our RNA-seq results, glycolysis was the most significantly upregulated metabolic pathway in diapause and diapause-like states (Figures 2.2D and 2.3A). We therefore analyzed glycolytic capacity of the cells in the induced diapause-like state. A glycolysis stress test assay was performed to measure the glycolytic function using the Seahorse flux analyzer. We measured extracellular acidification rate (ECAR), which is predominantly the result of the excretion of lactic acid derived from pyruvate that was generated through glycolysis (Wu et al., 2007).

mESCs under starvation or in the presence of INK-128 had a higher glycolytic capacity compared to untreated mESCs (Figures 2.5H and I). The result agreed with the diapause and diapause-like state RNA-seq data that showed upregulation of glycolysis (Figures 2.2D and 2.3A). Using starvation and INK-128, mESCs in a diapause-like state showed higher glycolytic reserve compared to control mESCs (Figures 2.5H and J)

Interestingly, the cells with only *Lkb1* short form without a regulatory C terminus (R1(SS)) had significantly higher glycolytic capacity both in the presence and absence of starvation compared to R1(LL) cells (Figures 2.5H and I). R1(SS) cells also had higher glycolytic reserve compared to R1(LL) cells under no starvation (Figures 2.5H–J). No glycolytic activity changes were detected with INK-128 for both splice variants (Figures 2.5H–J).

To further investigate and find an explanation for the variations between INK-128 and starvation treatments with respect to the glycolytic capacity of *Lkb1* splice variants, we postulated that this was due to the observed differential activation of the LKB1 target, AMPK (Figure 2.4E). We tested this hypothesis by activating AMPK by AICAR in R1(LL) conditions and analyzing the glycolytic capacity of these cells. Interestingly, there was no difference in the glycolytic capacity between the *Lkb1* splice variants under starvation when AICAR was added to the long form of *Lkb1* (Figure 2.5K). Furthermore, we tested if *Lkb1* R1(SS) effect in glycolysis requires AMPK, and show that AMPK inhibition using compound C reduces the starvation-induced glycolysis seen in SS. The results unequivocally show that the induction of glycolysis is AMPK dependent (Figure 2.5L). These data support the finding that *Lkb1* short form is constitutively active and thereby activates the AMPK and glucose uptake more than the regulatable *Lkb1* form.

When AMPK is phosphorylated, it inhibits the mTOR pathway (Inoki et al., 2003; Gwinn

et al., 2008) (Figure 2.3). In addition, AMPK activation causes GLUT4 expression and translocation in skeletal muscles (Holmes et al., 1999; Kurth-Kraczek et al., 1999; Zheng et al., 2001). We observed increased glucose transporter levels in R1(SS) (Figure Appendix 4E), in agreement with constitutive activation of AMPK in the presence of the LKB1 short isoform. INK-128 only inhibits mTOR, whereas activated AMPK can stimulate glucose uptake in addition to inhibiting mTOR. These data suggest that the glycolytic activity differences between the experimental ICM and diapause-like states are due to preferential AMPK activation in the diapause-like state (Figures 2.3B and 2.5M). Similarly, higher glycolytic activity observed in the cell line expressing only the short *Lkb1* isoform may be due to constitutive activation of AMPK observed in this line.

2.4.9 Metabolite analysis of *in vivo* diapause state

We analyzed the metabolome of diapause in *in vivo* embryos to better understand this unique metabolic stage. Three and a half days after mating, the pre-implantation contorl blastocysts were collected while diapause was induced on day 2.5 by tTamoxifen and Depo Provera as previously described (Yoshinaga and Adams, 1966). Diapause embryos were collected five days after diapause induction and both diapause and pre-implantation embryos were flash frozen for metabolite analysis (Figure 2.6A).

We first performed lipidomics to identify the lipid constituents of the diapause and pre-implantation blastocysts. To do this, we harvested the whole embryo with the trophectoderm. We used chemical similarity enrichment analysis (ChemRICH) (Barupal and Fiehn, 2017), a statistical enrichment approach to analyze lipidomic data (Figure 2.6B). In diapause, the major enriched lipid class compared to pre-implantation blastocysts was free fatty acids (FA), which made up about 54% of total lipid content, followed by the main phospholipid

phosphatidylcholine (PC, 26%). FA and PC contents of diapause were much higher than in pre-implantation blastocyst (16% and 11%, respectively) (Figures 2.6B, C, Appendix A5A,B). In diapause, triacylglycerol (TAG) and acyl carnitine (AC) constituted 14% and 1% of total lipid contents, respectively, significantly lower than those of pre-implantation blastocysts (38% and 29%, respectively) (Figures 2.6B and C). Phosphatidylethanolamine (PE), sphingomyelin (SM), ceramide (Cer), lysophosphatidylcholine (LPC), and diacylglycerol (DAG) constituted about 0.4%–3% of total lipids in both diapause and pre-implantation stages (Figures Appendix A5C–G). The high level of acylcarnitines in pre-implantation blastocysts suggests increased fatty acid transport into the mitochondria for β-oxidation. In contrast, the high abundance of fatty acids in diapause suggests an increased synthesis and/or decreased β-oxidation in diapause blastocyst.

We observed multiple categories of fatty acids in diapause and pre-implantation blastocysts: saturated fatty acids (SFAs), mono-unsaturated fatty acids (MUFAs), and poly-unsaturated fatty acids (PUFAs) (Figures Appendix A5H and A5I). MUFAs and PUFAs were enriched in diapause in the free fatty acid pool. Interestingly, high levels of PUFAs are shown to be important for the prolonged survival of *Caenorhabditis elegans* dauer larva (Lam et al., 2017). This suggests that PUFAs might also be important for the survival of mouse embryos in diapause. SFAs were also highly enriched in diapause (Figures Appendix A5H and A5I). Interestingly, it has been reported that in cancer, when the cells are under hypoxia, there is a build-up of saturated fatty acid, similar to diapause (Ackerman et al., 2018). Furthermore, since long chain SFAs are known to induce inflammation (Yang et al., 2015; Lancaster et al., 2018) and might activate NF-κB (Yang et al., 2015), it is possible that SFAs that accumulate in diapause are stimulating NF-κB, and thereby survival of the diapause embryo. Interestingly, a recent work has shown that inflammatory NF-κB can induce stem cell quiescence (Chen et al.,

2019).

In addition to lipidomic analysis, we measured polar metabolites in diapause and pre-implantation blastocysts using hydrophilic interaction chromatography (HILIC) and gas chromatography (GC) with accurate mass tandem mass spectrometry. These analyses identified 234 polar metabolites in the early embryos (Figures 2.6E and F). Using statistical analysis, we found multiple highly differential metabolites in these two stages, including AMP, serine, indoxyl sulfate, fructose-1-phosphate, and ergothioneine (ET; a scavenger of hydroxyl radicals (Franzoni et al., 2006)), in addition to leucine degradation intermediates such as 3-hydroxyisovaleroly carnitine (Figures 2.6E and F). AMP among metabolites that were up in diapause corroborates the gene expression data, and further supports AMPK activation during diapause (Figure Appendix A4F). Since serine can be generated by serine synthesis pathway from glycolysis (de Koning et al., 2003), serine upregulation in diapause may in part be due to high glycolysis at this stage. Furthermore, since indoxyl sulfate has been shown to activate NF-κB through reactive oxygen species (ROS), followed by expression of p53 that suppresses cell proliferation (Shimizu et al., 2011), its upregulation in diapause may be involved in halting the cell cycle observed in diapause.

The dramatic upregulation of fatty acids seen in diapause may be partly due to serine-derived lipid metabolism (Gao et al., 2018) (Figures 2.6C–E). A recent study found that serine levels were critical to avoid mitochondrial fragmentation by regulating ceramide and sphingomyelin metabolism and sphingolipid synthesis (Gao et al., 2018). We found intermediate lipid metabolites derived from serine were enriched in diapause and the enzyme that generates free fatty acids from ceramide, N-acylsphingosine amidohydrolase 1 (ASAH1), was significantly upregulated (Figure 2.6E).

Fatty acid synthesis may also be upregulated in diapause since the enzymes that generate free fatty acids from acetate and acetyl-CoA, acyl-CoA synthetase short (ACSS1), and fatty acid synthase (FASN), respectively, were significantly upregulated in the diapause state. A previous study suggested that acetyl-CoA can enhance acetylation levels of histones at FASN promoters, a positive feed-forward regulation to upregulate FASN expression (Gao et al., 2016). Furthermore, a dramatic downregulation of TAG and DAG were observed in diapause, suggesting a release of free fatty acids from their breakdown (Figures 2.6C and E).

One of the ways free fatty acids can be utilized in diapause is to incorporate them into highly enriched phosphatidylcholines (PCs). Accumulation of PCs can stimulate phosphatidylcholine phospholipase C (PC-PLC), which is significantly upregulated in diapause (Figure 2.6E). Previous studies suggest that PCs play a critical role in NF-κB activation (Kouba et al., 2001). We show that TNFα signaling via NF-κB pathway is upregulated in diapause (Figures 5E and Appendix A1A). These data suggest that PCs in diapause may aid in cell survival through the NF-κB pathway (Vuong et al., 2015; Schütze et al., 1992; Zamorano et al., 2003).

We previously found that the metabolic enzyme NNMT and its substrate, S-Adenosyl methionine (SAM), can regulate human pre- and post-implantation pluripotency *in vitro* by regulating histone methylation (Sperber et al., 2015). Interestingly, compounds that indicate SAM utilization beyond histone methylation (e.g., 1-MNA) are upregulated in diapause suggesting that epigenetic modifications may be differentially regulated in diapause.

Polar metabolite analysis revealed differential regulation of one-carbon metabolism between pre-implantation and diapause embryos (Figure 2.6F). In the diapause state, high serine may be used to generate SAM since serine can donate one-carbon unit to support the synthesis of

methionine (Maddocks et al., 2016). SAM furthermore acts as a methyl donor since accumulation of SAH and 1MNA are observed (Figure 2.6F). Interestingly, SAH was not used downstream in the pathway, indicated by low levels of the downstream metabolites and the enzymes involved in the process (Figure 2.6E). Since previous studies suggest that upregulation of SAH activates the NF-κB pathway, it is plausible that the NF-κB activation in diapause is partly affected by high SAH levels (Barroso et al., 2016). Cystine levels were moderately elevated possibly due to autophagy (Lee et al., 2011) (diapause upregulation of genes involved in autophagy, *Gpnmb*, *Ulk2*, *Uvrag*, *Gabarapl1*,and *Wipi1*) (Li et al., 2010; Tsuyuki et al., 2014) and serine increase in diapause. High hypotaurine and taurine levels suggest that cysteine is utilized to generate metabolites with antioxidant activities in diapause. The enrichment of antioxidants indicates the importance of preventing these dormant cells from potential oxidation (Figure Appendix A5J).

2.4.10 Lipolysis in diapause-like state and in *Rictor* KO

We observed a significant decrease of TAGs and DAGs and an increase in fatty acid levels in diapause compared to the pre-implantation state, consistent with increased lipolysis in diapause (Figure 2.7A). Interestingly, lipolysis has previously been connected with mTOR inhibition and starvation adaptation (Cai et al., 2016; Tao et al., 2016). We therefore proceeded to analyze the lipidomics profile in *Lkb1* splice variants in starved versus non- starved mESCs (Figures 2.7B and Appendix A6). Our data show that starved mESCs have an increase of lipolysis as seen by TAG and DAG depletion (Figure 2.7B). Interestingly, PUFAs are highly enriched in R1(SS) splice variant in free fatty acid pool (Figure Appendix A6H). To test if mTORC2 inhibition in mESCs increases lipolysis, we generated mESC *Rictor* KO clones and analyzed their lipidomic profile (Figures 2.7D–F and Appendix A6). *Rictor* KO mESCs were

generated using the CRISPR-Cas9 system (Figures 2.7C and D). As expected, *Rictor* KO clones do not express RICTOR protein and do not phosphorylate AKT(S473). In addition, mTORC2 also affects mTORC1 activity in mESCs, as seen by decrease of mTOR, S6, and S6K phosphorylation (Figure 2.7E). Rictor KO mutants show upregulation of lipolysis as seen by the reduced levels of TAGs (Figure 2.7F). Upregulation of lipolysis was therefore observed in diapause, diapause-like state, and Rictor KO mESCs, suggesting that mTOR inhibition is causal for lipolysis in diapause (Figure 2.7).

2.4.11 Inhibition of the glutamine transporter SLC38A1 blocks the mTOR-dependent diapause state

Amino acid transporters are essential for a variety of cellular processes such as nutrient uptake and energy metabolism (McGivan and Pastor-Anglada, 1994). They are also required for activation of mTORC1. SLC38A1 mediates the saturable, pH-sensitive, and electrogenic cotransport of glutamine and sodium ions. Previous studies have shown that glutamine is an essential and rate-limiting sensitizing factor that enables essential amino acids (EAAs) and growth factors to regulate mTOR in different tissues (Jewell et al., 2015; Altman et al., 2016). *Slc38a1* was highly upregulated in our diapause and diapause-like state gene expression data (Figures 2.2C, 2.8A, Appendix A7A, and A7B). We hypothesized that upregulation of the glutamine transporter SLC38A1 is required for the diapause state. We tested this hypothesis by inducing diapause and treating the diapause embryos with a glutamine transporter inhibitor, L-γ-glutamyl-p-nitroanilide (GPNA) (Figures 2.8B and C). The drug is not amenable to *in vivo* studies of diapause. Hence, to address this question, we utilized *ex vivo* assays for blastocysts. We induced diapause *in vivo* and tested the blastocyst diapause with and without the glutamine transporter inhibitor using epigenetic state as an endpoint assay (H4K16Ac). We show with

GPNA treatments that mouse embryos require glutamine transporters for diapause (Figures 2.8B and C).

We also designed gRNAs for mouse *Slc38a1* and *Slc38a2* to test their function in the diapause stage. We electroporated mouse zygotes with *Slc38a1/2* guides using the CRISPR/Cas9 system and tested for potential mutations and function. Both *Slc38a1* and *Slc38a2* are upregulated in diapause state. These proteins (and other SNAT glutamine transporters) most likely act in a redundant manner, making KO experiments complicated. However, we made a small number of mutations with both *Slc38a1* and *Slc38a2* and cultured them to blastocyst (about 4 days) and induced a diapause-like state using INK-128. We showed that mutations in these glutamine transporters are detrimental for functional diapause (Figures Appendix A7C–F).

2.5 DISCUSSION

Future treatments that enable control of entry into and exit from quiescence in aging stem cells, or cancer stem cells should significantly improve modern medicine. However, the regulation of quiescence in any stem cell stage or type is poorly understood. We have identified regulators of an *in vivo* quiescent stage, embryonic diapause, the environmentally inducible suspended stage in development and have generated an *in vitro* diapause-like model for further dissecting the process. With these new tools, we have shown that downregulation of mTOR by starvation-induced LKB1-AMPK activation is necessary for the induction of a diapause-like state and that glutamine transporter SLC38A1 primes for mTOR-dependent exit from the quiescence. Forced expression of a non-diapause *Lkb1* splice variant results in a constitutive diapause-like state due to a phospho-AMPK dependent increase in glucose transporters and decrease in mTOR activation. These data also explain why amino acid composition in uterine fluid is critical for diapause regulation (Renfree and Fenelon, 2017). The glutamine transporter

Slc38a1 is essential for the diapause state. These data show that amino acid composition and *Lkb1* splice variant regulate mTOR-dependent diapause metabolic and epigenetic state (Figure 2.8D). Since metabolism has recently been shown to be a critical determinant of cellular fate, it is likely to play a role in quiescence and may also contribute to the epigenetic state of the diapause stage (Sperber et al., 2015; Mathieu and Ruohola-Baker, 2017). These studies set the stage to better understand how cells communicate to synchronize this enigmatic, reversibly paused embryonic diapause stage (Figure 2.8D).

Diapause ICM, in contrast to ICM, has upregulated PFKPB2 levels catalyzing the formation of F2,6P2 that activates the key glycolytic enzyme PFK-1. Similarly, a diapause-like state has high glycolytic activity and *Lkb1* splice variants affect this glycolytic activity. These data have revealed a metabolic state for dormant ESCs. While previous studies showed a transcriptome profile of diapause that is associated with downregulation of metabolism (Renfree and Fenelon, 2017), the present study reveals a significant increase in a critical metabolic pathway, glycolysis. Since diapause is a cell cycle and growth dormant stage, an unanswered question is why diapause requires such a high glycolytic rate.

The present study suggests that the short *Lkb1* splice variant is eliminated in normal diapause since the short protein is not regulated as it is the wild-type long *Lkb1*. *Lkb1* short codes for a protein that has a C-terminal sequence lacking potentially critical regulation sites, a phosphorylation site (serine 431 in mouse) and a farnesylation site (cysteine 433 in mouse) (Denison et al., 2009). It is possible that these sites are involved in differential regulation and/or localization of the two forms of LKB1 protein (Towler et al., 2008). LKB1-based activation of AMPK under energetic stress has multiple beneficial metabolic effects. However, having a constitutive activation of AMPK by an LKB1 short splice variant leads to a chronic, low-level

activation of AMPK, and this can have an adverse metabolic consequence in embryonic diapause in the long-term. Constant activation of AMPK was found to cause obesity and diminishes B-cell function in mice while similar phenotype and increased adiposity were observed in humans bearing a mutation that leads to chronic activation of AMPK (Yavari et al., 2016).

The molecular mechanisms for regulation of the signaling pathways that control diapause are not well understood. In our studies, we observed high expression levels of genes involved with leucine degradation, high levels of leucine degradation metabolites and high levels of glutamine transporters in diapause. Pharmacological inhibition of the glutamine transporter SLC38A1 blocked the diapause-like state, consistent with the hypothesis that amino acid glutamine levels are critical regulators of mTOR activity and thereby the diapause state (Gonzalez et al., 2012; Jewell et al., 2015). We propose that the regulated high glutamine levels inhibit mTOR and thereby allow the blastocyst diapause state.

Taken together, this study has revealed that diapause and starvation-induced diapause-like cells have highly upregulated glycolytic activity, similar to that observed in cancer cells. We have also shown critical regulators of the mTOR pathway as the gateway to entry and exit from diapause. Starvation induces LKB1/AMP/AMPK-dependent repression of the mTOR pathway and thereby entry into diapause, while glutamine transporters are required for the diapause state. Stem cells and cancer stem cells share the capacity of controlled entry to and exit from a dormant state. Examples of abnormal control of these quiescent states include loss of regeneration due to aging and recurrence of cancer after remission. With the onset of aging, stem cells lose the ability to re-enter the cell cycle in order to regenerate tissues after injury (Artoni et al., 2017), while aggressive cancer cells with stem cell properties can enter quiescence and become resistant to conventional chemotherapy by withdrawing from the cell cycle. In our study, we identified

candidate regulators of diapause. Future studies will shed light on the functional roles of these regulators in stem cell quiescence, in both normal and pathological conditions.

2.6 ACKNOWLEDGMENTS AND FUNDING

We thank members of the Ruohola-Baker laboratory for helpful discussions throughout this work. We thank Logeshwaran Somasundaram, Ammar Alghadeer, and Alex Karin Fischer for technical help. We thank the Transgenic Resource Program and Lynn & Mike Garvey Imaging Core at the University of Washington. This work is supported by the ISCRM Fellows Program Award for A.M.H., ISCRM Innovation Pilot Award for J.M., support from the Hahn family and grants from the National Institute of Health R01GM097372, R01GM97372-03S1, and R01GM083867 for H.R.-B. and 1P01GM081619 for C.B.W. and H.R.-B.

2.7 FIGURES

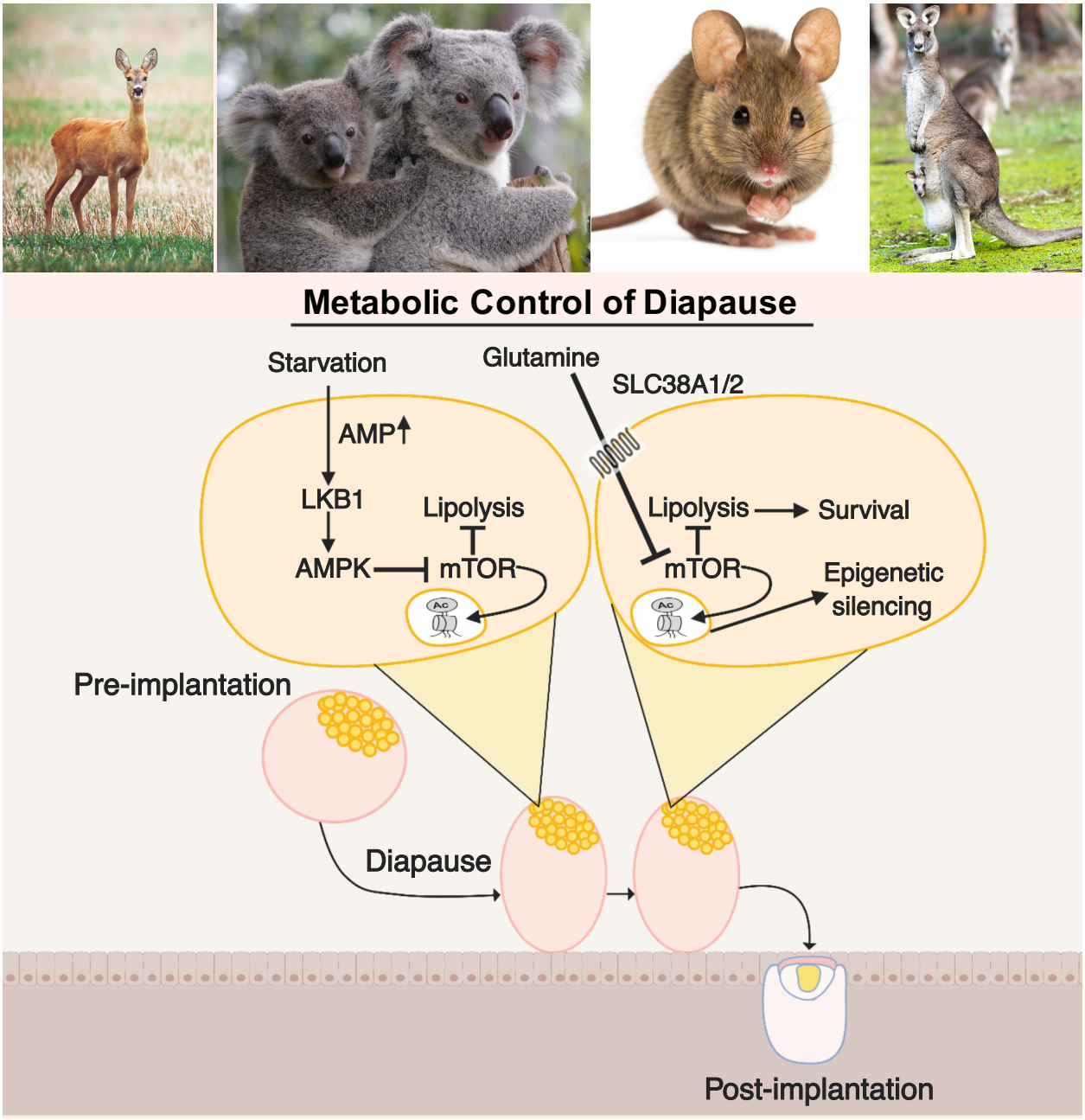

Figure 2.1: Graphical abstract briefly highlighting main findings of chapter 2. Diapause is associated with increased lipolysis and glutamine transporter expression. Upregulation of lipolysis in diapause is associated with downregulation of mTORC2. Starvation results in a diapause-like state, enriched in glutamine transporters. During starvation, mTOR is

repressed through LKB1-AMPK, inducing a reversible metabolically active but epigenetically silenced embryonic diapause-like state that upregulates expression of the glutamine transporters SLC38A1/2. These transporters are required for the H4K16ac-negative, diapause state because their inhibition leads to exit from the diapause epigenetic state.

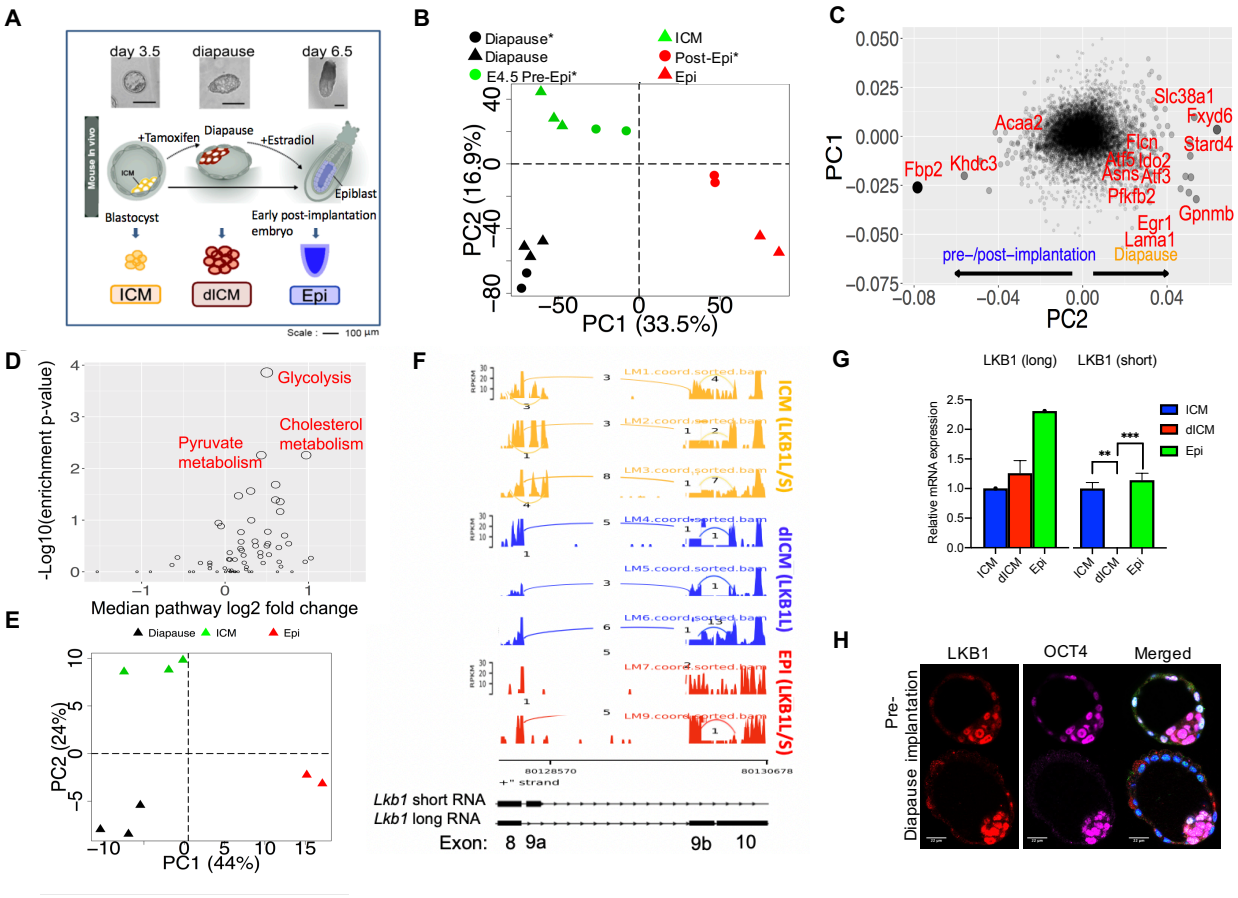

Figure 2.2: Gene Expression and Splice Variants Separate Diapause Stage from ICM and Post-implantation Stages.

(A) Schematic diagram depicting outline of the experiment. (B) PCA of our RNA-seq data showed that diapause is in a distinct transcriptional state compared to pre- and post-implantation epiblasts. (* = Boroviak et al., 2015) (C) Scatter plot of gene contributions to PC1 and PC2 in the PCA plot (in B) showing genes that are specifically up- or down-regulated in diapause compared to pre-/post-implantation. (D) Metabolic pathway enrichment of genes differentially expressed between diapause and ICM. (E) PCA plot using transcript splicing rate of our RNA-sequence samples clearly separates diapause and pre-/post-implantation samples. (F) Sashimi plot of *Lkb1* exons 8–10. Bar height represents expression level (FPKM). Arcs connect two exons that are spliced together. (G) qPCR analysis of *Lkb1* splice variant expression in ICM, dICM, and

epiblast. n = 2 for each group, p = 0.001965 for ICM versus dICM, and p = 0.000102 for dICM versus Epi. (H) Immunostaining of pre-implantation and diapause embryos with antibodies against both LKB1 isoforms (*red)*, OCT4 (*magenta*), or stained with DAPI (blue). Scale: 22 μm. ** indicates $p<0.001$ and *** indicates $p<0.0001$.

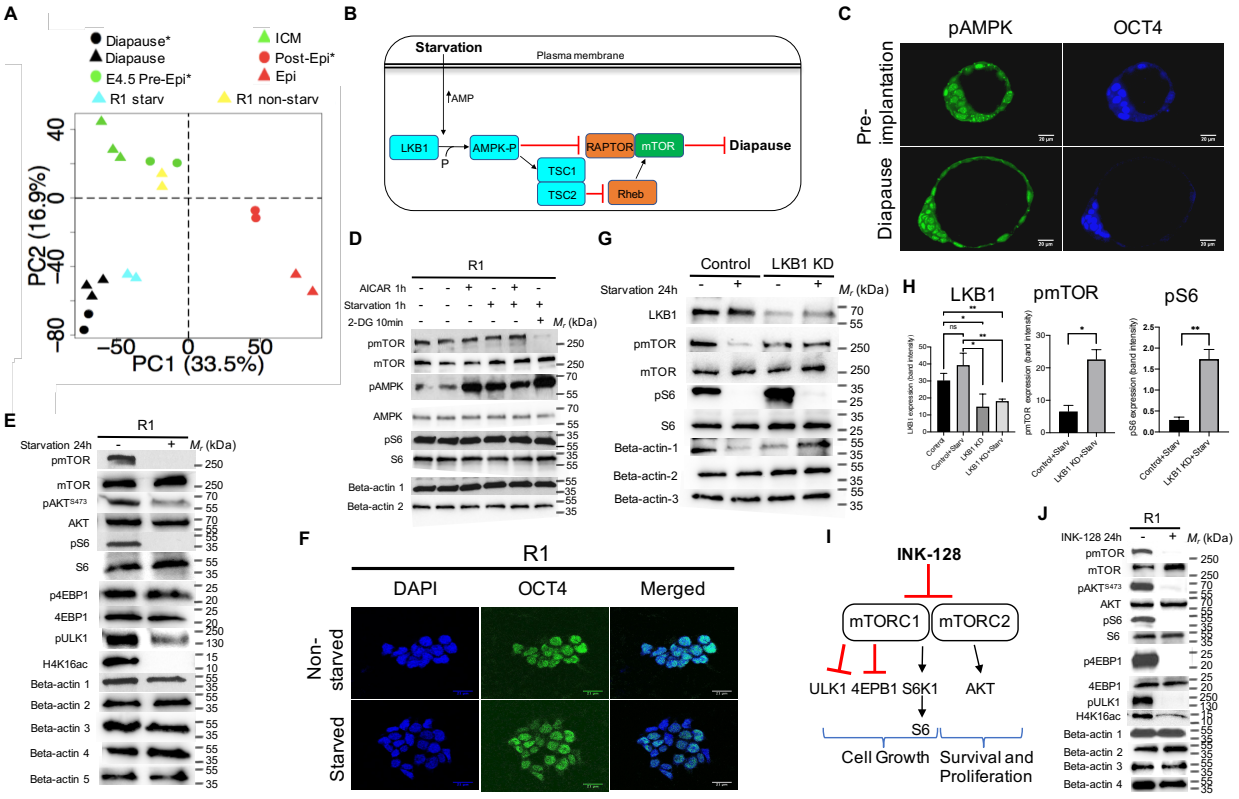

Figure 2.3: LKB1 Activation by Starvation Induces Diapause-like State.

(A) Starvation moved mESC samples (R1/*Lkb1*) toward a diapause state. Cell line samples are projected in the PCA of *in vivo* samples using a previously described method (Kho et al., 2004).* = Boroviak et al., 2015. (B) Model of LKB1 and starvation. AMPK is activated by starvation and is a target of LKB1. Activated AMPK inhibits mTOR and induces diapause. (C) Immunostaining of day 3.5 and diapause embryos with an antibody against pAMPKa2(Thr172) (*green*) and OCT4 (*blue*). Scale: 20 μm. (D) 1-h exposure to AICAR, starvation, or 2-DG (10 min) increased the activity of AMPK compared to untreated cells. β-actin 1: pmTOR, pAMPK and pS6; β- actin 2: mTOR, AMPK and S6. (E) Phosphorylation of mTOR, Akt(S473), S6, ULK1(S757), and acetylation of H4K16 in R1(LL) cells decreased after 24 h in starvation, whereas p4EBP1 did not change. β-actin 1, pmTOR and pS6; β-actin 2, mTOR and S6; β-actin 3, H4K16ac; β-actin 4, pAkt(S473) and p4EBP1; β-actin 5, Akt. (F) Immunostaining of mouse ESCs with or without

starvation. Staining was performed to detect the pluripotent marker, OCT4 (green). The nuclei of all cells were stained blue with DAPI. Scale: 21 μm. (G) *Lkb1* siRNAs effectively knocks down expression of LKB1 at the protein level compared to the control luciferase siRNA. The efficiency of the transient siRNA approach was assessed at the protein level by western blotting coupled with densitometry for LKB1, mTOR, and S6 in transiently transfected R1(LL) cells. (H) mTOR, and S6 phosphorylation were significantly reduced (KD) in the luciferase siRNA control under starvation compared to LKB1 siRNA under starvation. β-actin 1: LKB1 and pmTOR; β-actin 2: pS6; β-actin 3: mTOR and S6. n = 3 for pmTOR, p = 0.010 for control versus KD; n = 3 for pS6, p = 0.0039 for control versus KD; n = 3 for LKB1, p = 0.035 for control versus KD, p = 0.0068 for control+starved versus KD+starved, p = 0.0081 for control versus KD+starved, p = 0.014 for control+starved versus KD. (I) A simplified diagram of the mTOR signaling pathway and mTOR Complexes 1 and 2 inhibitor, INK-128. See text for details. (J) Phosphorylation of mTOR, Akt(S473), S6, 4EBP1, ULK1(S757), and acetylation of H4K16 in R1(LL) cells decreased after INK-128 treatment for 24h. β-actin 1: pmTOR, pAkt(S473), pS6, and p4EBP1, β-actin 2: mTOR, S6, and 4EBP1, β-actin 3: Akt, β-actin 4: pULK1 and H4K16ac.

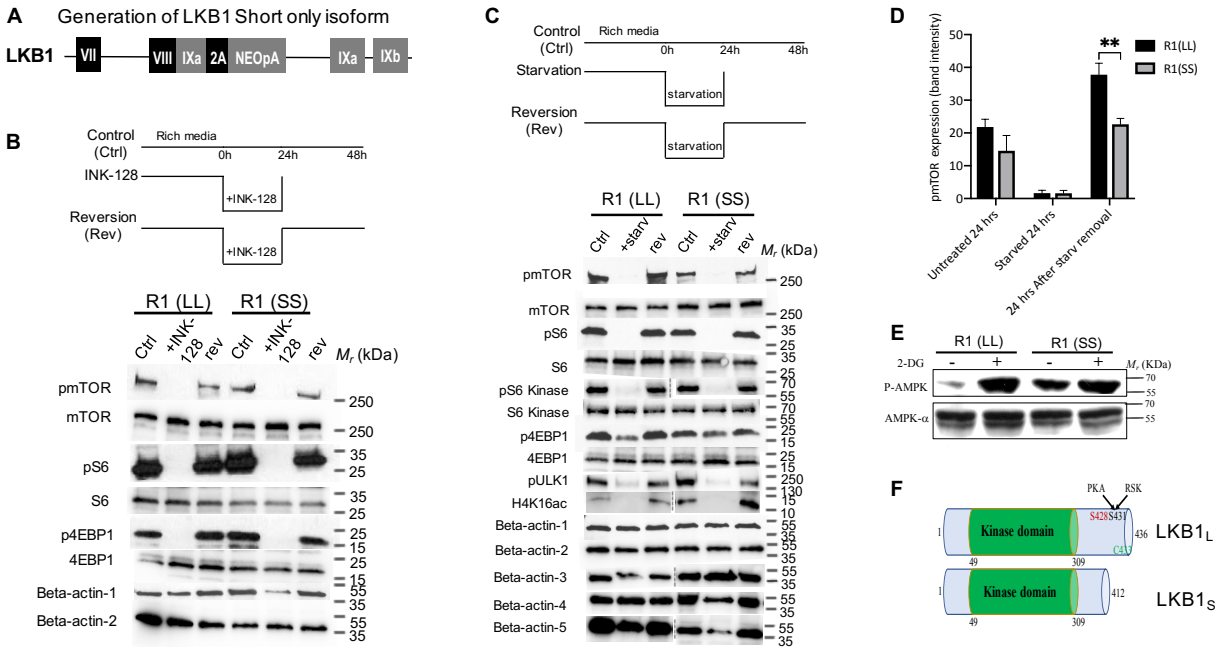

Figure 2.4: Reversible Diapause-like State Can Be Induced In Vitro by Starvation or Inhibition of mTOR.

(A) Generation of LKB1 short only isoform. A schematic of Talen-mediated gene editing of the endogenous *Lkb1* locus using donor construct that expresses LKB1-short form-specific exon 9A (Figure 1F) fused directly in frame with exon 8 followed by a 2A peptide. This modified LKB1 locus expresses only the short form of LKB1. (B and C) Pharmacological inhibition of mTOR and starvation can induce a reversible diapause-like state. (B) mTOR inhibition by INK-128 is reversible as indicated by the rephosphorylation of mTOR, S6 and 4EBP1 24 h after removal of INK-128 in R1(LL) and R1(SS) cells. β-actin 1: pmTOR, pS6 and p4EBP1, β-actin 2: mTOR, S6 and 4EBP1. (C) Starvation abolishes phosphorylation of mTOR and its substrates, S6 kinase, S6, ULK1, and 4EBP1 in 24 h. This inhibition is reversible as indicated by the rephosphorylation of those proteins 24 h after removal of starvation medium from culture both in R1(LL) and R1(SS) cells. Intriguingly, the mTOR signal in the untreated and the reversed R1(SS) samples is reduced compared to their respective R1(LL) samples. β-actin 1: pmTOR, pS6 and p4EBP1, β-

actin 2: mTOR, S6 kinase, S6 and 4EBP1, β-actin 3: pS6 kinase, β-actin 4: pULK1, β-actin 5: H4K16ac. (D) Quantification of pmTOR protein bands from C using ImageJ software. n = 3 for each sample, p = 0.0027 for R1(LL) versus R1(SS) 24h after starvation removal. (E) Western blot of pAMPK in mESCs expressing different forms of LKB1 splice variants. The phosphorylation of AMPK is increased in response to 2DG both in R1(LL) and R1(SS). However, higher levels of AMPK phosphorylation are observed in R1(SS) even in the absence of 2-DG. (F) A schematic representation of the two splice forms of LKB1. ** indicates $p<0.001$.

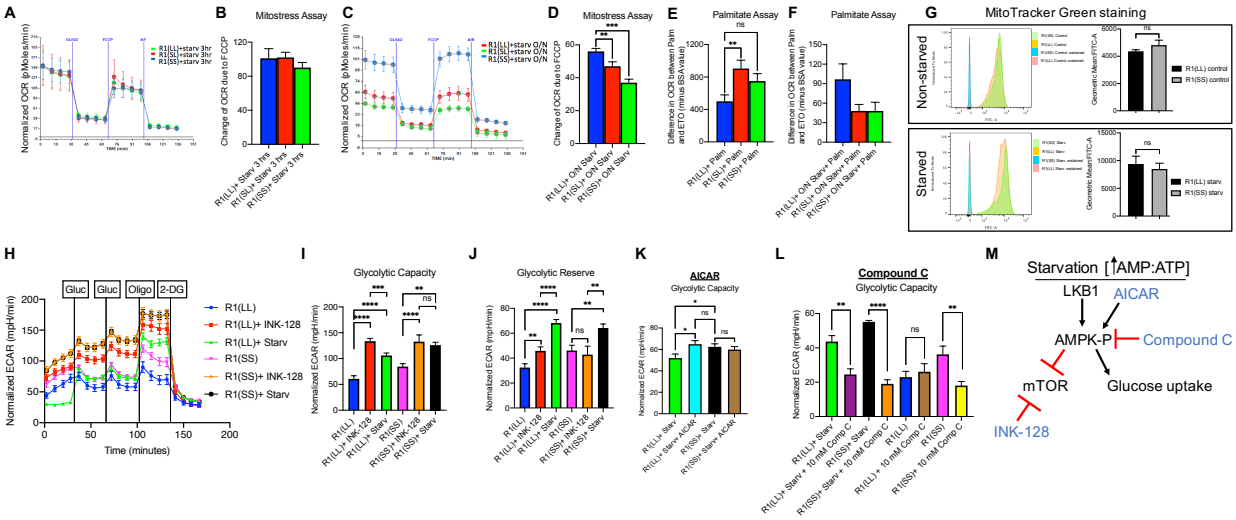

Figure 2.5: LKB1Short Does Not Respond Dynamically to Starvation, and Diapause-like State Cells Have Higher Glycolytic Activity Compared to Control Metabolic Flux in Mouse ESCs with Different LKB1 Splice Variants.

(A–F) Short *Lkb1* does not respond dynamically to starvation. Metabolic flux of mouse ESCs with different *Lkb1* splice variants using a Seahorse analyzer. (A) Representative trace of OCR changes is shown under a MitoStress protocol. (B) Quantification of A (4 independent experiments). (C) Representative trace of OCR changes of mouse ESCs with R1(SS) or R1(SL) lines have reduced OCR changes in response to FCCP compared to R1(LL). (D) Quantification of C (4 independent experiments). n = 28 per group, p = 0.0076 R1(LL) versus R1(SL), p < 0.0001 R1(LL) versus R1(SS). Mouse ESC lines with the short *Lkb1* splice variant cannot respond dynamically to stress. (E) mESCs with *Lkb1* short splice variant show high mitochondrial β-oxidation when substrate, fatty acid palmitate (Palm) is offered for oxidation in normal conditions. n = 7 per group, p = 0.0088 R1(LL) versus R1(SL), p = 0.062 R1(LL) versus R1(SS). (F) The mESC lines with *Lkb1* SL and SS splice variants show lower fatty acid β-oxidation levels than R1(LL, blue). n = 7 per group, p = 0.073 R1(LL) versus R1(SL). (G) MitoTracker Green staining of R1(LL) and R1(SS). No change in mitochondrial mass was

detected between R1(LL) and R1(SS) in normal or starvation conditions. (H) Representative trace of ECAR changes in response to glucose, oligomycin, and 2-DG is shown under a glucose stress protocol. (I and J) Using starvation and INK-128, naïve mESCs, R1(LL), and R1(SS), under starvation or INK-128, have higher glycolytic capacity (I) and glycolytic reserve (J) compared to naïve mESCs under normal conditions. (I) n = 12 for R1(LL) and R1(SS), n = 9 for R1(LL)+INK-128, n = 15 for R1(LL)+starv, n = 22 for R1(SS)+starv, n = 8 for R1(SS)+INK-128, $p < 0.0001$ for R1(LL) versus R1(LL)+INK-128, $p < 0.0001$ for R(LL) versus R1(LL)+starved, $p < 0.0007$ for R1(LL)+starved versus R1(LL)+INK-128, $p < 0.0026$ for R1(SS) versus R1(SS)+INK-128, $p < 0.0001$ for R1(SS) versus R1(SS)+starv, $p = 0.0088$ for R1(LL) versus R1(SS), $p = 0.0109$ for R1(LL)+starved versus R1(SS)+starved. (J) n values are the same as Figure 2.5I. $p = 0.0063$ for R1(LL) versus R1(LL)+INK-128, $p < 0.0001$ for R(LL) versus R1(LL)+starved, $p < 0.0001$ for R1(LL)+starved versus R1(LL)+INK-128, $p = 0.0022$ for R1(SS) versus R1(SS)+starved, $p = 0.0030$ for R1(SS)+starved versus R1(SS)+INK-128, $p = 0.0176$ for R1(LL) versus R1(SS). (K) No glycolytic capacity differences were observed between R1(LL) and R1(SS) under starvation when AICAR is added to R1(LL). n = 11 for R1(LL)+starved, n = 12 for the rest, $p = 0.537$ for R1(LL)+starved+AICAR versus R1(SS)+starved, $p = 0.0171$ for R1(LL)+starved versus R1(LL)+starved+AICAR, $p = 0.5267$ for R1(SS)+starved versus R1(SS)+AICAR, $p = 0.0350$ for R1(LL)+starved versus R1(SS)+starved. (L) Compound C, an inhibitor of AMPK, reduces the glycolytic capacity observed under starvation for both LKB1 splice variants. n = 4 for R1(SS), n = 5 for R1(LL) and R1(LL)+10 mM compound C, rest, n = 6. $p = 0.0027$ for R1(LL)+starved versus R1(LL)+starved+10 mM compound C, $p < 0.0001$ for R1(SS)+starved versus R1(SS)+starv+10 mM compound C, $p = 0.5978$ for R1(LL) versus R1(LL)+10 mM compound C, $p = 0.0056$ for R1(SS) versus

R1(SS)+10 mM compound C. (M) Model of AMPK pathway. AMPK, once phosphorylated by LKB1, can stimulate glucose uptake and inhibit mTOR while INK-128 inhibits mTOR. ns: not significant. * indicates $p<0.05$, ** indicates $p<0.001$, *** and **** indicates $p<0.0001$

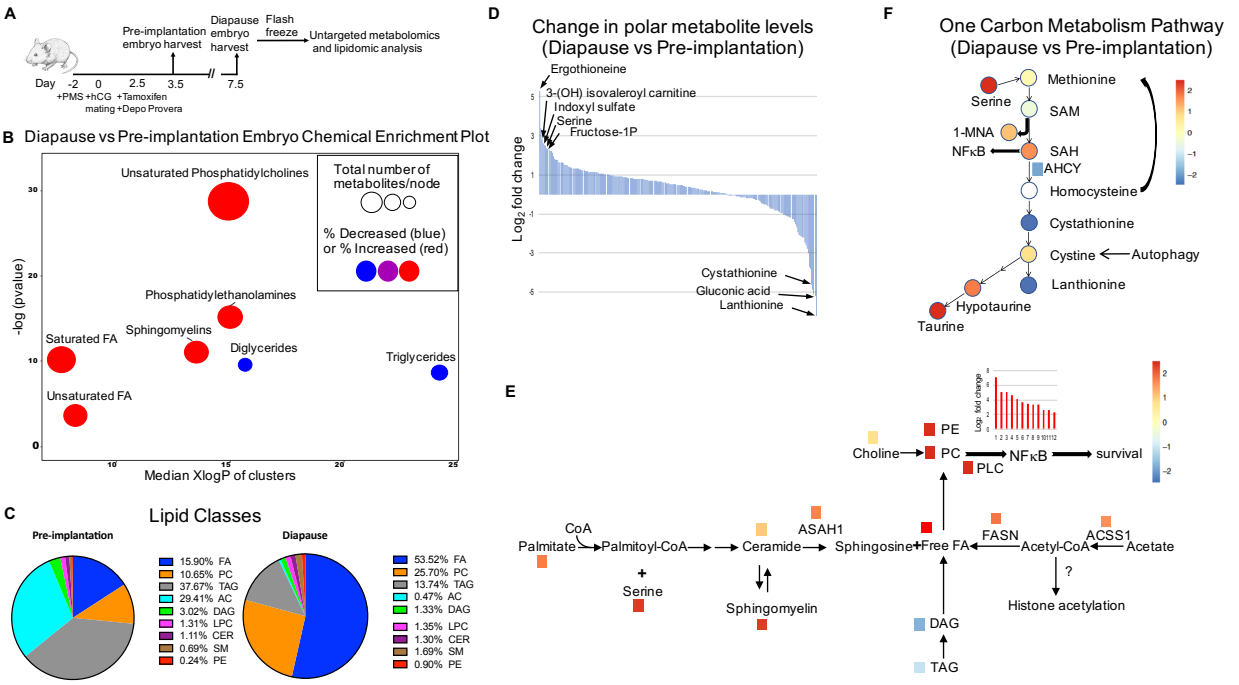

Figure 2.6: Overall Changes of Lipids and Polar Metabolites between Diapause and Pre-implantation Blastocyst.

(A) Schematic diagram depicting outline of the metabolomics experiment for pre-implantation or diapause embryos. (B) Chemical enrichment analysis of diapause blastocyst compared to pre-implantation blastocyst show dramatic differences in lipid composition. Node size reflects the number of metabolites and color indicates direction of change, blue is decreased and red increased. The Y axis indicates enrichment p values calculated by the Kolmogorov-Smirnov-test and the X axis shows the polarity of chemical clusters. (C) Relative lipid classes between diapause and pre-implantation blastocyst. (D) Log2 fold change of a total of 243 polar metabolites that were identified between diapause and pre-implantation blastocysts. (E) Schematic diagram of sphingolipid metabolism showing metabolites and genes that are upregulated in diapause compared to pre-implantation. D, diapause; PI, pre-implantation; TAG, Triacylglycerol; DAG, Diacylglycerol; ASAH1, N-acylsphingosine amidohydrolase 1; ACSS1, acyl-CoA synthetase short-chain family member 1; FASN, fatty acid synthase. (F) One-carbon

metabolism pathway indicating metabolites that are increased or decreased and their connections with other pathways.

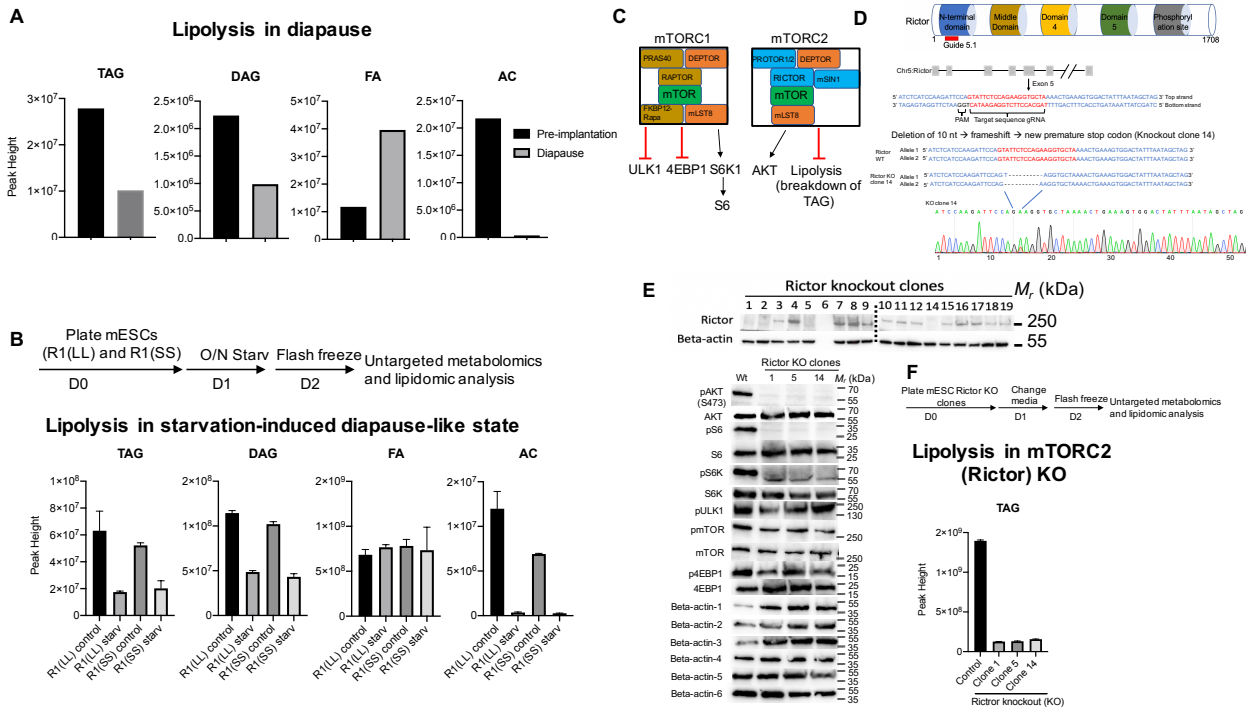

Figure 2.7: Lipolysis Is Upregulated in Embryonic Diapause, in Diapause-like State, and in Rictor Knockout mESCs.

(A) Abundance of TAG, DAG, FA, and AC in pre-implantation and diapause blastocyst. (B) Schematic diagram depicting outline of the LKB1 splice variant metabolomics experiment and abundance of TAG, DAG, FA, and AC in LKB1 splice variants, R1(LL) and R1(SS), under control and starvation conditions. (C) A simplified diagram of the mTOR signaling pathway, showing components, and downstream targets of mTORC1/2. (D) Schematic diagram of the CRISPR-Cas9 system–mediated homozygous Rictor (mTORC2 specific component) KO in mESCs. Sequence and chromatogram (homozygote) of Rictor KO clone 14 mESCs. (E) Screening of Rictor KO clones (top panel) by western blotting and analysis of Rictor knockout effect on mTOR and its downstream targets (bottom panel). (β-actin-1: pAkt and pmTOR, β-actin-2: pS6 Kinase and pS6, β-actin-3: Akt, S6 and 4EBP1, β-actin-4: mTOR, β-actin-5: pULK1 and p4EBP1, β-actin-6: S6 Kinase). (F) Schematic diagram depicting outline of the

Rictor KO metabolomics experiment and Rictor KO effect on lipolysis. TAGs are downregulated in Rictor knockout clones compared to wildtype.

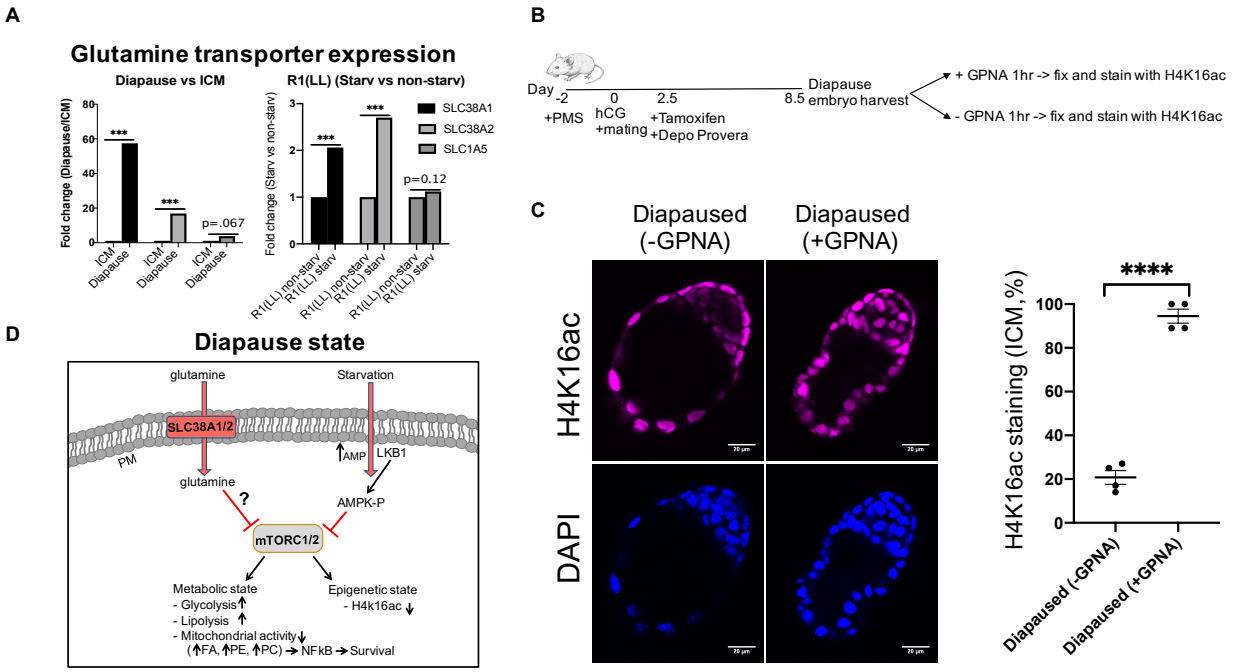

Figure 2.8: Inhibition of the Glutamine Transporters Leads to Exit from Diapause.

(A) Glutamine transporters, *Slc38a1*, *Slc38a2*, and *Slc1a5* are upregulated in diapause and starvation-induced diapause-like state. (B) Schematic diagram depicting outline of the glutamine transporter inhibition in mouse diapause embryos. (C) Immunostaining of diapause embryos with or without GPNA treatment (1h) for the H4K16ac mark (*magenta)*, and DAPI (*blue*). n = 4 diapaused embryos per treatment, $p < 0.0001$ for diapaused embryos versus diapaused embryo+10 mM GPNA. Scale: 20 mm. (D) Hypothetical model of mouse embryos in diapause state. Pre-implantation embryos enter the diapause state through LKB1-AMPK dependent downregulation of mTOR. Diapause is associated with upregulation of SLC38A1/2 and glycolysis, low mitochondrial activity, low fatty acid β-oxidation (FAO), increased NF-κB activity, and downregulation of mTOR. Downregulation of mTOR leads to upregulation of lipolysis, resulting in breakdown of TAGs. Glutamine transporters (*Slc38a1/2*) are required for diapause state, plausibly through prolonged mTOR inhibition. PM, plasma membrane.

CHAPTER 3

THE HISTONE METHYLTRANSFERASE GENE SUV420H2 IS REQUIRED FOR THE NAÏVE-TO-PRIMED TRANSITION OF HESCS, AND ITS MUTATION RESULTS METABOLIC REMODELING OF HESCS

3.1 ABSTRACT

Organismal health requires continuous regeneration. However, the mechanisms that govern the regenerative competence still remain unclear. The cells that are refractory for regenerative aging, pluripotent stem cells have the capacity to remain in a pluripotent stage either by culture conditions in vitro or by diapause conditions in vivo. We have previously identified metabolic differences that regulate the ESC epigenetic state. Here we define a novel epigenetic regulator during the implantation stage, SUV420H2. Our screen for early ESC regulators revealed SUV4020H2 as a critical component in naïve to primed transition. Using the CRISPR/Cas9 system, we generated SUV420H2 mutant naïve hESC line to study its role in the pre- and post-implantation embryonic stages. We show that SUV420H2 mutants do not enter in vitro diapause, but instead continue dividing. By immunoblotting, we also show mutant cells have higher levels of H4K16ac as well as increased rates of proliferation. These data suggest that mechanistically H4K20me3 repressive marks in key target genes are a pre-requisite for the diapause stage. Furthermore, our functional metabolic assays show that SUV420H2 mutant cells have an increased levels of fatty acid β-oxidation and increased mitochondrial respiration and glycolysis compared to wildtype, suggesting SUV420H2 as a potential metabolic inhibitor. We conclude that increased OXPHOS and glycolytic metabolism might be due to blocking the inhibitory effect of SUV420H2 on PPAR-γ. The data reveal the mechanism for SUV20H2 requirement during naïve to primed embryonic transition. The epigenetic repression by H4K20me3 marks is a pre-requisite for the potential diapause and metabolic reprogramming that takes place during the naïve to primed transition.

3.2 INTRODUCTION

Organismal health requires continuous regeneration. However, the mechanisms that govern the regenerative competence still remain unclear. Pluripotent stem cells have the potential to generate a whole organism, and multiple ESC states have been identified and stabilized both in mouse and human early embryos (Brons et al., 2007; Tesar et al., 2007; Nichols and Smith, 2009; Chan et al., 2013; Gafni et al., 2013; Takashima et al., 2014; Theunissen et al., 2014; Ware et al., 2014; Wu et al., 2015). However, today it is not fully understood how pluripotent states transition between naïve to primed and how they exit from pluripotent states.

H4K20 methylation marks are evolutionarily conserved from yeast (*S. pombe*) to humans (Lachner et al., 2004), and have diverse cellular functions such as heterochromatin formation, gene regulation, transcriptional repression (Karachentsev et al., 2005), genome stability (Schotta et al., 2008; Oda et al., 2009), DNA replication (Vermeulen et al., 2010) and DNA damage repair (Botuyan et al., 2006; Schotta et al., 2008). Histone 4 lysine 20 (H4K20) can be mono, di-, or tri-methylated by the histone methyltransferases SETD8 (KMT5A) (Nishioka et al., 2002), SUV420H1(KMT5B) and SUV420H2 (KMT5C) respectively (Schotta et al., 2008; Sanders et al., 2004). Both H4K20me2 and H4K20me3 were shown to cause chromatin compaction and gene repression (Schotta et al., 2004; Schotta et al., 2008; Hahn et al., 2013). H4K20me3 is an epigenetic modification to the DNA packaging protein H4. It is a mark that indicates the tri-methylation at the 20^{th} lysine residue of histone H4 protein, a mark that causes transcriptional repression of associated genes (Kourmouli et al., 2004; Schotta et al., 2004, 2008).

Embryonic expression of SUV420H2 is characterized by maternally inherited transcripts in the zygote and decreased expression by the two-cell stage in mice, corresponding with lack of H4K20me3 (Eid et al., 2016). Ectopic expression of SUV420H2 results in an increase of

H4K20me3 in both the zygote and two-cell stage, causing lower developmental rate attributed to a delayed entrance into S phase (Eid et al., 2016).

A recent study has shown that SUV420H2 affects metabolism through peroxisome proliferator activated receptor gamma (PPAR-γ) (Pedrotti et al., 2019). PPAR-γ is a master transcriptional regulator of glycemic metabolism, adipogenesis and lipid biosynthesis (Soccio et al. 2017; Lapa et al. 2017). SUV420H2 knockout mice display higher mitochondrial respiration and higher toleration of glucose than in WT mice (Pedrotti et al. 2019). RNA-seq of the KO mice showed enrichment in genes for oxidative phosphorylation metabolism and mitochondrial function.

To understand the differences between ESCs states, we performed a whole genome CRISPR screen to identify genes that are essential in the transition of naïve (pre-implantation) to primed (post-implantation) ESCs (Mathieu et al., 2019). Using this functional screen, we uncovered novel regulators of naïve-to-primed transitions and in a secondary screen, we validated genes from different classes that are required for the transition. The CRISPR screen identified genes that regulate human primed pluripotent stem cells (Mathieu et al., 2019; Chia et al., 2010) as well as many novel regulators, including GREB1, FLCN, MAP2K7, NELL2, GPR161, GPI, and SUV420H2. These known and novel potential regulators of the exit from the naïve state are involved in chromatin remodeling, metabolic switching, and signaling. We chose to further study the role of SUV420H2, a histone methyltransferase, and its mechanism of action in naïve to primed transition of human ESCs. *Suv420h1* knockout and *Suv420h1/2* double knockout mice are perinatally lethal (Schotta et al., 2008). Previous studies have shown that tri-methylation of H4K20 by SUV420H2 repressed the recruitment of the histone acetyltransferase MOF, which acetylates histone 4 lysine 16 (H4K16ac), causing RNA pol II pausing (Kapoor-

Vazirani et al., 2011).

3.3 MATERIALS AND METHODS

3.3.1 hESC Culture

Naïve hESCs [Elf-1 (NIH_hESC Registry #0156) were cultured as previously described (Sperber et al., 2014; Ware et al., 2014; Theunissen et al., 2016; Ferreccio et al., 2019). Briefly, cells were grown on a feeder layer of irradiated primary mouse embryonic fibroblasts (MEF) in naïve hESC media (2iL-I-F). 2iL-I-F media consisted of DMEM/F-12 media supplemented with 20% knockout serum replacer (KSR), 0.1 mM nonessential amino acids (NEAA), 1 mM sodium pyruvate, penicillin/streptomycin (all from Invitrogen, Carlsbad, CA), 0.1 mM β-mercaptoethanol (Sigma-Aldrich, St. Louis, MO), 1 μM GSK3 inhibitor (CHIR99021, Selleckchem), 1 μM of MEK inhibitor (PD0325901, Selleckchem), 10 ng/mL human LIF (Chemicon), 5 ng/mL IGF1 (Peprotech) and 10 ng/mL bFGF. Cells were passaged using 0.05% Trypsin-EDTA (Life Technologies). Cells were transferred to matrigel-coated plates prior to molecular analysis. Exit from the naïve state was achieved by culturing the cells in either mTeSR1 media (StemCell Technologies) or primed FGF hESC media (DMEM/F-12 media supplemented with 20% KSR, 0.1 mM NEAA, 1 mM sodium pyruvate, penicillin/streptomycin, 0.1 mM β-mercaptoethanol, and 10 ng/mL bFGF) on matrigel-coated plates. All cells were cultured at 5% O_2 and 5% CO_2 between passage p20 and p40.

3.3.2 Generation of CRISPR mutant lines

SUV420H2 mutants were generated in naïve hESC (Elf1 2iL-I-F) using CRISPR/Cas9. Guides were ordered through Synthego and cells were transfected with 40 nM of gRNA using Lipofectamine RNAiMAX (Life Technologies). Three days later, cells were dissociated into single cells and replated onto MEF-coated plates or collected for DNA analysis (pool). In the

next passage, single colonies from MEF- coated plates were randomly selected and amplified. The molecular characterization of the mutant lines and their phenotype were analyzed between passage 33 and 40 using controls with matching passage number. Genomic DNA was extracted using DNAzol reagent (Invitrogen) according to the manufacturer's instructions and quantified using Nanodrop ND-1000. Genomic regions flanking the CRISPR target sites were PCR amplified with the designed primers and sent for Sanger sequencing.

3.3.3 Secondary CRISPR screen

Newly generated naïve hESC (Elf1 2iL-I-F) SUV420H2 CRISPR KO were pushed to exit the naïve pluripotent state by switching their media to mTeSR1. Four days later, cells were treated with methotrexate (1 μM) and acetaldehyde (1 mM) for three additional days to selectively kill primed pluripotent state and hESCs exiting the naïve pluripotent state. Number of surviving cells was then assessed using NucleoCounter NC-200 (ChemoMetec).

3.3.4 SUV420H2 and mTORC1/2 chemical inhibition

SUV420H2 activity was inhibited in hESC Elf1 by treatment with A-196 (24 hours, 10 μM; Medchem). Dimethyl sulfoxide (DMSO) treatment was used as a vehicle control. mTORC1/2 activity was inhibited in hESC Elf1 wildtype and SUV420H2 knockout cells by treatment with INK-128 (100 nM-1 μM; Medchem).

3.3.5 Protein Extraction and Western Blots Analysis

For protein analysis,$1x10^5$ cells were plated on 35 mm plates coated with Matrigel. To harvest cells were lysed directly on the plate with a lysis buffer containing 20 mM Tris-HCl pH 7.5, 150 mM NaCl, 15% glycerol, 1% Triton x-100, 1 M ß-glycerolphosphate, 0.5 M NaF, 0.1 M sodium pyrophosphate, orthovanadate, PMSF, and 2% sodium dodecyl sulfate (SDS). Twenty-

five units of Benzonase® Nuclease (EMD Chemicals, Gibbstown, NJ) was added to the lysis buffer right before use. The protein samples were combined with the 4× Laemmli sample buffer, heated (95°C, 5 min), and run on SDS-PAGE (protean TGX pre-casted 4–20% gradient gel; Bio-rad) and transferred to the nitrocellulose membrane (Bio-Rad) by semi-dry transfer (Bio-Rad). Membranes were blocked for 1 h with 5% milk or 5% BSA (for antibodies detecting phosphorylated proteins), and incubated in the primary antibodies overnight at 4°C. The antibodies used for western blot were β-actin (Cell Signaling 4970 (1:10000), phospho-mTOR (Ser 2448) (Cell Signaling 5536, 1:1000), mTOR (Cell Signaling 2972, 1:1000), pS6 (Cell Signaling 2215, 1:1000), S6 (Cell Signaling 2117, 1:1000), histone 4 (Lys16) acetylation (H4K16Ac) (Millipore Sigma 07-329, 1:1000), pAkt(S473) (Cell Signaling 9271, 1:1000), pAkt(T308) (Cell Signaling 9275, 1:1000), Akt (Cell Signaling 9272, 1:1000); Histone 4 (Lys20) trimethylation (H4K20me3) (D84D2) (Cell Signaling 5737, 1:1000), OCT4 (Santa Cruz sc-5279, 1:500), KLF4 (Abcam ab129473, 1:1000), and NANOG (D73G4) (Cell Signaling 4903, 1:1000). The membranes were then incubated with secondary antibodies (1:10000, goat anti-rabbit or goat anti-mouse IgG HRP conjugate (Bio-Rad) for 1 hour and detection was performed using the Immobilon-luminol reagent assay (EMP Millipore).

3.3.6 OCR and ECAR Measurement Using Seahorse Cellular Flux Assays

Human ESCs (Elf1 2-I-L-IF wildtype and SUV420H2 KO clones) were seeded onto 96-well Seahorse plates at $2x10^4$ cells/well. Cells were cultured in DMEM with or without glucose, depending on starvation criteria, overnight. For SUV420H2 inhibition, cells were treated with A-196 overnight (10 μM, Medchem). Culture media were exchanged for base media (unbuffered DMEM (Sigma D5030) supplemented with sodium pyruvate (Gibco, 1mM) and with 25-mM glucose (for Mitostress assay), or 25-mM glucose and 50mM carnitine (for palmitate assay), 1 h

prior to the assay. For the glycolysis stress assay, DMEM base media were not supplemented with. Substrates and selective inhibitors were injected during the measurements to achieve final concentrations of glucose (2.5mM), 4-(trifluoromethoxy) phenylhydrazone (FCCP, 300nM–500nM), oligomycin (2.5 mM), antimycin (2.5mM), rotenone (2.5mM), palmitate (50mM in BSA), BSA and ETO (50mM). The OCR and ECAR values were normalized to the number of cells present in each well, quantified by the Hoechst staining (HO33342; Sigma-Aldrich). Changes in OCR and ECAR in response to addition of substrates and inhibitors were defined as the maximal change after the chemical injection compared to the last OCR or ECAR value before the injection. Glycolytic capacity is a measure of the maximum rate of conversion of glucose to lactate after using oligomycin to inhibit ATP synthase in the electron transport chain (ETC) and thus block generation of ATP. Measurements of ECAR before and after 2-DG addition is a readout of the maximum glycolytic capacity of the cell. Glycolytic reserve is a measure of ECAR differences before and after oligomycin and indicates the ability of a cell to respond to an energetic demand.

3.3.7 Statistical analysis

All data are presented as the mean of $n \geq 3$ experiments with the standard error of the mean (SEM) indicated by error bars, unless otherwise indicated. Statistical significance was determined using Student's t-test. Only p values of 0.05 or lower were considered statistically significant ($p > 0.05$ [ns, not significant], $p \leq 0.05$ [$*$], $p \leq 0.01$ [$**$], $p \leq 0.001$ [$***$], $p \leq 0.0001$ [$****$]). Data were compiled and analyzed with Excel for Mac (2020; Microsoft, Seattle, WA, USA).

3.4 RESULTS

3.4.1 SUV420H2 is not required to maintain the naïve pluripotent state

We investigated the role of SUV420H2 in human pluripotency by generating a SUV420H2 KO line in naïve human ESC (Elf1) using guide RNA targeting SUV420H2 (Fig. 1A-C). The guide RNA located in exon 3 created InDel mutations, introducing a STOP codon in three different mutant lines (Figure 1C and Supplementary Figure 1A). Western blot analysis shows that SUV420H2 KO naïve hESC (2iL-I-F) clones 35, 36 and 37, resulted in almost a complete loss of H4K20me3 expression, which is a target of SUV420H2 (Figure 1D and Supplementary Figure 1B-C). We tested whether SUV420H2 knockout clones can transition from a naïve to primed stage of hESCs. We performed a naïve pluripotency state exit assay (Figure 1E), allowing cells to exit the naïve state and selectively eliminating the primed state with methotrexate/acetaldehyde (M/A), which negatively selects primed hESCs (Sperber et al., 2015; Mathieu et al., 2019) (Figure 1F). SUV420H2 KO cells were not negatively selected by M/A treatment, whereas the number of wildtype naïve cells were significantly reduced in the exit assay. This further confirms that SUV420H2 knockout cells are not able to transition from naïve to primed hESCs. SUV420H2 mutation did not affect expression of the pluripotency markers, OCT4, KLF4 and NANOG (Supplementary Figure 1D-F). These data suggest that SUV420H2 is not required to maintain the naïve pluripotent state of human ESCs.

3.4.2 SUV420H2 mutation is associated with an increased proliferation

Since SUV420H2 knockout cells are not able to become primed cells, we asked whether they correspond to an intermediate stage between the pre-implantation and post-implantation stages. Embryonic diapause is known to be an intermediate stage, when embryos in more than 130 mammalian species do not implant (Fenelon et al., 2014), but remain in a suspended, reversible state (Hussein et al., 2020; Bulut-Karslioglu et al., 2016; Scognamiglio et al., 2016). We therefore tested whether SUV4202H KO hESCs can enter a diapause-like state (Figure 2A),

which can be induced in vitro by starvation (Hussein et al., 2016) or through pharmacological inhibition of mTOR (Bulut-Karslioglu et al., 2016; Hussein et al., 2020; Sousa et al., 2020). We found both WT naïve hESCs and SUV420H2 KO cells are able to go into a diapause-like state and reversibly come out based on the downregulation of mTOR and its downstream targets, pAKT and pS6, as well as the epigenetic marker H4K16ac (Figure 2B). Surprisingly, the H4K16 acetylation levels of the untreated sample were higher in SUV420H2 KO cells compared to the WT. We reasoned this increase in H4K16ac was due to inhibition of H4K20me3 by SUV420H2. We used A-196 (Bromberg et al., 2017), to inhibit SUV420H2 in both WT naïve hESCs and SUV420H2 KO cells (Supplementary Figure 1G). Upon 24-hour treatment with A-196 , followed by western blot analysis, we saw a strong band of H4K16ac only in the knockout cells (Figure 2C). This increase of H4K16Ac in the knockout cells was also associated with a significant increase in PCNA, a marker for proliferation (Figure 2C-D). Furthermore, an increase in proliferation was also evident upon culturing knockout cells in a dish and counting them 48, 72 and 96 hours after they were plated (Figure 2E). Loss of H4K20me3 genome wide has been observed in many types of human cancers (Fraga et al., 2005). Down-regulation of H4K20me3 and SUV420H2 has also been shown to contribute to migration and invasion of breast cancer cells (Wu et al., 2019) however, this invasion can be hindered by ectopic overexpression of SUV420H2 (Yokoyama et al., 2014). Our findings suggest mutating SUV420H2 and loss of H4K20me3 is associated with an increase in uncontrollable cell proliferation, consistent with previous findings in cancer studies were SUV420H2 was consistently mutated.

3.4.3 SUV420H2 knockout hESCs have higher mitochondrial respiration, increased glycolytic activity and increased fatty acid β-oxidation

Naïve-to-primed hESC transition involves an important metabolic switch from naïve cells being bivalent – using both OXPHOS and glycolysis, to primed cells which mainly depend on glycolysis and have a decreased mitochondrial respiration (Zhou et al., 2012). As primed cells exit the pluripotent state, mitochondrial respiration of differentiated cells increases (Zhou et al., 2012 Mathieu and Ruohola-Baker, 2017). We tested if SUV420H2 plays a role in metabolic regulation and whether SUV420H2 KO in hESCs shifts or changes the metabolic state observed in naïve hESCs. To do this, we performed functional analysis in live cells using the Seahorse extracellular flux analyzer as done before (Zhou et al., 2012; Mathieu et al., 2014; Sperber et al., 2015, Miklas et al., 2019; Hussein et al., 2020). We performed a glycolysis stress test assay to measure and analyze the glycolytic activities of WT naïve hESCs and *SUV420H2* KO clones 35, 36 and 37 (Figure 3B-E). We observed an increased glycolytic capacity, glycolytic reserve and glycolysis in the knockout cells compared to WT naïve hESCs. We also performed a mitostress test assay to measure maximum oxygen consumption rate (OCR) to determine the level of mitochondrial respiration. We found the knockout clones have higher maximum OCR than the WT cells when we measure their maximal respiration, basal respiration as well their ATP production (Figure 3F-I and Supplementary Figure 2). This is consistent, with previous findings that show naïve cells use both OXSPHOS and glycolysis, whereas primed cells exclusively rely upon glycolysis (Zhou et al., 2012; Sperber et al., 2015). Finally, we used palmitate as a substrate and performed a palmitate-oxidation assay to measure the levels of fatty acid β-oxidation. We found, overall, mutation to SUV420H2 led to an increase of fatty acid oxygen consumption compared to WT cells (Figure 3J). These data indicate that disruption of SUV420H2 increases their metabolic activities compared to naïve hESCs.

The increased levels of mitochondrial respiration seen in the SUV420H2 KO phenotype can be replicated in wildtype Elf1 cells in the presence of a SUV420H2 inhibitor, A-196. Elf1 cells treated with A-196 overnight have significantly increased basal OCR, maximal respiration, and ATP production compared to untreated Elf1 cells (Supplementary Figure 3A-C). Additionally, A-196 treated Elf1 cells have the same OCR levels compared to untreated SUV420H2 KO cells (Supplementary Figure 3A-C). These data suggest that the increase in mitochondrial respiration is due to knocking out or inhibiting SUV420H2.

3.5 DISCUSSION

Interestingly, previous studies in other cell types have shown that tri-methylation of H4K20 by the methyltransferase, SUV420H2, repressed the recruitment of the histone acetyltransferase MOF, which acetylates H4K16, causing RNA pol II pausing (Kapoor-Vazirani et al., 2011). Our data showing increased proliferation when SUV420H2 is mutated is consistent with de-repression of hMOF. Recent work has also shown that SUV420H2 might play a role in metabolism through its novel target, PPAR-γ, as SUV420H2 KO in mice led to upregulation of PPAR-γ related genes (Pedrotti et al., 2019). These upregulated genes were involved in oxidative metabolism, mitochondrial function and genes that are essential for fatty acid β-oxidation (Pedrotti et al. 2019). It is plausible that SUV420H2 is essential for regulating metabolism of naïve hESCs through PPAR-γ ,therefor knocking out SUV420H2 will increase mitochondrial oxidative phosphorylation and fatty acid β-oxidation observed in naïve hESCs. The metabolic remodeling observed in SUV420H2 KO cells might be due to removing the inhibitory influence of SUV420H2 towards PPAR-γ. However, further studies will be needed to establish a role for PPAR-γ with respect to the metabolic changes associated with SUV420H2 mutations. Currently, we are testing any potential metabolic role that PPAR-γ might be playing by generating PPAR-γ

mutant lines in both wildtype cells and the SUV420H2 KO cells, creating double knockout (SUV420H2 and PPAR-γ).

3.6 FIGURES

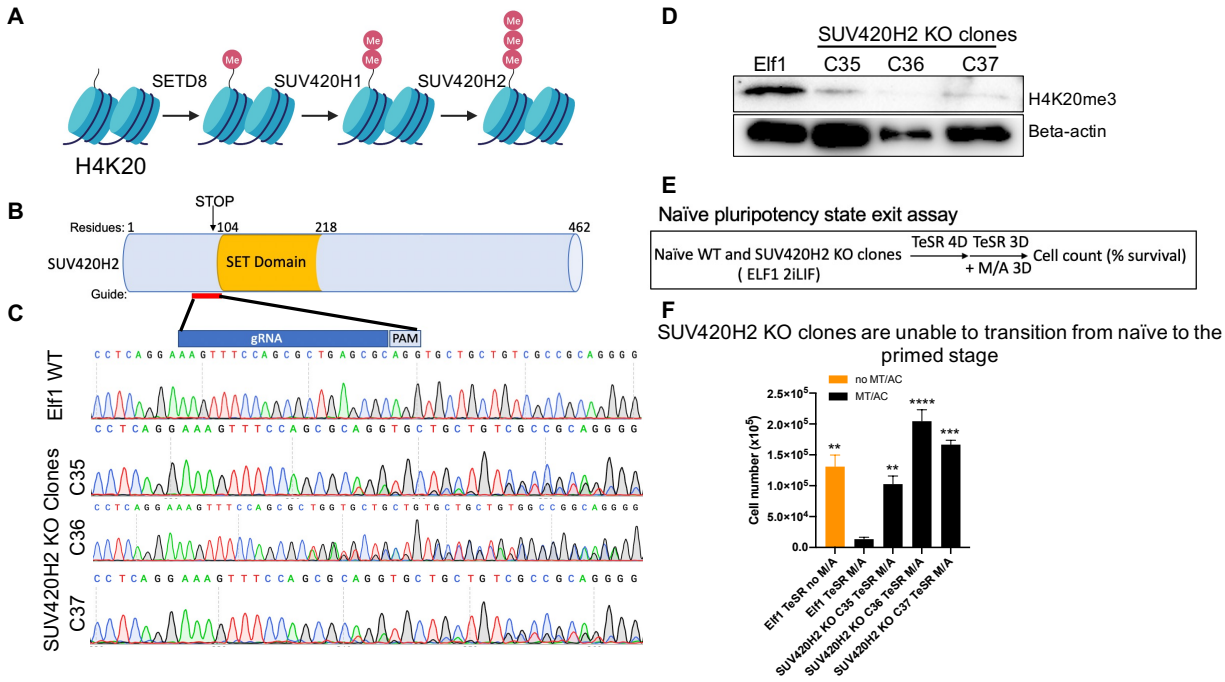

Figure 3.1: CRISPR-Cas9 screen reveals SUV420H2 as an essential gene during the exit from the naïve pluripotent state.

(A) The methyltransferase SUV420H2 is responsible for di- and trimethylation of H4K20me. (B) Schematic representation of SUV420H2 protein showing the catalytic set domain and location of CRISPR guide RNA used. (C) Sanger sequencing analysis of hESCs Elf1 SUV420H2 KO clones 35, 36 and 37 reveal introduction of a STOP codon in exon 3. (D) Western blot showing almost complete reduction of SUV420H2 target H4K20me3 in the mutant clones. (E) Secondary screen. Schematic of the naïve pluripotent state exit assay. (F) SUV420H2 wildtype and KO clones were induced to exit the naïve state in TeSR medium. The number of surviving cells after 3 days of methotrexate/acethaldehyde (M/A) was counted. S.e.m.; *: = $p < 0.05$; **= $p < 0.01$; ***: $p < 0.001$; ****: $p < 0.0001$; two-tailed t-test, n = 3 biological replicates.

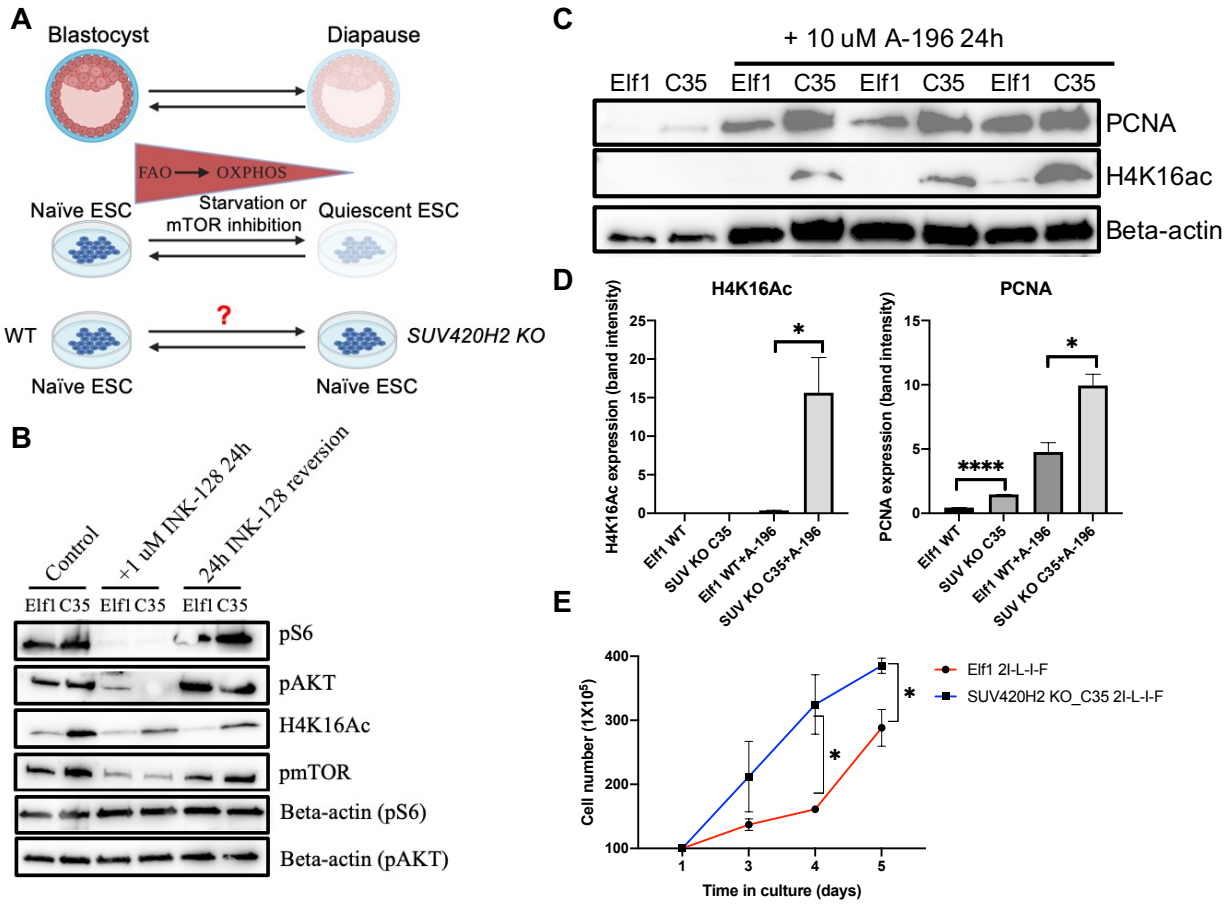

Figure 3.2: SUV420H2 KO hESCs have an increased proliferation.

(A) Schematic of starvation and mTOR-inhibition induced diapause-like state in hESCs. (B) Western blot showing downregulation of mTOR and its downstream targets as well H4K16Ac. (C) Western blot showing SUV420H2 wildtype Elf1 cells and KO clone 35 with and without SUV420H2 inhibitor (A-196) showing an increased proliferation in SUV420H2 KO cells. (D) Quantification of H4K16ac and PCNA from (C). (E) Growth curve of Elf1 wildtype cells and SUV420H2 KO cells cultured for 5 day. S.e.m.; *: = $p < 0.05$; **= $p < 0.01$; ***: $p < 0.001$; ****: $p < 0.0001$; two-tailed t-test, n = 3 biological replicates.

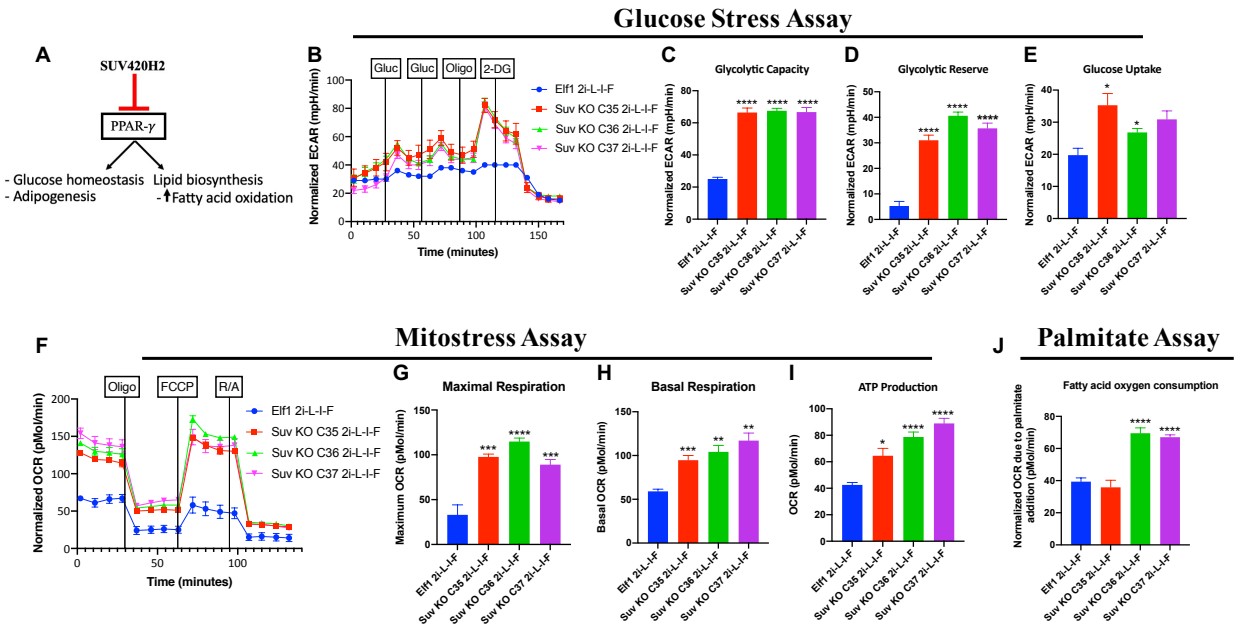

Figure 3.3: SUV420H2 KO hESCs have an increased metabolic function.

(A) Schematic of SUV420H2 metabolic regulation potentially through PPAR-γ. (B-D) SUV420H2 KO cells have an increased glycolytic activity. (B) Representative trace of ECAR changes in response to glucose, oligomycin, and 2-DG is shown under a glucose stress protocol. SUV420H2 KO clones have higher glycolytic capacity (C), higher glycolytic reserve (D), and an increased glucose uptake (E). (F-I) SUV420H2 KO cells have an increased mitochondrial respiration. (F) Representative trace of OCR changes is shown under a MitoStress protocol. SUV420H2 KO clones have an increased maximal respiration (G), basal respiration (H), and ATP production (I) compared to wildtype cells. (J) SUV420H2 KO clones 36 and 37 show high mitochondrial β-oxidation compared to wildtype cells when substrate, fatty acid palmitate (Palm) is offered for oxidation. S.e.m.; *: = $p < 0.05$; **= $p < 0.01$; ***: $p < 0.001$; ****: $p < 0.0001$; two-tailed t-test, n = 3 biological replicates.

CHAPTER 4

Human induced pluripotent stem cells (hiPSCs) require mitophagy to enter quiescence

Parts of this chapter are in the following manuscripts:

Stem cell quiescence requires PRC2/PRC1-mediated mitochondrial checkpoint

Julien R. Ishibashi, Tommy H. Taslim, Abdiasis M. Hussein, Daniel Brewer, Shuozhi Liu, Stuart Harper, Bich N. Nguyen, Jimmy Dang, Ashley Chen, Debra D. Castillo, Julie Mathieu, Hannele Ruohola-Baker

4.1 ABSTRACT

Both normal and tumor stem cells can arrest cell division, avoid apoptosis, and then regenerate following acute genotoxic insult. This protective, reversible proliferative arrest, known as “quiescence,” is still poorly understood. Here, we show that mTOR-regulated mitophagy is required for mTOR-inhibition induced quiescence in human induced pluripotent stem cells (hiPSCs). Depletion of mitophagy by mutating PINK, an essential protein for mitophagy, eliminates entry into quiescence, whereas wildtype cells can enter a reversible quiescent state. Mitochondrial number significantly decreases as cells enter a diapause-like state. Our data suggest that mitochondrial number coordinates reversible quiescence. We further identify that the mechanism of quiescence in human induced pluripotent stem cells (iPSCs) relies on mitophagy to deplete the mitochondrial pool of CycE and limit cell cycle progression. This alternative method of G1/S regulation may present new opportunities for therapeutic purposes.

4.2 INTRODUCTION

Diverse types of stem cells have the capacity to exit the cell cycle upon stress, only to reenter under the appropriate conditions; this process, coined quiescence, is distinct from senescence because quiescence can normally be reversed (van Velthoven and Rando, 2019; Cho et al., 2019). Nutrient-sensitive mechanistic target of rapamycin (mTOR) signaling has been implicated in quiescence, with mTOR activation promoting proliferation and exit from quiescence (Meng et al., 2018), and mTOR repression being a hallmark of stem cells in quiescence (van Velthoven and Rando, 2019; Cho et al., 2019; Meng et al., 2018; Artoni et al., 2017) and diapause (Bulut-Karslioglu et al., 2016; Hussein et al., 2020), with some exceptions (Mathieu et al., 2019). Epigenetic remodeling is another hallmark of the quiescent stem cell state (van Velthoven and Rando, 2019; Cho et al., 2019; Hussein et al., 2020; Somasundaram et al., 2020; Hu et al., 2020). However, it remains unknown whether there are overarching rules that control enter and exit from quiescence across different types of stem cells. Moreover, quiescence is associated with decreased mitochondrial metabolism and increased macroautophagy (van Velthoven and Rando, 2019; Cho et al., 2019), hereby referred to as autophagy.

Mitochondria are highly dynamic organelles and play key roles in signaling, energy metabolism and apoptotic cell death (Green and Kroemer, 2004). Mitochondria, considered the "powerhouse" of the cell, form a highly connected network regulated by continuous fusion and fission (Chan, 2006). Mitophagy, which is degradation of the mitochondrion, and mitochondrial biogenesis are critical to maintain mitochondrial morphology and homeostasis. Two important proteins that play key roles in mitophagy are the mitochondrial serine/threonine PTEN-induced kinase 1 (PINK1) and the E3 ubiquitin protein ligase PARKIN. Under normal conditions, PINK1 is targeted to mitochondria (Valente et al., 2004) while PARKIN is localized in the cytosol

(Shimura et al., 1999, 2004). In response to mitochondrial damage or dysfunction, PINK1 accumulates on the outer mitochondrial membrane (OMM) (Matsuda et al., 2010; Narendra et al., 2010; Geisler et al., 2010; Vives-Bauza et al., 2010) and PARKIN is subsequently recruited to mitochondria to mediate removal of damaged mitochondria (Narendra et al, 2008). Mutation in both PINK1 and PARKIN are the most common causes of early onset Parkinson's Disease (PD) (Corti et al., 2011). In flies, we found that in germline stem cells (GSCs) PINK1/PARKIN-mediated mitophagy to enter quiescence. Since mitochondrial activity is reduced in mouse diapause embryos (Hussein et al., 2020), we asked if mitophagy eliminates entry and exit of a diapause state using human induced pluripotent stem cells (hiPSCs). In this study, we show that mTOR-regulated mitophagy is required for a diapause-like state in hiPSCs. We further show that the mechanism of mTOR inhibition-induced diapause-like state relies on mitochondrial dynamics to temporally regulate a mitochondrial pool of Cyclin E (CyeE). We go on to characterize that human iPSCs couple cell cycle progression to mitochondrial count via the mitochondrial reserve of CycE.

4.3 MATERIALS AND METHODS

4.3.1 hiPSC culture conditions

The human pluripotent stem cell (hiPSC) line WTC-11 (Coriell Institute, GM25256), previously derived in the Conklin laboratory (Kreitzer et al., 2013) and the EGFP-tagged TOMM20 WTC iPSC line generated by the Allen Institute for Cell Science (Coriell Institute, AICS-0011) were cultured on Matrigel growth factor-reduced basement membrane matrix (Corning) in mTeSR media (StemCell Technologies). The cells were treated with Rapamycin (200nM– 2μM, Fisher Scientific) or DMSO for indicated periods, and thereafter tested for reversion in the absence of Rapamycin.

4.3.2 hiPSC gene knockout

Guide RNAs (gRNAs) targeting exon 2 of PINK1 were designed using CRISPOR.org (Concordet and Haeussler, 2018) and inserted into LentiCRISPRv2 plasmid (Shalem et al., 2014; Sanjana et al., 2014) (a gift from Feng Zhang (Addgene plasmid # 52961), as done before (Mathieu et al., 2019). LentiCRISPRv2 contains two expression cassettes, hSpCas9 and the chimeric guide RNA. The vector was digested using BsmBI, and a pair of annealed oligos was cloned into the single guide RNA scaffold.

4.3.3 hiPSCs transduction and selection

hiPSCs (WTC-11) were transduced with lentiCRISPR-v2/gRNA lentiviral particles targeting PINK1 or PARKIN in the presence of 4 μg/mL polybrene (Sigma Aldrich). The medium was changed the next day. Forty-eight hours after infection, cells were selected with puromycin (1 μg/ml) for two days and genomic DNA was extracted using DNAzol reagent (Invitrogen) according to the manufacturer's instructions and quantified using Nanodrop ND-1000. Genomic regions flanking the CRISPR target sites were PCR amplified with designed primers using GoTaq DNA polymerase (Promega) and sent for Sanger sequencing to determine the insertion and deletion errors generated by CRISPR-Cas9 system in exon 2 of the PINK1 gene. The editing efficiency and KO score were determined using the Synthego ICE analysis tool. The mutant lines were analyzed further in this study.

4.3.4 Protein Extraction and Western Blots Analysis

For protein analysis,$1x10^5$ hiPSCs were plated on 35 mm plates coated with Matrigel. Cells were lysed directly on the plate with a lysis buffer containing 20 mM Tris-HCl pH 7.5, 150 mM NaCl, 15% glycerol, 1% Triton X-100, 1 M ß-glycerolphosphate, 0.5 M NaF, 0.1 M sodium pyrophosphate, orthovanadate, PMSF protease inhibitor, and 2% sodium dodecyl sulfate (SDS).

Twenty-five units of Benzonase® Nuclease (EMD Chemicals, Gibbstown, NJ) was added to the lysis buffer immediately preceding use. The protein samples were combined with the 4× Laemmli sample buffer, heated (95 °C, 5 min), and run on SDS-PAGE (protean TGX pre-casted 4–20% gradient gel; Bio-rad) and transferred to the nitrocellulose membrane (Bio-Rad) by semi-dry transfer (Bio-Rad). Membranes were blocked for 1 h with 5% milk or 5% BSA (for antibodies detecting phosphorylated proteins), and incubated in the primary antibodies overnight at 4 °C. The antibodies used for western blot were β-actin (Cell Signaling 4970 (1:10000), phospho-mTOR (Ser 2448) (Cell Signaling 5536, 1:1000), mTOR (Cell Signaling 2972, 1:1000), pS6 (Cell Signaling 2215, 1:1000), S6 (Cell Signaling 2117, 1:1000), histone 4 (Lys16) acetylation (H4K16Ac) (Millipore Sigma 07-329, 1:1000), PINK1 (D8G3, Cell Signaling 6946, 1:1000). The membranes were then incubated with secondary antibodies (1:10000, goat anti-rabbit or goat anti-mouse IgG HRP conjugate (Bio-Rad) for 1 hour and detection was performed using the Immobilon-luminol reagent assay (EMP Millipore).

4.3.5 Immunofluorescence Staining of hiPSCs

Cells were washed with PBS (2 × 5 min) and then were fixed in 4% paraformaldehyde in PBS for 15 min and blocked for 1 h in 3% BSA+0.1% Triton X-100. The cells were then incubated in primary antibody overnight at 4 °C, washed with PBS (3 × 5 min), incubated with the secondary antibody in 3% BSA+0.1% Triton X-100 for 2 h at room temperature washed (3 × 10 min) and stained with 2 μM/mL DAPI diluted with 1X PBS for 15 min. Mounting medium was composed of 21mL of Glycerol, 2.4 mL of 10x PBS and 0.468g of N-Propyl Gallate. Analysis was done on a Leica SPE5 Confocal microscope using a 63x objective and Leica Software. The antibodies used for immunostaining were anti-ATP synthase β subunit (Abcam, Ab14730, 1:500), anti-cyclin E human (Santa Cruz, sc-481, 1:100), anti-Phospho-Histone 3

(Ser10) (Millipore Sigma, 06-570, 1:250), Alexa Fluor 568 Phalloidin (Invitrogen, Cat: A12380, 1:300) and Alexa 488- or 647-conjugated secondary antibody (Molecular Probes, 1:250).

4.3.6 Cell cycle Analysis via Flow Cytometry

hiPSC, either WT, or PINK1 mutants, were seeded in 35 mm dishes at a density of $1.0x10^5$ cells. After 48 h of culture, cells were treated with 2 μM rapamycin or 1% DMSO and 24 hours later, were harvested, and cell suspensions pelleted at 300 x g for 4 minutes and subsequently washed twice with PBS. Cells were resuspended in 2% FBS in PBS and fixed with 5 mL cold 70% ethanol for at least 24 hours (-20 °C). The next day they were centrifuged 10 minutes at 500 x g at 4 °C. Cells were subsequently washed twice with PBS, pelleted at 400 x g for 5 minutes at 4 °C when 500 uL PI staining buffer was added (1X PBS, 50 μg/mL PI (Calbiochem), 2μg/mL RNase A (Sigma) and 0.1% Igepal (Sigma)) to stain for 3 hours at 4 °C. Cell cycle analysis was performed using the FACS Canto II flow cytometer (BD Biosciences). Data analysis was performed using the FlowJo software (Tree Star, Ashland, OR, USA).

4.3.7 Image Deconvolution and 3D Imaging

Images taken from a SPE5 confocal laser-scanning microscope were deconvoluted using Leica LIGHTNING software. 3D hiPSCs images were taken using GE DeltaVision OMX SR super-resolution microscope. Deconvoluted confocal images and OMX images were further analyzed with the Imaris (Bitplane) program to construct respective 3D models in Maximum Intensity Projection (MIP) mode for Drosophila GSCs, and Normal Shading for hiPSCs.

4.3.8 Statistical analysis

All data are presented as the mean of $n \geq 3$ experiments with the standard error of the mean (SEM) indicated by error bars, unless otherwise indicated. Statistical significance was determined using chi-squared test (between timepoints) or Student's t-test (between conditions).

Only p values of 0.05 or lower were considered statistically significant ($p > 0.05$ [ns, not significant], $p \leq 0.05$ [∗], $p \leq 0.01$ [∗∗], $p \leq 0.001$ [∗∗∗], $p \leq 0.0001$ [∗∗∗∗]). For analysis of quiescence, only fold changes of ≥1.6 were evaluated for significance. Data were compiled and analyzed with Excel for Mac (2020; Microsoft, Seattle, WA, USA).

4.4 RESULTS

4.4.1 Cyclin E localized to the mitochondria is degraded upon chemical insult in hiPSCs

The importance of epigenetic regulation of mitophagy further suggests that mitophagy is the metabolic cornerstone of quiescence, as has been recently shown in colorectal cancer (Rehman et al., 2021). However, the question remains whether mitophagy affects quiescence strictly through bioenergetics, or if mitochondrial number can toggle cell cycle progression through more direct means. We asked whether mitochondria played a more direct role in cell cycle progression.

Recent work in mouse fibroblasts has shown that mitochondrial fission/fusion regulate cell cycle through maintenance of a reserve pool of the G1/S regulator Cyclin E (CycE) (Parker et al., 2015; Spurlock et al., 2020). CycE has also been reported to be targeted for degradation by ubiquitination by PARKIN (Staropoli et al., 2003), the E3 ubiquitin ligase required for mitophagy and CycE ubiquitination is PINK1-dependent (Ejma et al., 2020). Furthermore, Parkin mutations are associated with increased CycE in both cancer and Parkinson's neurons (Veeriah et al., 2010). Therefore, we hypothesized that PINK1/PARKIN-mediated mitophagy might also regulate stem cell quiescence by dictating the amount of available mitochondrial CycE. We used rapamycin, an inhibitor of mTORC1, to induce a diapause-like state in human induced pluripotent stem cells (hiPSCs) (Hussein et al., 2020). We show that rapamycin inhibits

mTORC1 by western blot analysis (Fig. 1A-B). Rapamycin-inhibited hiPSCs show inhibition of mTORC1 target, pS6, within 24 hours of treatment (Fig. 1B). We also show that this mode of inhibition is reversible as S6 is again phosphorylated within 3 days after mTORC1 reactivation (Fig. 1B). Furthermore, rapamycin treatment results in reversible reduction of the epigenetic H4K16 acetylation mark (Fig. 1B), indicating reduced cellular transcription and plausible quiescence.

We next analyzed if these quiescent hiPSCs show alterations to CycE or mitochondrial dynamics. We treated hiPSCs with 2μM rapamycin to inhibit mTORC1 or vehicle (1% DMSO) for 24 hours and stained them with CycE and ATPsynβ to analyze CycE and mitochondrial subcellular localization (Fig. 1C). By super resolution microscopy, we find that CycE colocalizes with the mitochondria with or without rapamycin treatment (Fig. 1C), confirming that human iPSC mitochondria harbor CycE. Interestingly, upon mTORC1 inhibition by rapamycin, overall CycE levels drop and the mitochondria fragment and degrade, suggesting that rapamycin-induced mitophagy also eliminates mitochondrial CycE (Fig. 1C).

In order to test if mitochondrial fragmentation and CycE depletion can reverse in hiPSCs, we treated cells with rapamycin for 7hr, and then allowed them to recover in rapamycin-free medium for up to 48hr (Fig. 1E-F). Control hiPSCs show robust mitochondria and CycE dynamics (Fig. 1F), but immediately after (0hr) the end of rapamycin treatment, both CycE and mitochondrial number are drastically decreased. After 24-48hr of recovery, the mitochondria and CycE have recovered to reflect the vehicle control. These data confirm that, under conditions of mTORC1 inhibition in hiPSCs mitochondria and CycE levels degrade and can be reversed if mTORC1 is no longer inhibited.

4.4.2 Mitophagy dictates quiescence in human iPSCs

To further investigate the importance of mitophagy in regulating the stability of CycE, we used a CRISPR/Cas9 system to generate hiPSC lines with mutations in the mitochondrial serine/threonine protein kinase, PTEN-induced kinase 1 (PINK1). The PINK1 protein contains a N- terminal mitochondrial localization sequence, transmembrane sequence, Ser/Thr kinase domain and C-terminal regulatory domain (Schubert et al., 2017). We engineered the CRISPR/Cas9 guide system to generate mutations prior to the kinase domain, thereby eliminating the protein's normal functions (Fig. 2A). Accordingly, using lentivirus-mediated CRISPR/Cas9, 90% of the cells generated had indels near the PAM region (Fig. 2B). We generated PINK1 mutant lines in two genetic backgrounds (WTC11 and WTC11 tagged with GFP) and showed that in both cases the mutations had dramatically reduced the level of PINK1 protein (Fig. 2B).

We treated both control hiPSC and PINK1 mutant hiPSC with rapamycin or vehicle for 24 hours and observed a dramatic change in the cellular behavior using immunofluorescence microscopy. As before (Fig. 1C,F), control hiPSCs show dense via fused mitochondrial networks, with only (~10%) of cells containing reduced mitochondria and CycE, but after 24 hour treatment with 2μM rapamycin, mitochondrial and CycE levels reduced significantly (~27-35%) (Fig. 2C-E; Fig. 3A). In contrast, PINK1 mutant hiPSCs showed relatively low (~5%) mitochondrial and CycE reduction regardless of whether they were treated with DMSO or rapamycin, suggesting that PINK1/PARKIN-mediated mitophagy is required for CycE degradation (Fig. 2C-E; Fig. 3A,C-E). Using PH3 to assess stem cell proliferation, we also found that, in control hiPSCs, roughly 50% fewer cells were dividing after rapamycin treatment (Fig. 2F-G, Fig. 3B,F). PINK1 mutant hiPSCs exhibit less cell cycle arrest following rapamycin

treatment, with 29% fewer stem cells still dividing relative to the control cultures (Fig. 2F-G Fig. 3B,F).

In addition to microscopic analysis, we also stained control iPSC and PINK1 mutant iPSC with PI for cell cycle analysis by flow cytometry. Control iPSCs treated with vehicle (DMSO) for 24hr show 25.5% of cells in G_0/G1 (25.5%), a 58.4% in S, and the remainder (14.7%) in G2/M (Fig. 2H, Fig. 3G). Conversely, after 24hr of rapamycin treatment, control iPSCs show significant G_0/G1 arrest (38.7% vs. 25.5% of non-rapamycin treated cells), consistent with the idea that rapamycin induces a diapause-like state of cellular quiescence in human iPSCs. Remarkably, rapamycin treated PINK1 mutant iPSCs show no significant difference when compared to vehicle treated PINK1 mutant iPSCs. Moreover, neither vehicle- nor rapamycin-treated PINK1 mutant iPSCs differ significantly from vehicle treated control iPSCs (Fig. 2H, Fig. 3G). In addition to PINK1 knockdown cells, we generated PINK1 knockout homozygous null mutant cells missing one base (deletion of G), which introduced an early stop codon and eliminated the protein's normal functions (Fig. 4A). Using PINK1 knockout clones 1 and 2, genetically identical knockout clones, we performed similar experiments as PINK1 KD cells. Mitochondrial and CycE levels were reduced dramatically when wildtype cells were treated with rapamycin (Fig. 4B-D). However, PINK1 knockout clones 1 and 2 had no mitochondrial and CycE reductions regardless of whether they were treated with DMSO or rapamycin (Fig. 4B-D). In addition, by staining cells with PH3, we found that, in control hiPSCs, about 50% fewer cells were dividing after rapamycin treatment relative to vehicle exposure (Fig. 4E). Compared to control, PINK1 knockout clones 1 and 2 show less cell cycle arrest and had the same levels of PH3 with or without rapamycin (Fig. 4E). The inability for PINK1 mutant iPSCs to arrest in G_0/G1 is consistent with mitophagy reducing CycE and thereby reducing G1-S

transition in controls. These data indicate that hiPSCs utilize a non-canonical method of regulating the available reservoir of CycE via PINK1/PARKIN-mediated mitophagy. Together, these findings across stem cell types suggest that diverse stem cells may rely on mitochondrial count to regulate available CycE, and consequently stem cell quiescence.

4.5 DISCUSSION

In this study, we show that quiescence in human induced pluripotent stem cells relies on the amount of mitochondria; failure to fragment and degrade mitochondria abolishes quiescence, allowing the cell cycle to continue. We found that mitochondria co-localized with CycE, raising the possibility that the abnormal accumulation of CycE previously observed may represent an undiscovered mitochondria-associated pool of CycE in hiPSCs. Mitophagy in this case would reduce the CycE protection and allow cells to enter G_0 (Fig. 4F), explaining how mitochondrial network integrity controls cell cycle progression. We found that in human induced pluripotent stem cells (hiPSC) show mitochondrial localization of CycE. Furthermore, rapamycin-induced mitophagy reduced mitochondrial CycE and increased G1 cell cycle arrest. Both PINK1 knockdown and knockout impair the response to rapamycin, revealing that mitochondrial morphology actively regulates CycE in iPSC quiescence.

Human iPSCs use an atypical cell cycle regulation in that they are refractory to the typical G1/S phase checkpoint regulators, CDKIs (Artoni et al., 2007; Zhan et al., 2019; Zhan et al., 2019; Chu et al., 2007; Padgett and Santos, 2020; Qi et al., 2009). Lack of CDKI inhibitor function in iPSC was recently demonstrated by findings revealing that absence of CDKIs increases the iPSC reprogramming efficiency (Zhan et al., 2019). mTOR-inhibited hiPSCs can enter a quiescent stage called diapause for an undetermined, but reversible period. In both cases, once conditions are again favorable, the quiescent cell can re-enter cell cycle and continue

proliferation. This is a particularly extraordinary detour for pluripotent stem cells in the blastocyst, as the zygote would normally proceed from fertilization, through implantation and embryogenesis, to fetal development without halt. This begs the question, if iPSCs do not rely on CDKI to halt the cell cycle, then how is quiescence induced in this unrestrained cell type? We have now identified an alternative method: mitochondrial count, which in turn stabilizes the critical G1/S cell cycle regulator, CycE. We show that mitochondrial count regulates whether the stem cell divides, or not. When mitochondrial number is reduced by mitophagy, CycE levels drop and cells halt in G1/S transition, entering a reversible quiescence. It will be important to interrogate which stem cell types can utilize this alternative method of G1/S control, and whether this phenomenon can be leveraged for therapeutic purposes.

4.6 FIGURES

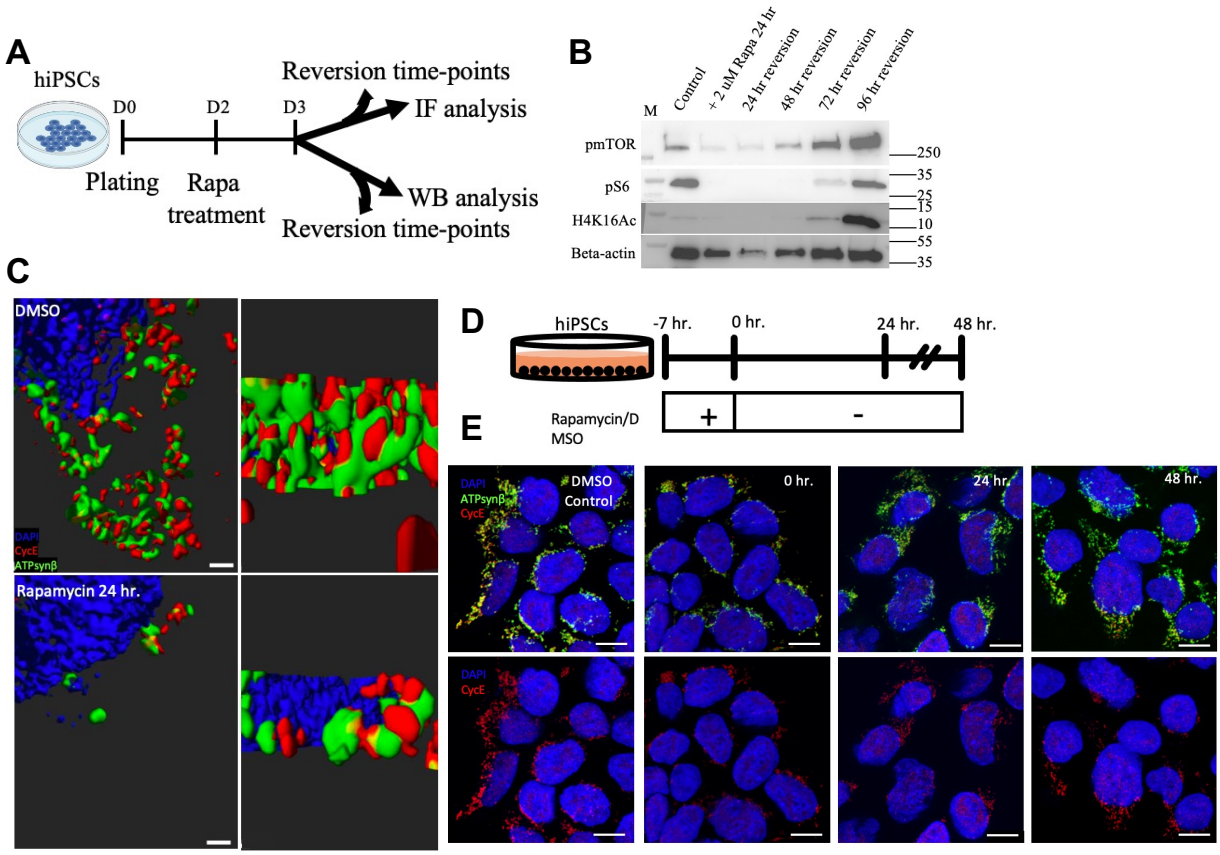

Figure 4.1: Pool of Cyclin E is observed on Mitochondria in iPSCs.

(A) Schematic of iPSC reversion experiment for western blot and immunofluorescence (IF) analysis. (B) Western blot analysis after a pulse chase experiment of WT iPSCs treated with either vehicle control (DMSO) or rapamycin (2μM) for 24 hours followed by reversion (normal iPSC growth medium) for another 96 hours. pmTOR, pS6 and H4K16Ac level is seen to be low by 24 hours post 2μM rapamycin treatment while the level increases to more than the control by 96 hours post reversion. (C) Representative 3D-reconstructed OMX super resolution microscopy images of WTC Tom20 (WTCT) cells treated with vehicle control (DMSO) or 2μM rapamycin for 24 hours. Stained with ATPsynβ (mitochondria, green), cyclin E (red) and DAPI (blue)

(Scale bar 0.5μm). (D) Pulse-chase experiment setup model for immunofluorescence. (E) Representative confocal microscopy images of WT iPSCs treated with either vehicle control (DMSO) or rapamycin (2μM) pulse-chase stained with ATPsynβ (mitochondria, green), Cyclin E (red) and DAPI (blue) (Scale bar 10μm). iPSCs show reduction in both mitochondrial and cyclin E density compared to vehicle control after 7 hours of 2μM rapamycin treatment. Both mitochondria and Cyclin E density increases after 24 hours, and 48 hours, post rapamycin treatment.

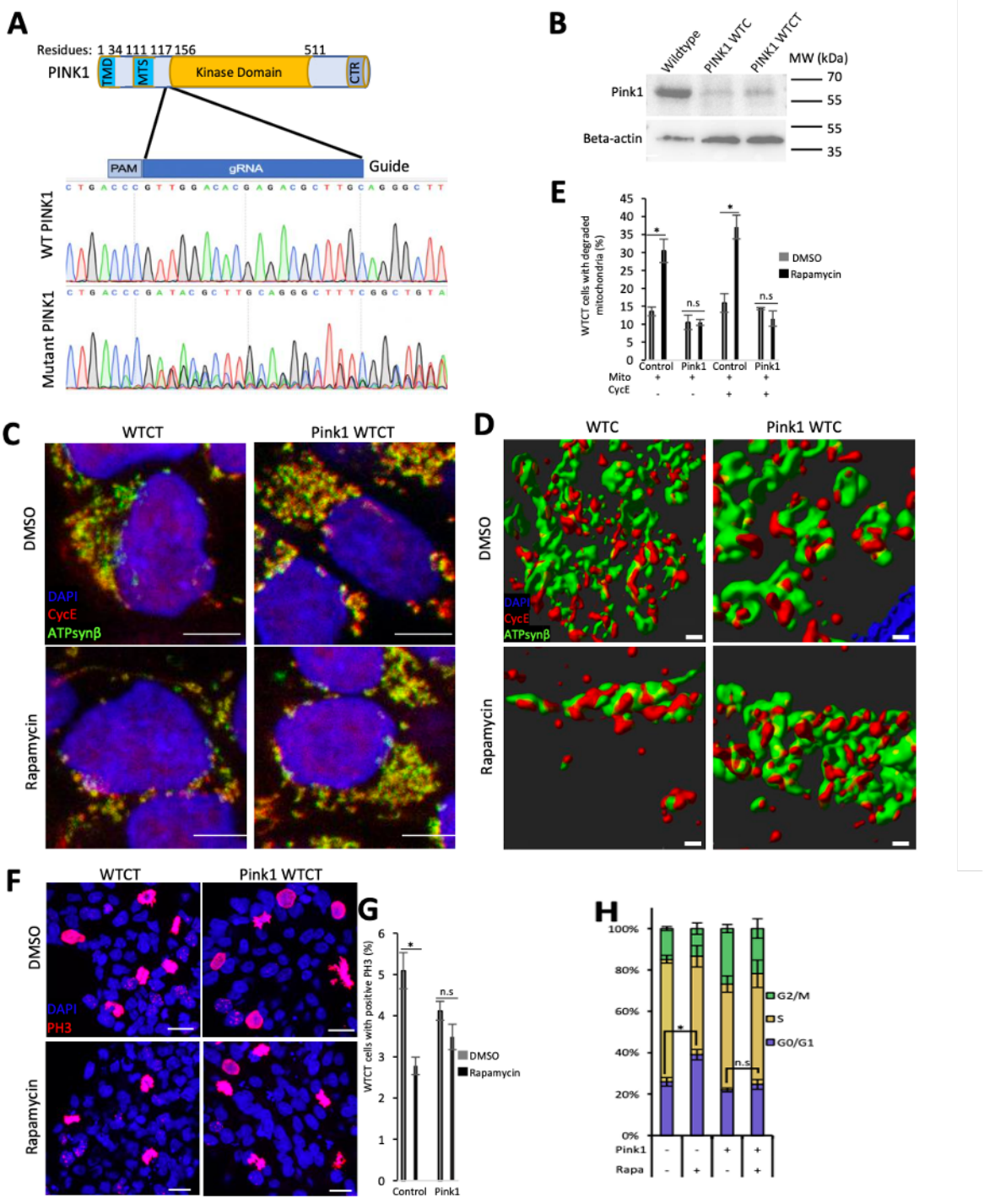

Figure 4.2: Mitophagy in iPSCs controls both mitochondrial Cyclin E and cell cycle.

(A) Schematic of PINK1 structure with guide RNA location indicated and DNA sequencing

chromatogram comparing wildtype (WT) PINK1 to mutant PINK1, showing a mixed pool of mutants and a loss of the wildtype sequence. (B) Western blot showing lysates from Control WTC-11, PINK1 mutant WTC and PINK1 mutant WTCT, showing PINK1 protein knocked down in both mutant pools when compared to control. (C) Representative confocal microscopy images of wildtype WTCT or PINK1 mutant WTCT treated with either vehicle control (DMSO) or rapamycin (2μM) stained with DAPI (blue), CycE (red) and ATPsynβ (mitochondria, green) (Scale bar 5μm). (D) Representative 3D reconstructed OMX super resolution microscopy images of wildtype WTC or PINK1 mutant WTC stained with DAPI (blue), CycE (red), and ATPsynβ (mitochondria, green) (Scale bar 0.2μm). (E) Quantification of mitochondrial degradation in WTCT vs PINK1 mutant treated with either vehicle control (DMSO) or rapamycin (2μM), suggesting that PINK1 mutants can't degrade their mitochondria in response rapamycin. (F) Representative confocal microscopy images of wildtype WTCT or PINK1 mutant WTCT treated with either vehicle control (DMSO) or rapamycin (2μM) stained with DAPI (blue), PH3 (proliferating cell nuclei, red) (Scale bar 15μm). (G) Quantification of PH3 incidence in WTCT vs PINK1 mutant treated with either vehicle control (DMSO) or rapamycin (2μM), suggesting that PINK1 mutants fail to halt cell cycle progression as efficiently as wildtype. (H) Quantification of FACS analysis of cell cycle by propidium iodide staining in WTC or PINK1 KD treated with DMSO or rapamycin (2μM). S.e.m.; ns: $P > 0.05$; *: = $p < 0.05$; **= $p < 0.01$; ***: $p < 0.001$; ****: $p < 0.0001$; two-tailed t-test, n = 3 biological replicates.

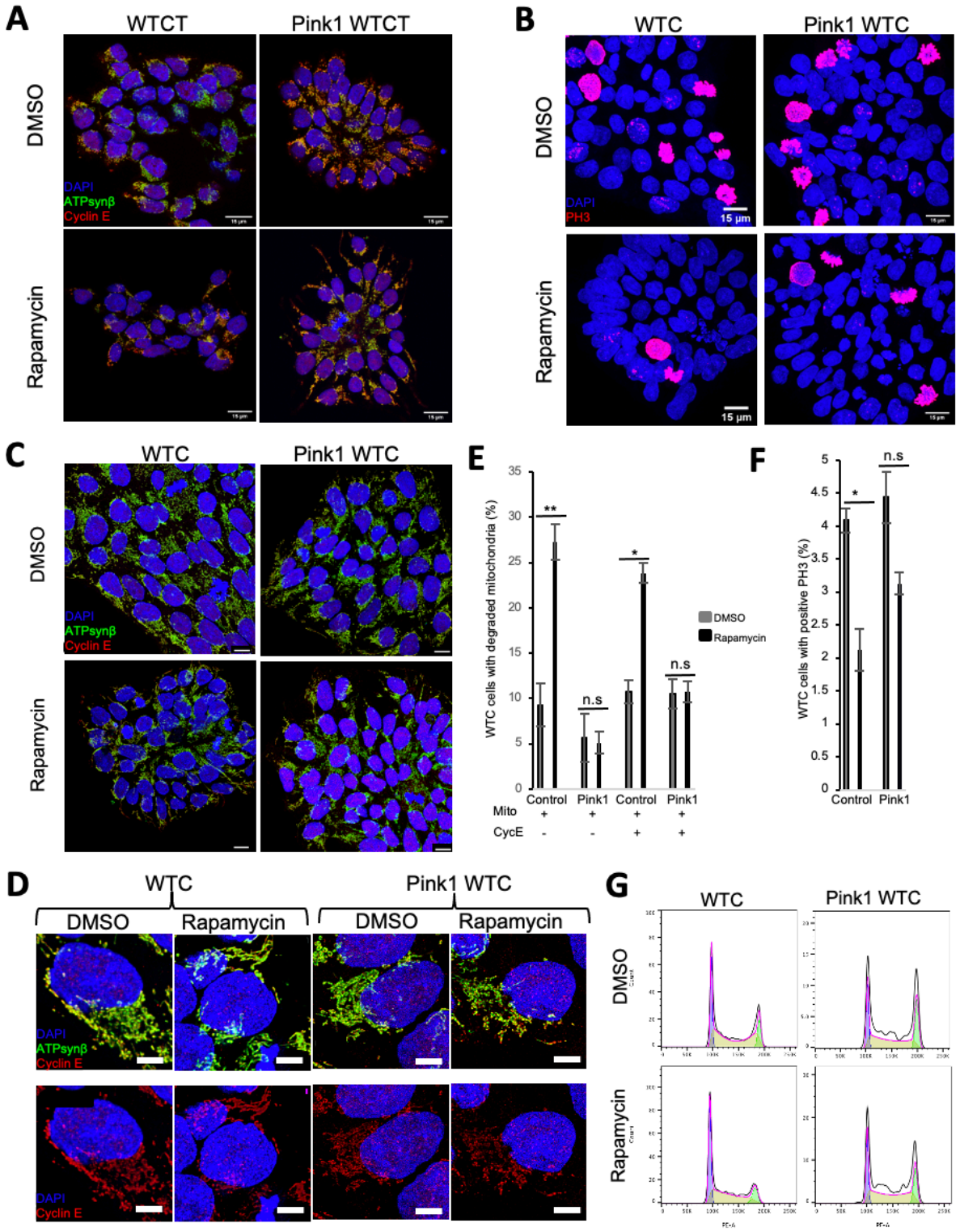

Figure 4.3: iPSCs require mitophagy to regulate Cyclin E.

(A-D) Representative confocal microscopy images of control and PINK1 KD iPSCs, treated with either DMSO or 2μM rapamycin for 24 hours. (A) Control and PINK1 KD WTCT cells stained with ATPsynβ (mitochondria, green), Cyclin E (red) and DAPI (blue) (Scale bar 15μm). (B) Control and PINK1 KD WTC cells stained with PH3 (mitosis marker, red), and DAPI (blue) (Scale bar 15μm). (C-D) Deconvoluted images taken from SP8 confocal microscope. (C) Control and PINK1 KD WTC cells stained with ATPsynβ (mitochondria, green), Cyclin E (red) and DAPI (blue) (Scale bar 10μm). (D) High magnification of control and PINK1 KD WTC cells stained with ATPsynβ (mitochondria, green), Cyclin E (red) and DAPI (blue) (Scale bar 5μm). (E) Quantification of cells without a dense cluster of mitochondria in control vs PINK1 KD WTC treated with control DMSO or 2μM rapamycin for 24 hours. One group of control and PINK1 KD (left half) is quantified based on the mitochondria, the other group (right half) includes the criteria of only quantifying mitochondrial-CycE positive cells. Each group shows control WTC increase in cells without dense cluster of mitochondria when treated with rapamycin vs DMSO, whereas PINK1 KD WTC cells maintain their dense cluster of mitochondria when treated with rapamycin. Grey bar shows quantification for DMSO treated cells and black bar for 2μM rapamycin treated cells. Data is from duplicate experiments. (F) Quantification of PH3 positive cells in control vs PINK1 KD WTC treated with DMSO control vs 2μM rapamycin for 24 hours. Control WTC shows decrease in positive PH3 cells by half when treated with rapamycin compared to DMSO control, whereas PINK1 KD WTC shows slightly higher PH3 positive cells when treated with rapamycin compared to control WTC cells. n=3. (G) Representative FACS cell cycle analysis traces from WTC or PINK1 mutant WTC treated with vehicle (DMSO) or rapamycin (2μM) for 24 hours. S.e.m.; ns: $P > 0.05$; *: = $p <$

0.05; **= p < 0.01; ***: p < 0.001; ****: p < 0.0001; two-tailed t-test, n = 3 biological replicates.

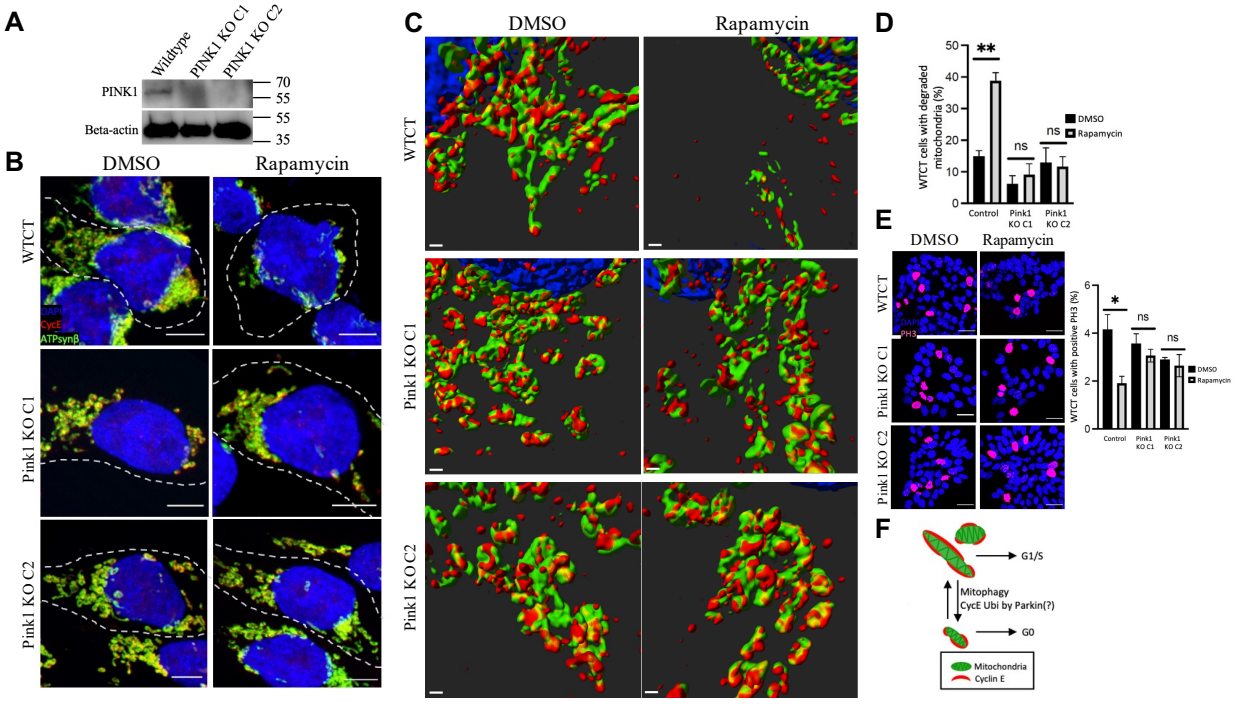

Figure 4.4: PINK1 is required in iPSCs to control both mitochondrial Cyclin E and cell cycle.

(A) Western blot showing lysates from control WTC-11, PINK1 knockout clones 1 and 2 (C1 and C2) showing no expression of PINK1 protein. (B) Representative confocal microscopy images of wildtype WTCT or PINK1 KO clones 1 and 2 treated with either vehicle control (DMSO) or rapamycin (2μM) stained with DAPI (blue), CycE (red) and ATPsynβ (mitochondria, green) (Scale bar 5μm). (C) Representative 3D reconstructed OMX super resolution microscopy images of wildtype WTCT or PINK1 KO Clones 1 and 2 corresponding to (B) (Scale bar 5 μm). (D) Quantification of mitochondrial degradation in WTCT vs PINK1 KO clones 1 and 2 treated with either vehicle control (DMSO) or rapamycin (2μM), suggesting that PINK1 mutants can't degrade their mitochondria in response rapamycin. (E) Quantification of

PH3 incidence in WTCT vs PINK1 KO clones 1 and 2 treated with either vehicle control (DMSO) or rapamycin (2μM), suggesting that PINK1 mutants fail to halt cell cycle progression as efficiently as wildtype. (F) Model of proposed mechanism in which mitochondria can normally stabilize CycE and promote G1-S transition, while mitophagy induction will reduce CycE – perhaps through direct ubiquitination by PARKIN – to keep the stem cells in quiescence/G_0.

CHAPTER 5

SUMMARY AND FUTURE DIRECTIONS

5.1 ABSTRACT

For the diapause project, we characterized the transcriptional and metabolite profiles of mouse pre-implantation, post-implantation and diapause embryos. We have shown diapause is a distinct state compared to pre/post-implantations stages. We also found that in addition to gene expression, splice variants also separate diapause from pre/post-implantation stages. We found that starvation through the LKB1-AMPK pathway can induce a diapause-like state *in vitro* which mimics *in vivo* diapause that activates expression of glutamine transporters (*Slc38a1* and *Slc38a2*). These glutamine transporters are required for the diapause state as both starvation and glutamine transporter activity repress the mTOR pathway. Both chemical and genetic manipulation of these glutamine transporters in a diapause embryo led to exit from the diapause state. Inhibition of mTOR causes upregulation of lipolysis and epigenetic silencing, as shown by the downregulation of H4K16 acetylation marks. Lipolysis, which is breakdown of fats and other lipids, supplies free fatty acids to support cell survival through the NF-κB pathway. mTORC2 downregulation causes lipolysis during diapause, as seen by inactivation of mTORC2 in mouse ESCs. In mESC null mutation of the mTORC2 component *Rictor*, increases lipolysis. Our findings suggest that glutamine might be acting as an mTOR inhibitor. In addition to increased lipolysis, other metabolic signatures associated with both diapause and the starvation-induced diapause-like state include increased glycolysis and metabolic pathways regulated by AMPK and decreased mitochondrial activity. It is interesting but also perplexing that cells that are in a dormant state would have activated glycolysis, but further studies are needed to examine this phenomenon.

5.2 DIAPAUSE METABOLISM

Embryonic diapause is associated with reduced metabolic activities including protein and DNA synthesis and carbohydrate metabolism (Fenelon et al., 2014; Menke and McLaren, 1970; Pike, 1981; Van Blerkom et al., 1978). Previous studies suggest that autophagy is activated in a dormant blastocyst compared to a reactivated blastocyst (Lee et al., 2011). Activation of autophagy might provide essential nutrients allowing the prolonged survival of embryos during diapause. Interestingly, using transcriptomic studies, a recent study has shown that some of the pathways enriched in diapause include glycolysis, pyruvate and cholesterol metabolism (Hussein et al., 2020).

Lipolysis, breakdown of triacylglycerol, the lipid storage components, into free fatty acids and glycerol, was also highly upregulated in diapause compared to pre-implantation blastocysts (Hussein et al., 2020). Lipolysis has been connected with starvation adaptation (Tao et al., 2016), suggesting that energy from oxidation of fats can be utilized instead of glucose oxidation. Furthermore, glycerol released from triacylglycerol breakdown can enter the glycolytic pathway as DHAP (dihydroxyacetone-3-phosphate), in line with observations of increased glycolytic pathway activity in diapause (Hussein et al., 2020).

A recent study proposed that the diapause blastocyst uses lipid droplets to survive while it remains in a dormant state (Arena et al., 2021). Furthermore, the authors suggested that lipid droplets are not essential at the pre-implantation stage or during implantation but only in the diapause state. Interestingly, levels of lipids decreased with the progression of embryonic diapause suggesting lipid catabolism was possibly occurring instead of carbohydrate catabolism (Arena et al., 2021). This was consistent with transcriptomic data showing downregulation of carbohydrate metabolism and upregulation of lipid metabolism pathways in diapausing mouse embryos compared to embryos that were not in diapause (Arena et al., 2021). Although gene

expression studies can illuminate our understanding of diapause metabolic profiles, it is essential to perform metabolomics to detect levels of endogenous metabolites such as those in glycolysis and the TCA cycle.

5.3 EPIGENETIC REMODELING IN DIAPAUSE

During embryonic development, an extensive chromatic remodeling at promoters and enhancers accompanies the transition from the pre-implantation to the post-implantation stage (Battle et al., 2019). Both DNA and histone methylation in mammals are epigenetic modifications that can impact gene expression and affect cell fate. Epigenetic remodeling has been shown to play an important role in regulating embryonic diapause (Fu et al., 2014; Bulut-Karslioglu et al., 2016; Hussein et al., 2020). Based on proteomic studies, proteins involved in chromatin remodeling are differentially expressed between dormant and reactivated blastocysts (Fu et al., 2014). The expression of these proteins increases upon reactivation of the dormant blastocyst (Fu et al., 2014). More recently, immunofluorescence staining in the ICM of diapause blastocysts has highlighted a significant reduction of histone marks associated with active transcription: H4K5/8/12 acetylation and H3K36me2 (Bulut-Karslioglu et al., 2016), H4K16 acetylation (Hussein et al., 2020; Bulut-Karslioglu et al., 2016) and H3K4me3 (He et al., 2019) compared to pre-implantation blastocysts. In contrast, the repressive histone modification mark H3K27me3 was significantly increased in the ICM of diapause blastocysts compared to reactivated blastocysts (He et al., 2019). These data suggest that the chromatin landscape of embryonic diapause is remodeled, and that diapause has a distinct epigenetic signature, that encompasses an increase of repressive marks and a significant reduction of activating marks.

5.4 IMPLICATIONS IN CANCER STEM CELLS

In the United States, cancer is the second leading cause of death as of 2020 according to the Centers for Disease Control and Prevention (CDC). Cancer can arise in many different ways, but a subpopulation of cancer cells has characteristics of both stem cells and cancer cells. These cancer stem cells in a tumor, like stem cells, have the capacity to self-renew and give rise to progenitor cells that are committed to different lineages of cancer cells within the tumor (Clarke et al., 2006). Cancer stem cells could arise from normal stem, progenitor, or differentiated cells due to environmental alterations or genetic mutations (Rapp et al., 2008). Cancer stem cells, like normal stem cells, can into transit into dormancy when they are known to be resistant to most clinical treatments, such as chemotherapy, and can contribute to tumor recurrence (Tang, 2012).

Our studies can have clinical implications in cancer and can potentially contribute to treatments that target cancer stem cells. Studies have suggested cytotoxic treatment of tumor cells followed by therapeutics, such as mTOR or Myc inhibition, can keep cancer stem cells in a dormant state to prevent regrowth (Dhimolea et al., 2021). However, this strategy might fail because cancer stem cells will remain dormant but alive, and they will still have the potential to exit this state at some point. We propose using cytotoxic drugs to target the cancer and combined with activation of the dormant state, allowing cancer stem cells to exit their "hideout" and become sensitized to the chemotherapeutic agents. One way to terminate dormancy that we have shown in our studies is chemical inhibition of the glutamine transporter, SLC38A1/2, to cause exit from the diapause-state. Control of activity of the transcription factor Myc plays a key role in the generation of cancer stem cell specific therapeutics. Depletion of Myc was found to induce a diapause-like state and proliferative arrest (Scognamiglio et al., 2016). Inhibition of Myc in tumor cells also caused resistance to cytotoxic treatments (Dhimolea et al., 2021). These findings related to Myc can be used to design CSC specific drug cocktails in combination with existing

cancer treatments to drive CSC out of dormancy and eradicate tumor recurrence. This can be achieved by activation of Myc, allowing CSCs to proliferate again, enter a biosynthetically active state and exit the dormant state. This will allow cytotoxic treatments to target cancer cells and reduce their ability to survive in an environment that hinders their capacity to enter dormancy and evade chemotherapeutic drugs.

5.5 EMBRYONIC DIAPAUSE IN HUMANS

Embryonic diapause can occur in over 130 mammalian species (Fenelon et al., 2014). Although embryonic diapause is evolutionarily conserved across mammals, it is not known whether diapause occurs in humans or other primates. Several reports have previously suggested that embryonic diapause might occur in humans (Grinsted and Avert, 1996; Tarín and Cano, 1999; Ptak et al., 2013), but testing this hypothesis has not been possible because of ethical limitations. Interestingly, studies have shown that in sheep, that have not been previously observed to be capable of diapause, embryos can be induced to display embryonic diapause (Ptak et al., 2012). The authors transferred blastocysts from sheep into pseudo-pregnant mice in which diapause conditions were hormonally induced. The sheep embryos entered diapause as shown by arrest of DNA replication, decreased expression of proliferation genes and increased expression of anti-proliferation genes. The diapausing embryos also developed into normal lambs after they were transferred to surrogate ewe recipients. These findings challenge and question the belief that only the embryos of certain mammalian species evolutionarily developed the capacity to enter diapause. This study also postulates that all species can potentially enter diapause if there are circumstances impacting the mother that allow embryonic development to pause.

Before we ask whether human embryos can enter a diapause state, we should ask what are the circumstances that lead to induction of diapause in other mammals? Some of the conditions

that induce diapause in other species include environmental stresses such as starvation, lactation, cold and overcrowding (Lopes et al., 2004, Renfree and Shaw, 2000). These are conditions that most modern humans do not commonly experience today and therefore there is no adaptive advantage for humans to undergo diapause. However, inducing diapause artificially in humans might have clinical implications including advancing assisted reproductive technology such as *in vitro* fertilization (IVF) and intracytoplasmic sperm injection (ICSI). Defects in implantation is the main cause of human pregnancy failure (Norwitz et al., 2001). Thirty percent of implantation failure is due to a dysfunctional blastocyst (Achache and Revel, 2006). This highlights the importance of the timing of blastocyst development and uterine receptivity. Previous studies in mouse have shown that the activity and condition of the blastocyst is a critical factor for the implantation process in the receptive uterus (Paria et al., 1993). Studies from embryonic diapause can generate a guide to determine blastocysts with high implantation potential in the context of in vitro fertilization and culture.

A surrogate model can be used to test if human ESCs can go into diapause. My studies have shown that human embryonic stem cells derived from the pre-implantation stage can be manipulated pharmacologically to go into a reversible diapause-like state. mTOR inhibition has been shown before to induce a diapause-like state both in mouse ESCs and mouse embryos (Bulut-Karslioglu et al., 2016; Hussein et al., 2020). I have shown mTOR-inhibited hESCs are void of epigenetic H4K16 acetylation, a mark that is associated with diapause embryos (Bulut-Karslioglu et al., 2016; Hussein et al., 2020). RNA-sequencing analysis of mTOR inhibited,hESC, in a diapause-like state, and comparison of their gene expression profile to those of published mouse *in vivo* embryonic diapause will provide an evidence of mechanistic conservation between species . hESCs induced to enter a diapause-like state should also have a

similar metabolic profile compared to mouse, and especially they should have increased lipolysis as shown before (Hussein et al., 2020). These findings should inform us if human embryos can be used to induce an in vitro diapause (followed by release) to analyze whether these human embryos behave as do mouse embryos. There are ethical limits to length of intact culture of human embryos cultured *in vitro* within two weeks from fertilization (Shahbazi et al., 2016). It is suspected that these studies could be informative well within these limits. There are alternative approaches to this limitation. A research group in the UK developed synthetic embryo-like structures using mouse stem cells which grew to resemble the embryo after implantation (Harrison et al., 2017). The synthetic embryo from mouse stem cells might pave the way for researchers to create similar embryo-like structures using human stem cells. Both the synthetic embryo and actual embryos cultured in vitro for two weeks might be good models to test whether humans can undergo diapause.

For our naïve-to-primed pluripotent stem cell project, we studied how the naïve cells transition to the primed stage and we found essential genes for this transition. One of the critical genes for this transition was the histone methyltransferase SUV420H2. Using the CRISPR/Cas9 system, we made SUV420H2 mutant naïve hESC lines to investigate the role of SUV420H2 in the pre- and post-implantation embryonic stages. We found that SUV420H2 mutant cells are not able to enter an *in vitro* diapause state, but instead continue dividing. By western blot analysis, we also found SUV420H2 mutant cells have higher levels of H4K16 acetylation and increased rates of proliferation compared to wildtype control cells. Our data suggest that mechanistically H4K20me3 repressive marks in key target genes are required for the induction of the diapause stage. In addition, our functional metabolic assays of live cells show that SUV420H2 mutant cells have an increased level of fatty acid β-oxidation, mitochondrial respiration and glycolysis

compared to wildtype, suggesting that SUV420H2 might be a potential metabolic inhibitor. Our findings uncover the mechanism for SUV20H2 requirement during naïve to primed embryonic stem cell transition. The epigenetic repression of SUV420H2 by trimethylation of H4K20 of target genes is a pre-requisite for the potential diapause and metabolic reprogramming that occurs during naïve to primed transition.

5.6 PERSPECTIVE

Regulation of embryonic diapause is under maternal control (Fenelon et al., 2014). A multitude of factors have been implicated in the control of induction of embryonic diapause including transcription factors and uterine microRNAs. Here, we highlight the role of a few transcription factors and microRNA let-7, that were shown to play a key role in embryonic diapause, and connect their activity with new findings that might inform us of their possible mechanisms of action. We combine our findings to what is known in the field about the molecular mechanism of diapause induction.

5.6.1 THE TRANSCRIPTION FACTOR HESX1

The homeobox transcriptional repressor *Hesx1* (Homeobox gene expressed in stem cells 1) was recently found to play a key role in early development and in embryonic diapause (Pozzi et al., 2019). *Hesx1*$^{-/-}$ mouse embryos die perinatally (Dattani et al., 1998; Andoniadou et al., 2007), and this suggest that lack of *Hesx1* might not be detrimental for in utero development. *Hesx1* is expressed in the mouse pre-implantation embryo and previous research suggests that Hesx1 might be required for human ESCs to remain pluripotent (Richards et al., 2004). It was proposed that Hesx1 might repress differentiation-related genes to maintain the pluripotent state (Li et al., 2015). However, the role of *Hesx1* in diapause hasn't been investigated. *Hesx1* was found to be essential during diapause (Pozzi et al., 2019) and lack of *Hesx1* resulted decreased

expression of post-implantation epiblast and primitive endoderm (Pozzi et al., 2019). Deletion of *Hesx1* was not only found to impair self-renewal of ESCs, but also diapaused embryos failed to continue embryonic development after implantation (Pozzi et al., 2011). Homozygous mutant *Hesx1* embryos, from a heterozygous cross, were shown to have reduced expression of NANOG and GATA6 for epiblast and primitive endoderm respectively. This suggests that these mutant embryos are not fully able to enter diapause, which remains to be determined.

Naïve and primed pluripotent cells exhibit different epigenetic signatures (Sperber et al., 2015, Mathieu and Ruohola-Baker., 2017, Guo et al., 2014; Somasundaram et al., 2020; Ehnes et al., 2020) and pre-implantation development is associated with a global reduction in DNA methylation (Guo et al., 2014). DNA methylation levels are reduced as cells progress from fertilization to the induction of the inner cell mass in vitro equivalent naïve stage, which is marked by a reversible genome-wide DNA hypomethylation (Theunissen et al., 2016). Afterward, DNA methylation levels increase as cells transition from the pluripotent stem cell naïve to the primed stage (Theunissen et al., 2016). Previous studies have shown that DNMT1 has an essential function in human and mouse primed ESCs (Liao et al., 2015; Geula et al., 2015). These findings suggest that DNA methylation is not required in mouse naïve ESCs, but it is essential in both mouse and human primed ESCs. However, as the pre-implantation blastocyst enters *in vivo* embryonic diapause, it is not clear, whether or not DNA methylation is required in diapause. The *de novo* DNA methyltransferase, DNMT1, was found to be a HESX1 binding protein (Sajedi et al., 2008). Mutations that lead to disruption of Hesx1 DNA binding properties had phenotypes similar to those observed in *Hesx1* deficient mice (Sajedi et al., 2018). It is possible that DNA methylation is also essential in embryonic diapause and that might explain why homozygous mutant Hesx1 embryos are unable to enter diapause state.

5.6.2. THE TRANSCRIPTION FACTORS MSX1 AND MSX2

Muscle segment homeobox (MSX) genes *Msx1* and *Msx2*, were found to be the first uterine factors associated with blastocyst dormancy (Cha et al., 2013). Msx1 expression is high in diapause (Cha et al., 2020) and its expression is reduced upon reactivation of the dormant blastocyst with replacement of estrogen or LIF (Daikoku et al., 2011). Mice with a uterine-specific deletion of *Msx1*and *Msx2* are not able to maintain uterine quiescence, which is required for the embryo to survive while in the diapause state (Cha et al., 2013) and this deletion is associated with increased NF-κB-mediated inflammation (Cha et al., 2015). Mechanistically, the role of MSX in the induction of diapause is not entirely clear. Findings from a recent paper suggest that Msx1 inhibits the PI3K-mTOR mediated signaling pathway as phosphorylation levels of PI3K, mTOR and Akt proteins were reduced in the presence of Msx1 or Msx1 with its interactor PIASy in HUVEC cells (Son et al., 2020). Although this is an exciting finding, additional studies and validations in different cell lines are needed to consolidate an inhibitory role for Msx1 in the PI3K-mTOR signaling pathway.

Several other factors are known to regulate embryonic diapause in rodents in cases of unfavorable environmental conditions, such as nutritional deprivation or energetic stress (Renfree and Shaw 2000; Renfree and Fenelon, 2017). Recent work has revealed that inhibition of the mechanistic target of rapamycin (mTOR) pathway or downregulation of the transcription factor, Myc can induce a diapause-like state (Bulut-Karslioglu et al., 2016; Hussein et al., 2020; Scognamiglio et al., 2016). Furthermore, it was shown that during starvation, mTOR is inhibited by LKB1-AMPK in mouse ESCs and this *in vitro* starvation model has a gene expression signature that mimics a diapause state (Hussein et al., 2020). The signals that reduce Myc or influence how mTOR is downregulated in diapause and the signals that reactivate both of these

signaling factors are poorly understood in any mammal both *in vitro* and *in vivo* (Fenelon et al., 2014; Van Blerkom et al., 1978; Shaw and Renfree, 1986; Renfree and Shaw, 2014; Murphy, 2012; He et al., 2019, Bulut-Karslioglu et al., 2016; Hussein et al., 2020; Scognamiglio et al., 2016).

5.6.3 MICRORNA LET-7

A role for microRNAs have been implicated in embryonic diapause (Liu et al., 2012; Renfree and Fenelon, 2017; Cheong et al., 2014). MicroRNAs are highly conserved small, ~ 22 bp nucleotide, non-coding RNA that play critical roles in the post-transcriptional regulation of gene expression. They regulate their target genes primarily by binding the 3′ UTR region of the protein-coding mRNA, which results translational repression or transcript destabilization (Bartel, 2019). MicroRNAs are crucial for animal development (Alvarez-Garcia and Miska, 2005) as they play critical roles in diverse cellular processes such as proliferation, differentiation, cell cycle progression and apoptosis (Bartel, 2019; Hatfield et al., 2005; Shcherbata et al., 2006).

MicroRNAs were shown to be differentially expressed in pre-implantation naïve and post-implantation primed human and mouse embryonic stem cells (Wang et al., 2019). Both diapause, which is an intermediate step between naïve and primed stages, and reactivated dormant blastocysts are associated with changes in microRNAs expression (Liu et al., 2012). The Let-7 family is highly upregulated in mouse embryonic diapause compared to reactivated embryos (Liu et al., 2012). A member of this family, microRNA let-7a was found to block implantation of embryos, keeping embryos in a dormant state (Liu et al., 2012). However, it was not clear how let-7a was able to do this and what targets were involved in this process.

A recent paper has shown that maternal origin let-7a reversibly induces embryonic diapause, which was associated, as expected, with decreased proliferation and reduced DNA

synthesis (Liu et al., 2020). Overexpression of pre-let-7a blastocysts cultured *ex vivo* remained viable for more than 12 days compared to control blastocysts, which had shrunken in size or degenerated by day 7 (Liu et al., 2020). By comparing the gene expression profiles of *in vivo* dormant blastocysts, *in vitro* let-7a-induced dormant blastocysts and activated blastocysts, the authors show similar profiles for the in vivo and let-7a-induced dormant blastocysts which is distinct from activated blastocysts (Liu et al., 2020). Interestingly, the transcript expression of the transcription factor c-myc, and Akt, an mTORC1 activator (Inoki et al., 2002; Manning et al., 2002), were shown to be highly reduced in the let-7-induced dormant blastocysts compared to control untreated blastocysts (Liu et al., 2020). Immunofluorescence staining has shown a decreased expression of *Rictor*, a component of mTORC2, in diapause embryos compared to estrogen-induced reactivated embryos (Liu et al., 2020). Using Targetscan, the authors identified *Rictor* as a potential target gene for let-7a and this was consistent with the IF data. Both mTOR inhibition and MYC depletion was previously found to induce a diapause-like state in mouse (Bulut-Karslioglu et al., 2016; Hussein et al., 2020; Scognamiglio et al., 2016). Mechanistically, let-7a was found to inhibit c-MYC, mTORC1 and mTORC2 and pharmacological manipulation of C-MYC and mTORC2 has shown decreased phosphorylation of only mTORC1 targets when C-MYC is inhibited, whereas inhibition of mTORC2 had no effect on C-MYC, suggesting that C-MYC is upstream of only mTORC1 and not mTORC2.

Other microRNAs are potentially involved in regulating embryonic diapause. We have looked at a few microRNAs that were highly either upregulated or downregulated and the status of their target genes in diapause compared to reactivated embryos. Using microarray data of diapause and re-activated embryos (Liu et al., 2012) and RNA-seq of diapause and post-implantation embryos (Hussein et al., 2020), 379 consistent connections were found between 38

microRNAs and 274 of their target genes (Wang et., 2019). In Table 1, we are highlighting a few of the genes that were highly upregulated in diapause in several studies (Liu et al., 2012; Hussein et al., 2020; Liu et al., 2020) and the microRNAs that target them based on predictions from Targetscan (Agrawal et al., 2015).

The transcription factor and stress response gene EGR1 is essential for early reproductive development (Lee et al., 1996). *Egr1* expression is highly upregulated in embryonic diapause and the microRNAs that targets *Egr1* (microRNA 199 and microRNA 181) are suppressed in diapause (Wang et al., 2019; Hussein et al., 2020). Expression of EGR1 is increased in this quiescent state because it might play a role in ensuring that diapause embryos remain viable for implantation as knockdown of *Egr1* results reduction of implantation sites (Guo et al., 2014). The diapause enriched glutamine transporters, *Slc38a1* and *Slc38a2*, also show the same trends in that the microRNAs that target them for degradation are downregulated in diapause compared to pre-implantation embryos (Wang et al., 2019; Hussein et al., 2020). Knocking out *Slc38a1* and *Slc38a2* results in loss of viable embryos (Hussein et al., 2020). Using chemical inhibitors against these glutamine transporters in diapause embryos caused the exit from the diapause state (Hussein et al., 2020). Further studies are needed to shed light on the role of these glutamine transporters and whether glutamine is acting as an inhibitor of mTOR to keep embryos in a diapause state.

We propose a model for the molecular regulation of embryonic diapause (Figure 5.1). The activity of several transcription factors changes upon induction of diapause. Both MSX and glutamine transporters (SLC38A1/2) can potentially inhibit mTOR, which is known to be downregulated in diapause. MicroRNA let-7 was also shown to inhibit both mTOR and the transcription factor Myc. Depletion of Myc in diapause is associated with downregulation of

biosynthetic pathways in diapause. Another transcription factor, which is essential for development of the diapause embryo is *Hesx1*. A *Hesx1* mutation in diapause embryos results in failure of embryos to continue embryonic development after implantation. However, *Hesx1* mechanism of action, besides self-renewal of ESCs, is poorly understood both in diapause and in during post-implantation development.

5.7 FIGURES

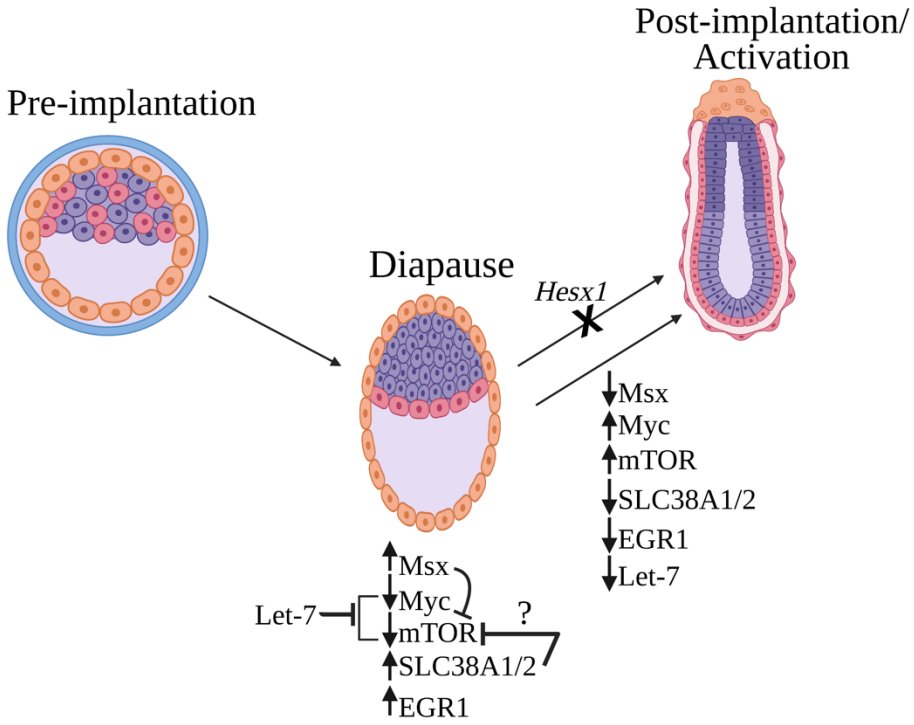

Figure 5.1: proposed model of embryonic diapause molecular regulation.

induction of diapause is associated with elevated levels of *Msx1*, *Egr1*, glutamine transporters *Slc38a1/2*, downregulation of Myc and mTOR. The microRNA let-7 is also highly upregulated in diapause and induces embryonic diapause by inhibiting both Myc/mTORC1 and mTORC2. MSX can potentially repress mTOR, whereas SLC38A1/2 might also inhibit activation of the mTOR complex. Mutation of the transcriptional repressor hesx1 in diapause disrupts exit from embryonic diapause and continuation of embryonic development after implantation. The figure was created with biorender.com.

Table 5.1: Changes in microRNA and their target genes in diapause compared to reactivated and post-implantation embryos

MicroRNA	Target gene	Context++ score percentile
mmu-miR-199a-3p	SLC38A1	75
mmu-miR-199b-3p	SLC38A1	75
mmu-miR-199a-3p	EGR1	87
mmu-miR-199b-3p	EGR1	87
mmu-miR-181-5p	EGR1	85
mmu-miR-181-5p	SLC38A2	84
mmu-let-7a-5p	RICTOR	83
mmu-let-7b-5p	RICTOR	83
mmu-let-7c-5p	RICTOR	83
mmu-let-7d-5p	RICTOR	85
mmu-let-7e-5p	RICTOR	83
mmu-let-7f-5p	RICTOR	82
mmu-let-7g-5p	RICTOR	84
mmu-let-7i-5p	RICTOR	84
mmu-let-7k	RICTOR	83

Red: upregulation; Blue: downregulation

APPENDIX A

Appendix A. Supplementary Information for Chapter 2

A.1 *Supplemental figures for Chapter 2*

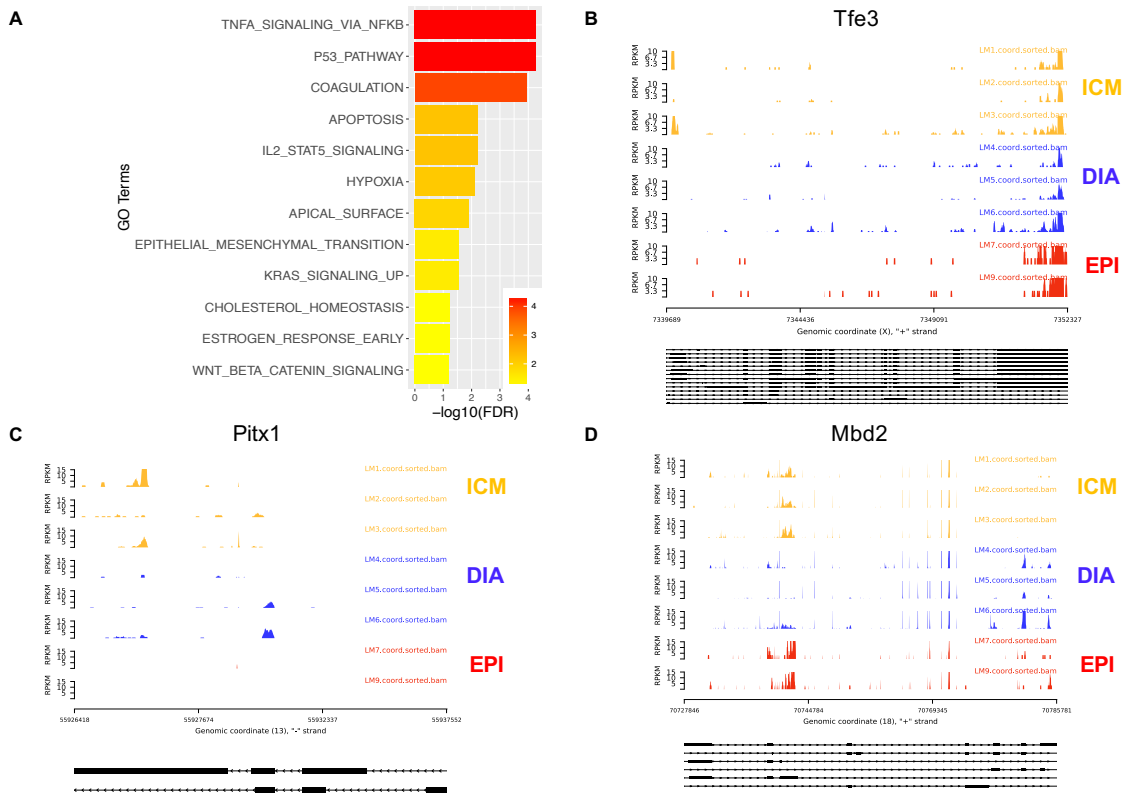

Figure Appendix A1: Differential splicing separates diapause from pre-implantation and post-implantation stages. *Related to Figure 2.2*

A. GO terms of pathways that were significantly enriched in genes upregulated in the diapause state compared to ICM. B-D. Differential splicing (long and short isoforms) of *Tfe3* (B), *Pitx1* (C), and *Mbd2* (D) between ICM, diapause and Epi.

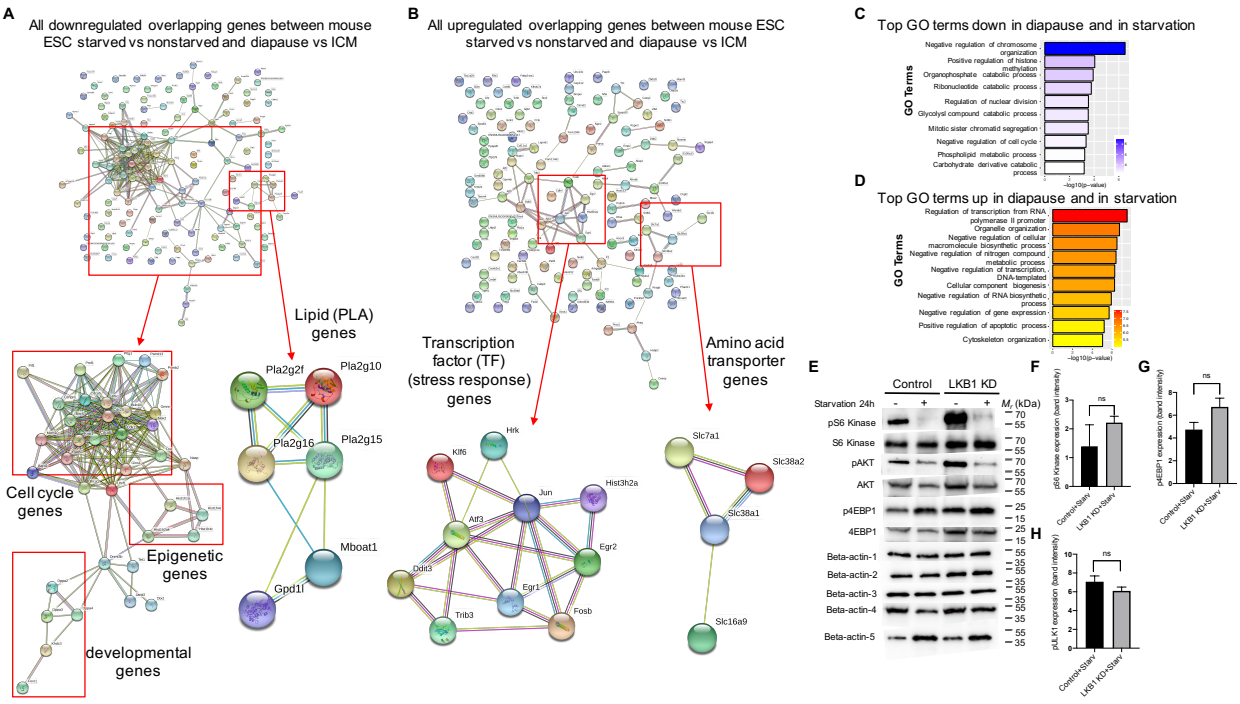

Figure Appendix A2: Starvation mimics diapause transcriptional profile. *Related to Figure 2.3*

A-B. String analysis of downregulated (A) and upregulated (B) overlapping genes between mouse ESC starved vs non-starved and diapause vs ICM. C-D. Top GO terms that were up (C) and down (D) in diapause were also highly upregulated (C) and downregulated (D) in starvation. E-H. Effect of *Lkb1* knock down (KD) in control and starved mESCs. E. Lkb1 siRNA knockdown expression of pS6 kinase, pAkt(S473), p4EBP1 at the protein level compared to the control luciferase siRNA. The efficiency of the transient siRNA approach was assessed at the protein level by western blotting coupled with densitometry for F) pS6 kinase, G) p4EBP1 and H) pULK1 in transiently transfected R1(LL) cells. (n=3 for all samples, S.e.m.; two-tailed t-test, ns: not significant). β-actin 1: for S6 kinase, β-actin 2: pS6 kinase, β-actin 3: pAkt(S473), β-actin 4: Akt, β-actin 5: p4EBP1.

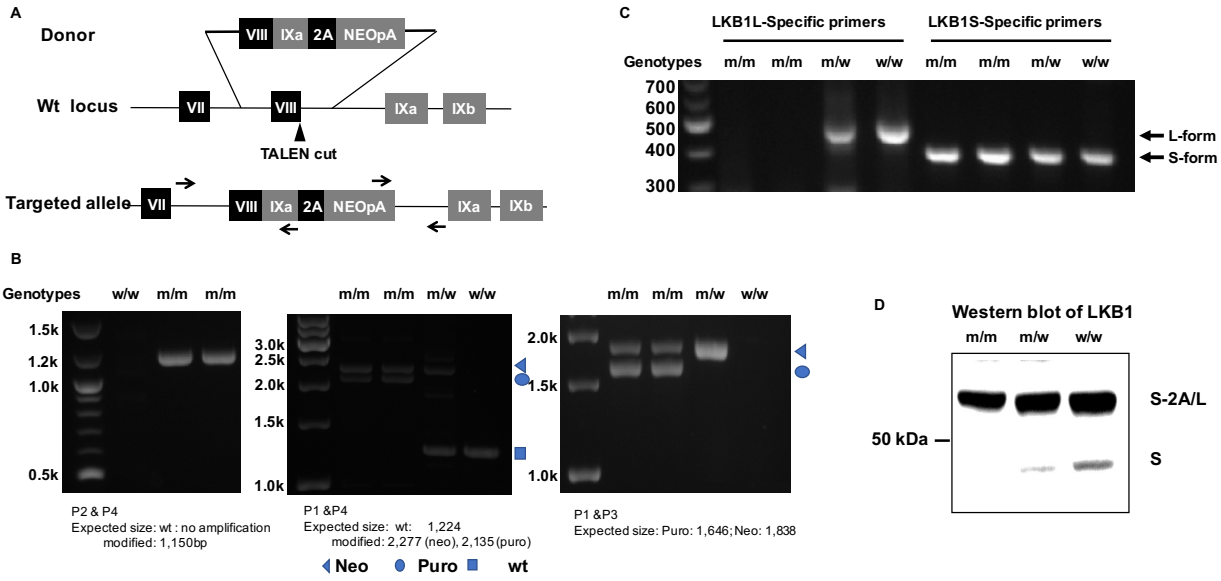

Figure Appendix A3: Generation of mESCs that express the short form of LKB1 using TALEN-based gene editing. *Related to Figure 2.4*

(A) Schematics of the donor, wt locus of *Lkb1* and the targeted allele. (B) Genotyping of mESCs. The primers are shown in A as arrows. The wt and modified alleles are indicated. M: modified alleles that express LKB1S only. W: wild type alleles. (C) RT-PCR analysis of LKB1L/S expression using long and short forms specific primers. (D) Western blot analysis showed that mESCs with both alleles modified express LKB1S only. mESCs with one allele modified express reduced level of LKB1S. The wild type mESCs express mostly LKB1L. LKB1S+2A peptide and LKB1L are the same size.

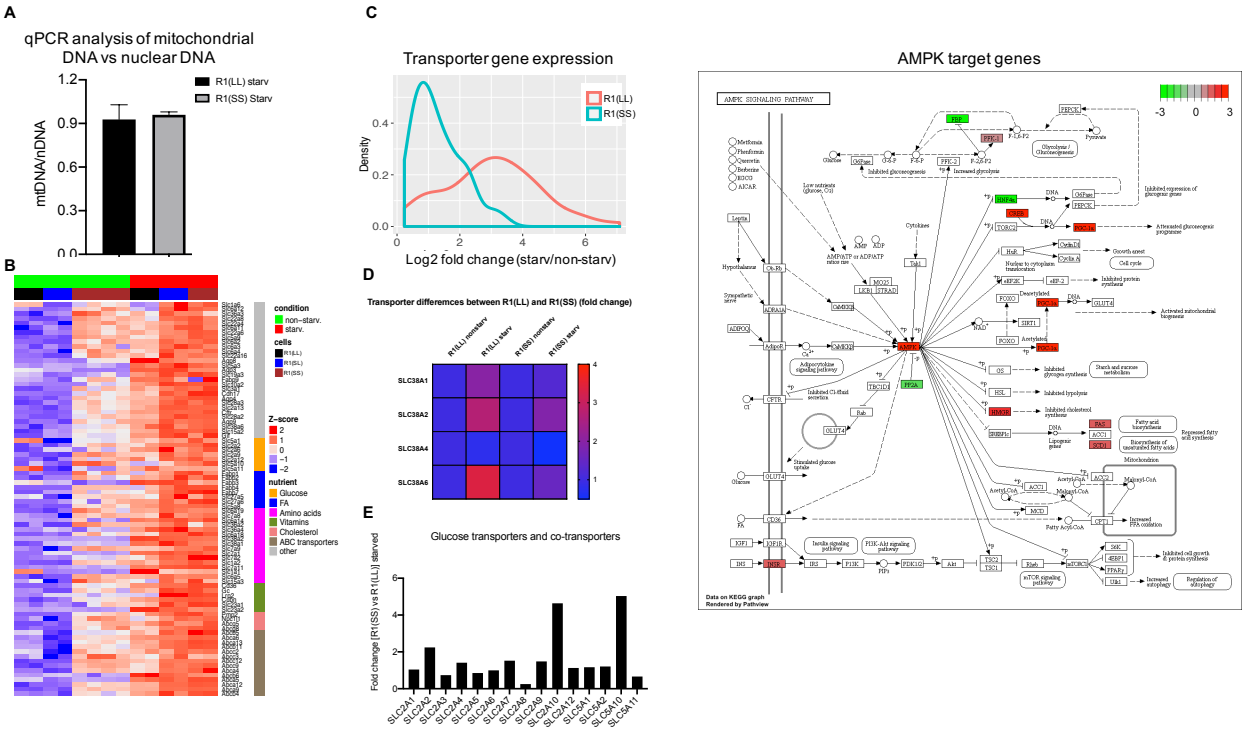

Figure Appendix A4: Lkb1 short lacks the capacity to respond to stress since most metabolic transporters are not upregulated. *Related to Figure 2.5*

(A) Mitochondrial DNA amount was assessed by measuring the ratio of mitochondrial DNA (mtDNA) versus nuclear DNA (nDNA) by qPCR analysis. (B) Heat map of metabolically relevant gene expression in response to starvation of cells carrying defined Lkb1 isoforms of R1(SS) cannot tolerate starvation since the metabolite transporters are not upregulated. (C) Log2 fold increase of transporter genes in response to starvation is larger in ESC with R1(LL) (diapause-like) than in R1(SS) isoform. Median log2 increase for 3.1 and 1.1 for R1(LL) and R1(SS) respectively. (D) Heat map of glutamine transporter differences between R1(LL) and R1(SS) in starved and non-starved conditions. (E) Some glucose transporters and co-transporters are upregulated in *Lkb1* short, R1(SS), compared to *Lkb1* long, R1 (LL) under starvation. *Slc2a2* (glut 2), *Slc2a10*, and *Slc5a10* were highly upregulated in *Lkb1* short, R1(SS) compared to *Lkb1*

long, R1(LL) under starvation. (F) AMPK target genes are upregulated in diapause. AMPK and its target genes are upregulated in diapause compared to ICM.

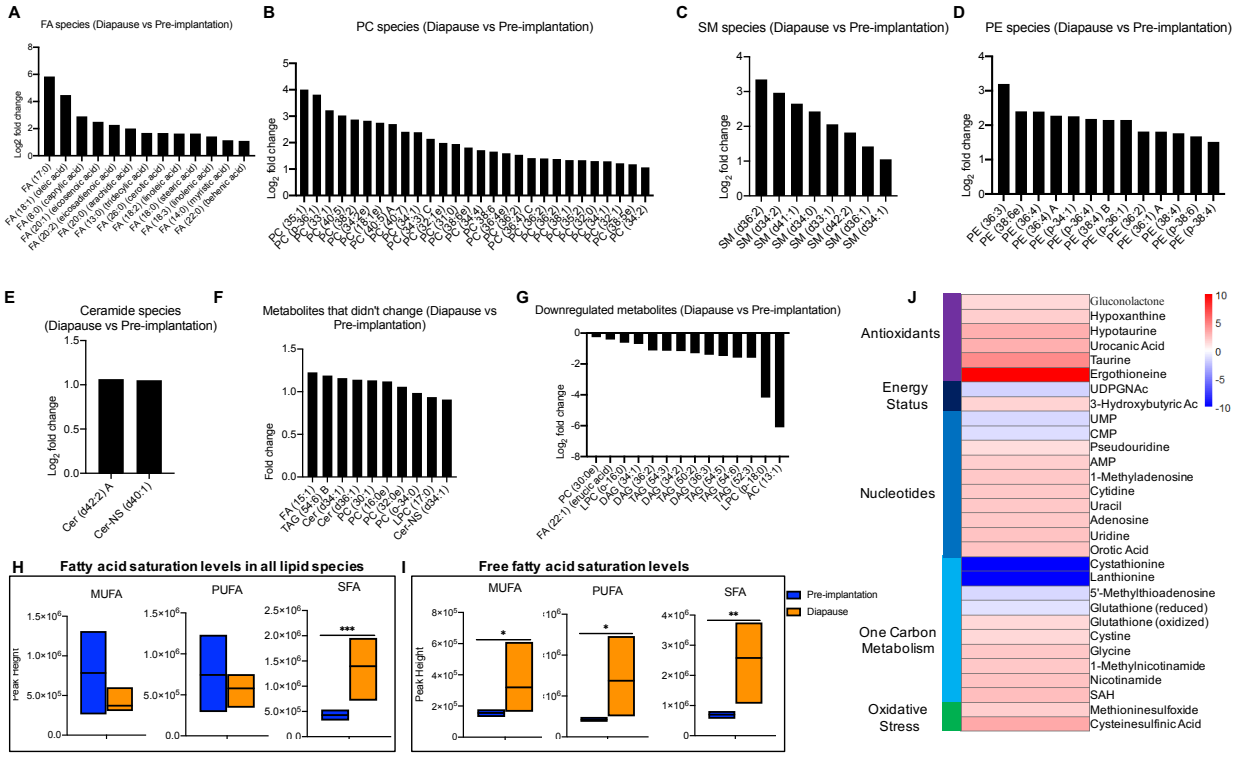

Figure Appendix A5: Lipidome changes during diapause and pre-implantation blastocyst.

Related to Figure 2.6

(A-E) Lipid species that were upregulated in diapause compared to pre-implantation. Log2 fold change of fatty acid (A), phosphatidylcholine (PC), (B), sphingomyelin (C), phosphatidylethanolamine (PE) (D), and ceramide species (E) between the diapause and pre-implantation blastocyst. (F) Fold change of lipid metabolites that didn't change between the 2 stages. (G) Log2 fold change of metabolites that were downregulated in diapause blastocysts. (H,I) Ratio of SFA, MUFA and PUFA of diapause and pre-implantation in all lipids (H) and free fatty acids (I). (J) Heat map of polar metabolites grouped based on their physiological activities or the metabolic pathways they are involved. SFA: saturated fatty acid; MUFA: mono-unsaturated fatty acid; PUFA: poly-unsaturated fatty acid.

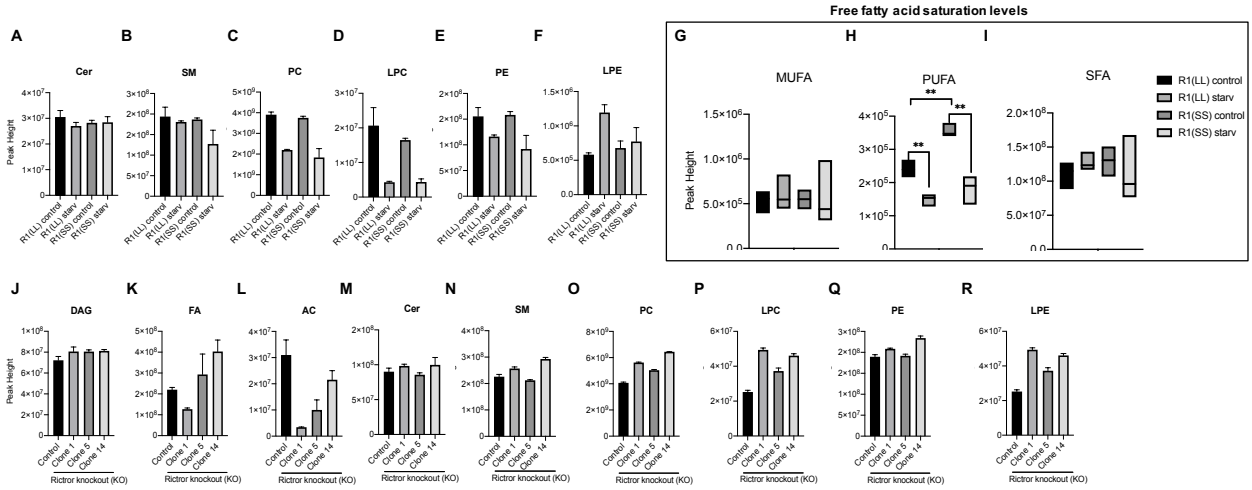

Figure Appendix A6: Starvation of mESCs and mTORC2 inactivation upregulates lipolysis. *Related to Figure 2.7*

Starvation of mESCs upregulates lipolysis resulting in a diapause-like lipidomics pattern (A-F) Changes in lipid species between R1(LL) starved vs non-starved and R1(SS) starved vs non-starved. Peak heights of ceramide (Cer) (A), sphingomyelin (SM) (B), phosphatidylcholine (PC) (C), Lyso-phosphatidylcholine (LPC) (D) phosphatidylethanolamine (PE) (E), and Lyso-phosphatidylethanolamine (LPE) (F) in a diapause-like state. (G,H,I) Ratio of MUFA (G), PUFA (H) and SFA (I) levels of both R1(LL) and R1(SS) in control and in starvation-induced diapause-like state in free fatty acids.

mTORC2 inactivation by *Rictor* KO in mESCs upregulates lipolysis resulting in diapause-like lipidomics pattern (J-R). Changes in lipid species between wild-type *Rictor* and *Rictor* knockout mutant clones. Peak heights of diacylglycerol (DAG) (J), fatty acids (FA) (K), acylcarnitine (AC) (L), ceramide (Cer) (M), sphingomyelin (SM) (N), phosphatidylcholine (PC) (O), Lyso-phosphatidylcholine (LPC) (P) phosphatidylethanolamine (PE) (Q), and Lyso-phosphatidylethanolamine (LPE) (R).

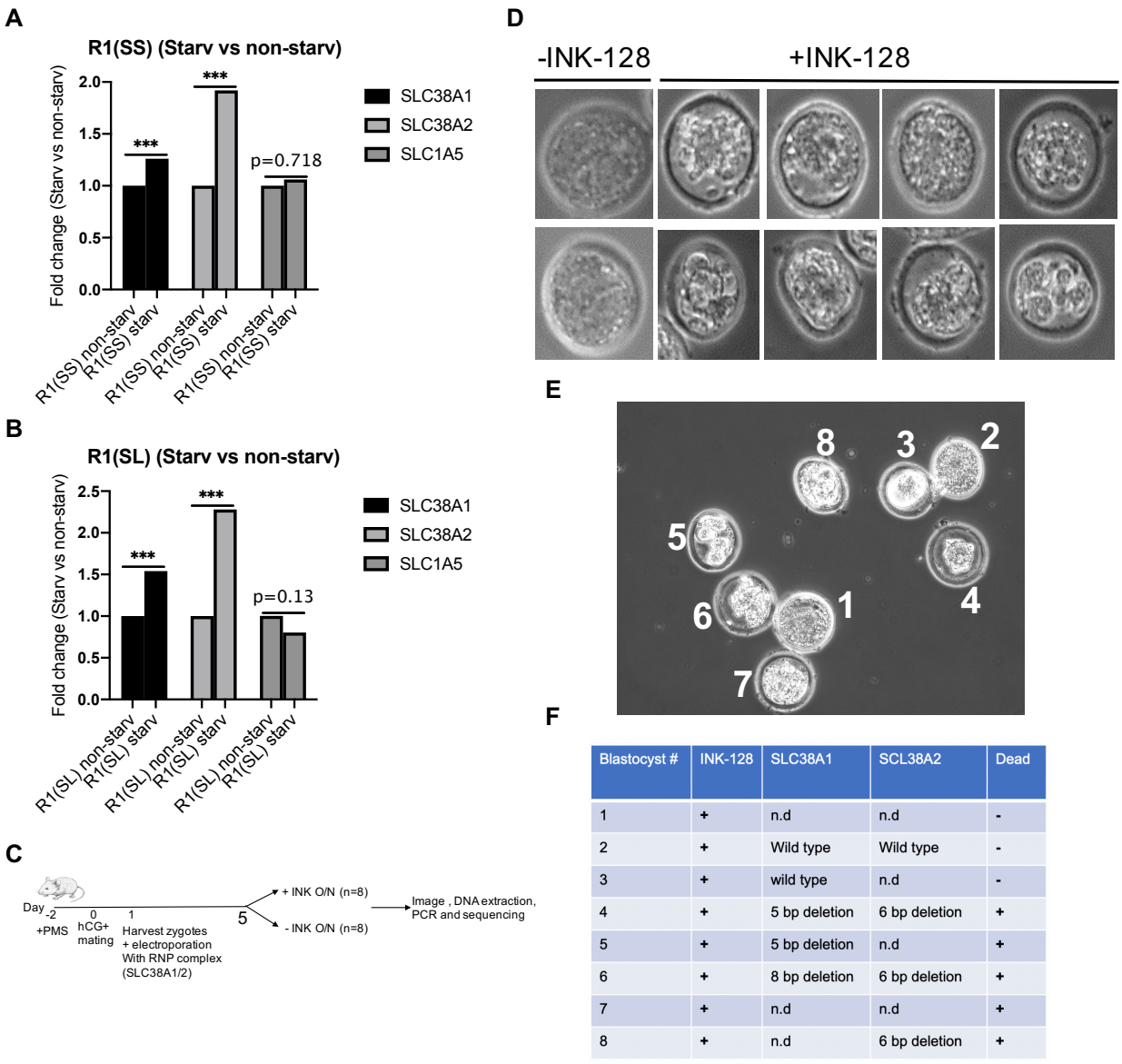

Blastocyst #	INK-128	SLC38A1	SCL38A2	Dead
1	+	n.d	n.d	-
2	+	Wild type	Wild type	-
3	+	wild type	n.d	-
4	+	5 bp deletion	6 bp deletion	+
5	+	5 bp deletion	n.d	+
6	+	8 bp deletion	6 bp deletion	+
7	+	n.d	n.d	+
8	+	n.d	6 bp deletion	+

Figure Appendix A7: Knockout (KO) of SLC38A1 and SLC38A2 in mouse embryos prevents a diapause-like stage induced by INK-128. *Related to Figure 2.8*

Differential expression of glutamine transporters between starvation-induced diapause-like state and non-starved cells (A,B) Glutamine transporters, *Slc38a1*, *Slc38a2* and *Slc1a5* were upregulated in LKB1 splice variants, R1(SS) (A) and R1(SL) (B), between starvation-induced diapause-like state and non-starved cells. (C) Schematic diagram depicting outline of the

CRISPR knockout of glutamine transporters (SLC38A1 and SLC38A2) in mouse zygotes. (D) Images of glutamine transporter knockout mouse embryos treated with or without INK-128 to induce a diapause-like state. (E,F) INK-128 treated mouse embryos (E) and their corresponding DNA sequencing results (F) after extracting DNA from the glutamine transporters knockout mouse embryos. n.d: not detected.

APPENDIX B

Appendix B. Supplementary Information for Chapter 3

B.1 *Supplemental figures for Chapter 3*

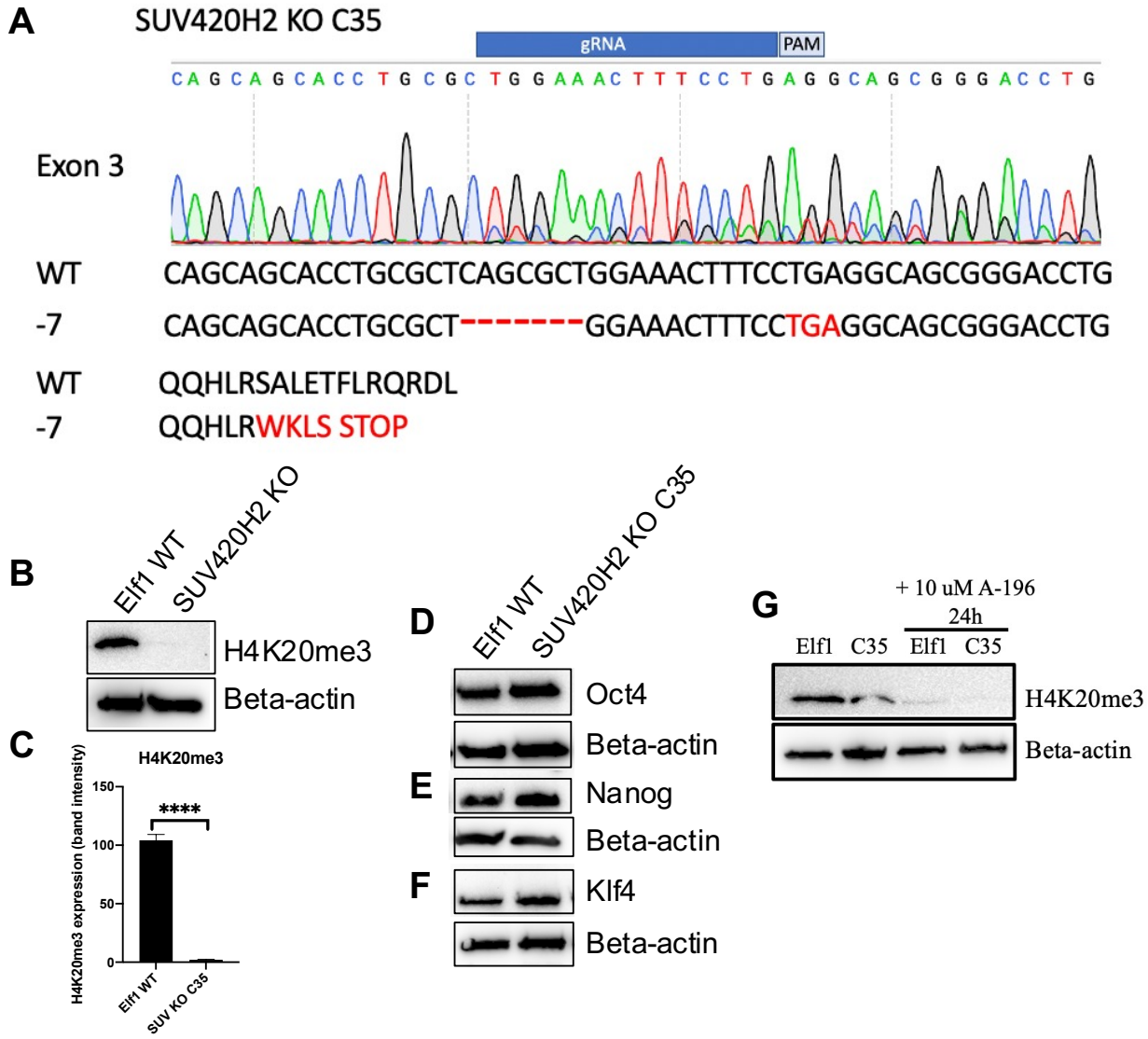

Figure Appendix B1: SUV420H2 KO hESC express naïve pluripotency markers. *Related to Figure 3.1 and 3.2*

(A) Sanger sequencing analysis of Elf1 2iL-I-F SUV420H2 KO hESC clone 35 reveals introduction of STOP codons in exons 3 after 7 base pair deletions. (B) Western blot showing

absence of H4K20me3 protein expression in the mutant line. (C) Quantification of H4K20me3 expression from (B). Expression of pluripotent markers OCT4 (D), NANOG (E) and KLF4 (F). (G) Western blot analysis showing H4K20me3 expression after treatment of wildtype and SUV420H2 mutant cells with A-196 for 24 hours. S.e.m.; *: = $p < 0.05$; **= $p < 0.01$; ***: $p < 0.001$; ****: $p < 0.0001$; two-tailed t-test, n = 3 biological replicates.

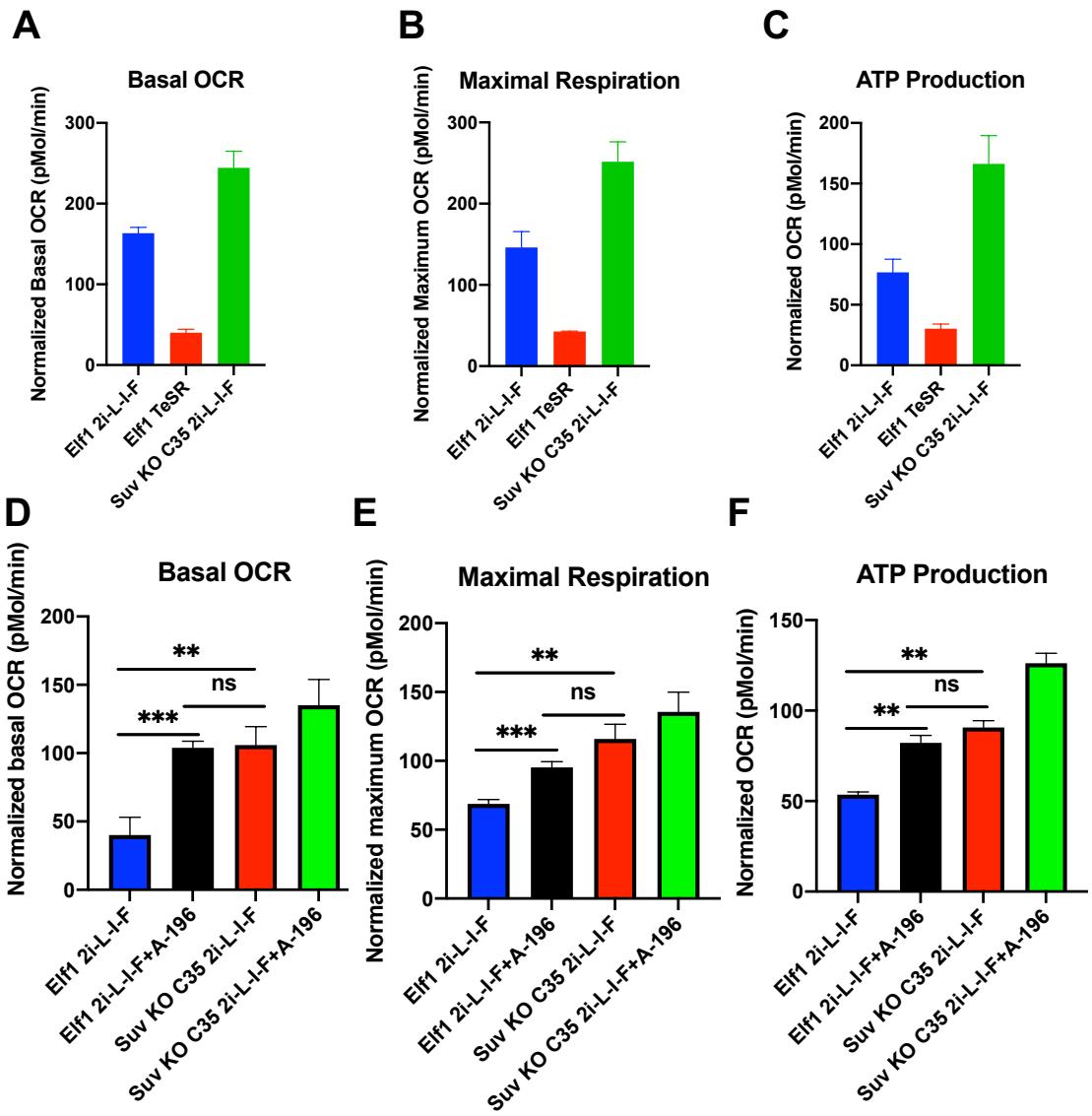

Figure Appendix B2: SUV420H2 KO hESCs have an increased mitochondrial activity compared to wildtype naïve and primed hESCs. *Related to Figure 3.3*

(A) Metabolic flux of wildtype and KO SUV420H2 hESCs using the Seahorse analyzer. Quantification of basal OCR (A), maximum OCR (B), and maximum ATP production (C) between SUV420H2 KO C35 2i-L-I-F compared to Elf1 wildtype 2i-L-I-F and Elf1 TeSR. Wildtype Elf12i-L-I-F and SUV420H2 KO C35 2i-L-I-F were treated with SUV420H2 inhibitor, A-196, and a mitostress assay was performed. Quantification of basal OCR (D), maximum OCR

(E), and maximum ATP production (F) after overnight A-196 treatment. S.e.m.; ns: P >0.05; *: = $p < 0.05$; **= $p < 0.01$; ***: $p < 0.001$; ****: $p < 0.0001$; two-tailed t-test, n = 3 biological replicates.

VITA

Abdiasis Hussein Mohamed Jama Farah was born in Somalia and lived in Kenya before he moved to San Diego, California, USA as a teenager. Abdiasis obtained an Associate of Science in Chemistry from San Diego Mesa College. He was a Research Trainee in the NIH/NIGMS-funded San Diego Mesa College Bridges to the Baccalaureate Program and worked under the supervision of Dr. Edward Alexander. Abdiasis completed his Bachelor of Science in Biochemistry from the University of California Los Angeles (UCLA), where he was a Jack Kent Cooke, American Chemical Society and UCLA IMSD Scholar. At UCLA, he was an undergraduate researcher in the laboratories of Professors James Gober and Catherine Clarke. In the fall of 2015, Abdiasis moved to Seattle, Washington to pursue his PhD in Biochemistry at the University of Washington and performed his doctorate work at UW Institute for Stem Cell and Regenerative Medicine (ISCRM) in the laboratory of Dr. Hannele Ruohola-Baker. Abdiasis was a trainee in UW Biological Mechanisms of Healthy Aging Training Grant and UW Institute for Stem cells and Regenerative Medicine Fellows Program. When not working in the laboratory, Abdiasis enjoys traveling the world, spending quality time with his wife and kids and playing soccer with his friends. In the spring of 2021, he earned a Doctor of Philosophy (Ph.D.) at the University of Washington in Biochemistry.

REFERENCES

Achache, H., and Revel, A. (2006). Endometrial receptivity markers, the journey to successful embryo implantation. Hum Reprod Update *12*, 731-746. 10.1093/humupd/dml004.

Ackerman, D., Tumanov, S., Qiu, B., Michalopoulou, E., Spata, M., Azzam, A., Xie, H., Simon, M.C., and Kamphorst, J.J. (2018). Triglycerides Promote Lipid Homeostasis during Hypoxic Stress by Balancing Fatty Acid Saturation. Cell Rep *24*, 2596-2605.e2595. 10.1016/j.celrep.2018.08.015.

Agarwal, V., Bell, G.W., Nam, J.W., and Bartel, D.P. (2015). Predicting effective microRNA target sites in mammalian mRNAs. Elife *4*. 10.7554/eLife.05005.

Alexa, A., Rahnenführer, J., and Lengauer, T. (2006). Improved scoring of functional groups from gene expression data by decorrelating GO graph structure. Bioinformatics *22*, 1600-1607. 10.1093/bioinformatics/btl140.

Altman, B.J., Stine, Z.E., and Dang, C.V. (2016). From Krebs to clinic: glutamine metabolism to cancer therapy. Nat Rev Cancer *16*, 749. 10.1038/nrc.2016.114.

Alvarez-Garcia, I., and Miska, E.A. (2005). MicroRNA functions in animal development and human disease. Development *132*, 4653-4662. 10.1242/dev.02073.

Amundson, S.A., Myers, T.G., and Fornace, A.J. (1998). Roles for p53 in growth arrest and apoptosis: putting on the brakes after genotoxic stress. Oncogene *17*, 3287-3299. 10.1038/sj.onc.1202576.

Anders, S., and Huber, W. (2010). Differential expression analysis for sequence count data. Genome Biol *11*, R106. 10.1186/gb-2010-11-10-r106.

Anders, S., Pyl, P.T., and Huber, W. (2015). HTSeq--a Python framework to work with high-throughput sequencing data. Bioinformatics *31*, 166-169. 10.1093/bioinformatics/btu638.

Andoniadou, C.L., Signore, M., Sajedi, E., Gaston-Massuet, C., Kelberman, D., Burns, A.J., Itasaki, N., Dattani, M., and Martinez-Barbera, J.P. (2007). Lack of the murine homeobox gene Hesx1 leads to a posterior transformation of the anterior forebrain. Development *134*, 1499-1508. 10.1242/dev.02829.

Arena, R., Bisogno, S., Gąsior, Ł., Rudnicka, J., Bernhardt, L., Haaf, T., Zacchini, F., Bochenek, M., Fic, K., Bik, E., et al. (2021). Lipid droplets in mammalian eggs are utilized during embryonic diapause. Proc Natl Acad Sci U S A *118*. 10.1073/pnas.2018362118.

Artoni, F., Kreipke, R.E., Palmeira, O., Dixon, C., Goldberg, Z., and Ruohola-Baker, H. (2017). Loss of. Elife *6*. 10.7554/eLife.27842.

Aubrey, B.J., Kelly, G.L., Janic, A., Herold, M.J., and Strasser, A. (2018). How does p53 induce apoptosis and how does this relate to p53-mediated tumour suppression? Cell Death Differ *25*, 104-113. 10.1038/cdd.2017.169.

Barroso, M., Kao, D., Blom, H.J., Tavares de Almeida, I., Castro, R., Loscalzo, J., and Handy, D.E. (2016). S-adenosylhomocysteine induces inflammation through NFkB: A possible role for EZH2 in endothelial cell activation. Biochim Biophys Acta *1862*, 82-92. 10.1016/j.bbadis.2015.10.019.

Bartel, D.P. (2009). MicroRNAs: target recognition and regulatory functions. Cell *136*, 215-233. 10.1016/j.cell.2009.01.002.

Barupal, D.K., and Fiehn, O. (2017). Chemical Similarity Enrichment Analysis (ChemRICH) as alternative to biochemical pathway mapping for metabolomic datasets. Sci Rep *7*, 14567. 10.1038/s41598-017-15231-w.

Battle, S.L., Doni Jayavelu, N., Azad, R.N., Hesson, J., Ahmed, F.N., Overbey, E.G., Zoller, J.A., Mathieu, J., Ruohola-Baker, H., Ware, C.B., and Hawkins, R.D. (2019). Enhancer Chromatin and 3D Genome Architecture Changes from Naive to Primed Human Embryonic Stem Cell States. Stem Cell Reports *12*, 1129-1144. 10.1016/j.stemcr.2019.04.004.

Blanpain, C., Lowry, W.E., Geoghegan, A., Polak, L., and Fuchs, E. (2004). Self-renewal, multipotency, and the existence of two cell populations within an epithelial stem cell niche. Cell *118*, 635-648. 10.1016/j.cell.2004.08.012.

Boroviak, T., Loos, R., Lombard, P., Okahara, J., Behr, R., Sasaki, E., Nichols, J., Smith, A., and Bertone, P. (2015). Lineage-Specific Profiling Delineates the Emergence and Progression of Naive Pluripotency in Mammalian Embryogenesis. Dev Cell *35*, 366-382. 10.1016/j.devcel.2015.10.011.

Botuyan, M.V., Lee, J., Ward, I.M., Kim, J.E., Thompson, J.R., Chen, J., and Mer, G. (2006). Structural basis for the methylation state-specific recognition of histone H4-K20 by 53BP1 and Crb2 in DNA repair. Cell *127*, 1361-1373. 10.1016/j.cell.2006.10.043.

Brons, I.G., Smithers, L.E., Trotter, M.W., Rugg-Gunn, P., Sun, B., Chuva de Sousa Lopes, S.M., Howlett, S.K., Clarkson, A., Ahrlund-Richter, L., Pedersen, R.A., and Vallier, L. (2007). Derivation of pluripotent epiblast stem cells from mammalian embryos. Nature *448*, 191-195. 10.1038/nature05950.

Bulut-Karslioglu, A., Biechele, S., Jin, H., Macrae, T.A., Hejna, M., Gertsenstein, M., Song, J.S., and Ramalho-Santos, M. (2016). Inhibition of mTOR induces a paused pluripotent state. Nature *540*, 119-123. 10.1038/nature20578.

Cai, H., Dong, L.Q., and Liu, F. (2016). Recent Advances in Adipose mTOR Signaling and Function: Therapeutic Prospects. Trends Pharmacol Sci *37*, 303-317. 10.1016/j.tips.2015.11.011.

Cajka, T. (2016). Increasing lipidomic coverage by selecting optimal mobile-phase modifiers in LC–MS of blood plasma. Metabolomics *12*, 1-11.

Cha, J., Burnum-Johnson, K.E., Bartos, A., Li, Y., Baker, E.S., Tilton, S.C., Webb-Robertson, B.J., Piehowski, P.D., Monroe, M.E., Jegga, A.G., et al. (2015). Muscle Segment Homeobox Genes Direct Embryonic Diapause by Limiting Inflammation in the Uterus. J Biol Chem *290*, 15337-15349. 10.1074/jbc.M115.655001.

Cha, J., Fenelon, J.C., Murphy, B.D., Shaw, G., Renfree, M.B., and Dey, S.K. (2020). A role for Msx genes in mammalian embryonic diapause. Biosci Proc *10*, 44-51. 10.1530/biosciprocs.10.002.

Cha, J., Sun, X., Bartos, A., Fenelon, J., Lefèvre, P., Daikoku, T., Shaw, G., Maxson, R., Murphy, B.D., Renfree, M.B., and Dey, S.K. (2013). A new role for muscle segment homeobox genes in mammalian embryonic diapause. Open Biol *3*, 130035. 10.1098/rsob.130035.

Chan, D.C. (2006). Mitochondria: dynamic organelles in disease, aging, and development. Cell *125*, 1241-1252. 10.1016/j.cell.2006.06.010.

Chan, Y.S., Göke, J., Ng, J.H., Lu, X., Gonzales, K.A., Tan, C.P., Tng, W.Q., Hong, Z.Z., Lim, Y.S., and Ng, H.H. (2013a). Induction of a human pluripotent state with distinct regulatory circuitry that resembles preimplantation epiblast. Cell Stem Cell *13*, 663-675. 10.1016/j.stem.2013.11.015.

Chan, Y.S., Göke, J., Ng, J.H., Lu, X., Gonzales, K.A., Tan, C.P., Tng, W.Q., Hong, Z.Z., Lim, Y.S., and Ng, H.H. (2013b). Induction of a human pluripotent state with distinct regulatory circuitry that resembles preimplantation epiblast. Cell Stem Cell *13*, 663-675. 10.1016/j.stem.2013.11.015.

Chao, H.X., Poovey, C.E., Privette, A.A., Grant, G.D., Chao, H.Y., Cook, J.G., and Purvis, J.E. (2017). Orchestration of DNA Damage Checkpoint Dynamics across the Human Cell Cycle. Cell Syst *5*, 445-459.e445. 10.1016/j.cels.2017.09.015.

Chen, J. (2016). The Cell-Cycle Arrest and Apoptotic Functions of p53 in Tumor Initiation and Progression. Cold Spring Harb Perspect Med *6*, a026104. 10.1101/cshperspect.a026104.

Chen, M., Reed, R.R., and Lane, A.P. (2019). Chronic Inflammation Directs an Olfactory Stem Cell Functional Switch from Neuroregeneration to Immune Defense. Cell Stem Cell *25*, 501-513.e505. 10.1016/j.stem.2019.08.011.

Chen, S., Lee, B., Lee, A.Y., Modzelewski, A.J., and He, L. (2016). Highly Efficient Mouse Genome Editing by CRISPR Ribonucleoprotein Electroporation of Zygotes. J Biol Chem *291*, 14457-14467. 10.1074/jbc.M116.733154.

Cheong, A.W., Pang, R.T., Liu, W.M., Kottawatta, K.S., Lee, K.F., and Yeung, W.S. (2014). MicroRNA Let-7a and dicer are important in the activation and implantation of delayed implanting mouse embryos. Hum Reprod *29*, 750-762. 10.1093/humrep/det462.

Cheshier, S.H., Morrison, S.J., Liao, X., and Weissman, I.L. (1999). In vivo proliferation and cell cycle kinetics of long-term self-renewing hematopoietic stem cells. Proc Natl Acad Sci U S A *96*, 3120-3125. 10.1073/pnas.96.6.3120.

Cheung, T.H., and Rando, T.A. (2013). Molecular regulation of stem cell quiescence. Nat Rev Mol Cell Biol *14*, 329-340. 10.1038/nrm3591.

Chia, N.Y., Chan, Y.S., Feng, B., Lu, X., Orlov, Y.L., Moreau, D., Kumar, P., Yang, L., Jiang, J., Lau, M.S., et al. (2010a). A genome-wide RNAi screen reveals determinants of human embryonic stem cell identity. Nature *468*, 316-320. 10.1038/nature09531.

Chia, N.Y., Chan, Y.S., Feng, B., Lu, X., Orlov, Y.L., Moreau, D., Kumar, P., Yang, L., Jiang, J., Lau, M.S., et al. (2010b). A genome-wide RNAi screen reveals determinants of human embryonic stem cell identity. Nature *468*, 316-320. 10.1038/nature09531.

Cho, I.J., Lui, P.P., Obajdin, J., Riccio, F., Stroukov, W., Willis, T.L., Spagnoli, F., and Watt, F.M. (2019). Mechanisms, Hallmarks, and Implications of Stem Cell Quiescence. Stem Cell Reports *12*, 1190-1200. 10.1016/j.stemcr.2019.05.012.

Chu, I., Sun, J., Arnaout, A., Kahn, H., Hanna, W., Narod, S., Sun, P., Tan, C.K., Hengst, L., and Slingerland, J. (2007). p27 phosphorylation by Src regulates inhibition of cyclin E-Cdk2. Cell *128*, 281-294. 10.1016/j.cell.2006.11.049.

Clarke, M.F., Dick, J.E., Dirks, P.B., Eaves, C.J., Jamieson, C.H., Jones, D.L., Visvader, J., Weissman, I.L., and Wahl, G.M. (2006). Cancer stem cells--perspectives on current status and future directions: AACR Workshop on cancer stem cells. Cancer Res *66*, 9339-9344. 10.1158/0008-5472.CAN-06-3126.

Codega, P., Silva-Vargas, V., Paul, A., Maldonado-Soto, A.R., Deleo, A.M., Pastrana, E., and Doetsch, F. (2014). Prospective identification and purification of quiescent adult neural stem cells from their in vivo niche. Neuron *82*, 545-559. 10.1016/j.neuron.2014.02.039.

Coller, H.A., Sang, L., and Roberts, J.M. (2006). A new description of cellular quiescence. PLoS Biol *4*, e83. 10.1371/journal.pbio.0040083.

Concordet, J.P., and Haeussler, M. (2018). CRISPOR: intuitive guide selection for CRISPR/Cas9 genome editing experiments and screens. Nucleic Acids Res *46*, W242-W245. 10.1093/nar/gky354.

Corti, O., Lesage, S., and Brice, A. (2011). What genetics tells us about the causes and mechanisms of Parkinson's disease. Physiol Rev *91*, 1161-1218. 10.1152/physrev.00022.2010.

Daignan-Fornier, B., and Sagot, I. (2011). Proliferation/quiescence: the controversial "aller-retour". Cell Div *6*, 10. 10.1186/1747-1028-6-10.

Daikoku, T., Cha, J., Sun, X., Tranguch, S., Xie, H., Fujita, T., Hirota, Y., Lydon, J., DeMayo, F., Maxson, R., and Dey, S.K. (2011). Conditional deletion of Msx homeobox genes in the uterus inhibits blastocyst implantation by altering uterine receptivity. Dev Cell *21*, 1014-1025. 10.1016/j.devcel.2011.09.010.

Dattani, M.T., Martinez-Barbera, J.P., Thomas, P.Q., Brickman, J.M., Gupta, R., Mårtensson, I.L., Toresson, H., Fox, M., Wales, J.K., Hindmarsh, P.C., et al. (1998). Mutations in the homeobox gene HESX1/Hesx1 associated with septo-optic dysplasia in human and mouse. Nat Genet *19*, 125-133. 10.1038/477.

de Koning, T.J., Snell, K., Duran, M., Berger, R., Poll-The, B.T., and Surtees, R. (2003). L-serine in disease and development. Biochem J *371*, 653-661. 10.1042/BJ20021785.

Deng, X., Berletch, J.B., Ma, W., Nguyen, D.K., Hiatt, J.B., Noble, W.S., Shendure, J., and Disteche, C.M. (2013). Mammalian X upregulation is associated with enhanced transcription initiation, RNA half-life, and MOF-mediated H4K16 acetylation. Dev Cell *25*, 55-68. 10.1016/j.devcel.2013.01.028.

Denison, F.C., Hiscock, N.J., Carling, D., and Woods, A. (2009). Characterization of an alternative splice variant of LKB1. J Biol Chem *284*, 67-76. 10.1074/jbc.M806153200.

Dhimolea, E., de Matos Simoes, R., Kansara, D., Al'Khafaji, A., Bouyssou, J., Weng, X., Sharma, S., Raja, J., Awate, P., Shirasaki, R., et al. (2021). An Embryonic Diapause-like Adaptation with Suppressed Myc Activity Enables Tumor Treatment Persistence. Cancer Cell *39*, 240-256.e211. 10.1016/j.ccell.2020.12.002.

Ehnes, D.D., Hussein, A.M., Ware, C.B., Mathieu, J., and Ruohola-Baker, H. (2020). Combinatorial metabolism drives the naive to primed pluripotent chromatin landscape. Exp Cell Res *389*, 111913. 10.1016/j.yexcr.2020.111913.

Eid, A., Rodriguez-Terrones, D., Burton, A., and Torres-Padilla, M.E. (2016). SUV4-20 activity in the preimplantation mouse embryo controls timely replication. Genes Dev *30*, 2513-2526. 10.1101/gad.288969.116.

Ejma, M., Madetko, N., Brzecka, A., Guranski, K., Alster, P., Misiuk-Hojło, M., Somasundaram, S.G., Kirkland, C.E., and Aliev, G. (2020). The Links between Parkinson's Disease and Cancer. Biomedicines *8*. 10.3390/biomedicines8100416.

el-Deiry, W.S., Tokino, T., Velculescu, V.E., Levy, D.B., Parsons, R., Trent, J.M., Lin, D., Mercer, W.E., Kinzler, K.W., and Vogelstein, B. (1993). WAF1, a potential mediator of p53 tumor suppression. Cell *75*, 817-825. 10.1016/0092-8674(93)90500-p.

Farioli-Vecchioli, S., Micheli, L., Saraulli, D., Ceccarelli, M., Cannas, S., Scardigli, R., Leonardi, L., Cinà, I., Costanzi, M., Ciotti, M.T., et al. (2012). Btg1 is Required to Maintain the Pool of Stem and Progenitor Cells of the Dentate Gyrus and Subventricular Zone. Front Neurosci *6*, 124. 10.3389/fnins.2012.00124.

Fenelon, J.C., Banerjee, A., and Murphy, B.D. (2014). Embryonic diapause: development on hold. Int J Dev Biol *58*, 163-174. 10.1387/ijdb.140074bm.

Ferreccio, A., Mathieu, J., Detraux, D., Somasundaram, L., Cavanaugh, C., Sopher, B., Fischer, K., Bello, T., M Hussein, A., Levy, S., et al. (2018). Inducible CRISPR genome editing platform in naive human embryonic stem cells reveals JARID2 function in self-renewal. Cell Cycle *17*, 535-549. 10.1080/15384101.2018.1442621.

Filosa, S., Fico, A., Paglialunga, F., Balestrieri, M., Crooke, A., Verde, P., Abrescia, P., Bautista, J.M., and Martini, G. (2003). Failure to increase glucose consumption through the pentose-phosphate pathway

results in the death of glucose-6-phosphate dehydrogenase gene-deleted mouse embryonic stem cells subjected to oxidative stress. Biochem J *370*, 935-943. 10.1042/BJ20021614.

Forster, N., and Ellisen, L.W. (2011). Notch signaling mediates p63-induced quiescence: a new facet of p63/Notch crosstalk. Cell Cycle *10*, 3632-3633. 10.4161/cc.10.21.18182.

Fraga, M.F., Ballestar, E., Villar-Garea, A., Boix-Chornet, M., Espada, J., Schotta, G., Bonaldi, T., Haydon, C., Ropero, S., Petrie, K., et al. (2005). Loss of acetylation at Lys16 and trimethylation at Lys20 of histone H4 is a common hallmark of human cancer. Nat Genet *37*, 391-400. 10.1038/ng1531.

Franzoni, F., Colognato, R., Galetta, F., Laurenza, I., Barsotti, M., Di Stefano, R., Bocchetti, R., Regoli, F., Carpi, A., Balbarini, A., et al. (2006). An in vitro study on the free radical scavenging capacity of ergothioneine: comparison with reduced glutathione, uric acid and trolox. Biomed Pharmacother *60*, 453-457. 10.1016/j.biopha.2006.07.015.

Fu, Z., Wang, B., Wang, S., Wu, W., Wang, Q., Chen, Y., Kong, S., Lu, J., Tang, Z., Ran, H., et al. (2014). Integral proteomic analysis of blastocysts reveals key molecular machinery governing embryonic diapause and reactivation for implantation in mice. Biol Reprod *90*, 52. 10.1095/biolreprod.113.115337.

Gafni, O., Weinberger, L., Mansour, A.A., Manor, Y.S., Chomsky, E., Ben-Yosef, D., Kalma, Y., Viukov, S., Maza, I., Zviran, A., et al. (2013). Derivation of novel human ground state naive pluripotent stem cells. Nature *504*, 282-286. 10.1038/nature12745.

Gao, X., Lee, K., Reid, M.A., Sanderson, S.M., Qiu, C., Li, S., Liu, J., and Locasale, J.W. (2018). Serine Availability Influences Mitochondrial Dynamics and Function through Lipid Metabolism. Cell Rep *22*, 3507-3520. 10.1016/j.celrep.2018.03.017.

Gao, X., Lin, S.H., Ren, F., Li, J.T., Chen, J.J., Yao, C.B., Yang, H.B., Jiang, S.X., Yan, G.Q., Wang, D., et al. (2016). Acetate functions as an epigenetic metabolite to promote lipid synthesis under hypoxia. Nat Commun *7*, 11960. 10.1038/ncomms11960.

Gardner, D.K., and Lane, M. (1993). Amino acids and ammonium regulate mouse embryo development in culture. Biol Reprod *48*, 377-385.

Gebert, L.F.R., and MacRae, I.J. (2019). Regulation of microRNA function in animals. Nat Rev Mol Cell Biol *20*, 21-37. 10.1038/s41580-018-0045-7.

Geisler, S., Holmström, K.M., Treis, A., Skujat, D., Weber, S.S., Fiesel, F.C., Kahle, P.J., and Springer, W. (2010). The PINK1/Parkin-mediated mitophagy is compromised by PD-associated mutations. Autophagy *6*, 871-878. 10.4161/auto.6.7.13286.

Geula, S., Moshitch-Moshkovitz, S., Dominissini, D., Mansour, A.A., Kol, N., Salmon-Divon, M., Hershkovitz, V., Peer, E., Mor, N., Manor, Y.S., et al. (2015). Stem cells. m6A mRNA methylation facilitates resolution of naïve pluripotency toward differentiation. Science *347*, 1002-1006. 10.1126/science.1261417.

González, I.M., Martin, P.M., Burdsal, C., Sloan, J.L., Mager, S., Harris, T., and Sutherland, A.E. (2012). Leucine and arginine regulate trophoblast motility through mTOR-dependent and independent pathways in the preimplantation mouse embryo. Dev Biol *361*, 286-300. 10.1016/j.ydbio.2011.10.021.

Green, D.R., and Kroemer, G. (2004). The pathophysiology of mitochondrial cell death. Science *305*, 626-629. 10.1126/science.1099320.

Grinsted, J., and Avery, B. (1996). A sporadic case of delayed implantation after in-vitro fertilization in the human? Hum Reprod *11*, 651-654. 10.1093/humrep/11.3.651.

Gründemann, D., Harlfinger, S., Golz, S., Geerts, A., Lazar, A., Berkels, R., Jung, N., Rubbert, A., and Schömig, E. (2005). Discovery of the ergothioneine transporter. Proc Natl Acad Sci U S A *102*, 5256-5261. 10.1073/pnas.0408624102.

Guo, B., Tian, X.C., Li, D.D., Yang, Z.Q., Cao, H., Zhang, Q.L., Liu, J.X., and Yue, Z.P. (2014a). Expression, regulation and function of Egr1 during implantation and decidualization in mice. Cell Cycle *13*, 2626-2640. 10.4161/15384101.2014.943581.

Guo, H., Zhu, P., Yan, L., Li, R., Hu, B., Lian, Y., Yan, J., Ren, X., Lin, S., Li, J., et al. (2014b). The DNA methylation landscape of human early embryos. Nature *511*, 606-610. 10.1038/nature13544.

Gwinn, D.M., Shackelford, D.B., Egan, D.F., Mihaylova, M.M., Mery, A., Vasquez, D.S., Turk, B.E., and Shaw, R.J. (2008). AMPK phosphorylation of raptor mediates a metabolic checkpoint. Mol Cell *30*, 214-226. 10.1016/j.molcel.2008.03.003.

Hahn, M., Dambacher, S., Dulev, S., Kuznetsova, A.Y., Eck, S., Wörz, S., Sadic, D., Schulte, M., Mallm, J.P., Maiser, A., et al. (2013). Suv4-20h2 mediates chromatin compaction and is important for cohesin recruitment to heterochromatin. Genes Dev *27*, 859-872. 10.1101/gad.210377.112.

Hamatani, T., Daikoku, T., Wang, H., Matsumoto, H., Carter, M.G., Ko, M.S., and Dey, S.K. (2004). Global gene expression analysis identifies molecular pathways distinguishing blastocyst dormancy and activation. Proc Natl Acad Sci U S A *101*, 10326-10331. 10.1073/pnas.0402597101.

Harper, J.W., Adami, G.R., Wei, N., Keyomarsi, K., and Elledge, S.J. (1993). The p21 Cdk-interacting protein Cip1 is a potent inhibitor of G1 cyclin-dependent kinases. Cell *75*, 805-816. 10.1016/0092-8674(93)90499-g.

Harrison, S.E., Sozen, B., Christodoulou, N., Kyprianou, C., and Zernicka-Goetz, M. (2017). Assembly of embryonic and extraembryonic stem cells to mimic embryogenesis in vitro. Science *356*. 10.1126/science.aal1810.

Hatfield, S.D., Shcherbata, H.R., Fischer, K.A., Nakahara, K., Carthew, R.W., and Ruohola-Baker, H. (2005). Stem cell division is regulated by the microRNA pathway. Nature *435*, 974-978. 10.1038/nature03816.

He, B., Zhang, H., Wang, J., Liu, M., Sun, Y., Guo, C., Lu, J., Wang, H., and Kong, S. (2019). Blastocyst activation engenders transcriptome reprogram affecting X-chromosome reactivation and inflammatory trigger of implantation. Proc Natl Acad Sci U S A *116*, 16621-16630. 10.1073/pnas.1900401116.

Holmes, B.F., Kurth-Kraczek, E.J., and Winder, W.W. (1999). Chronic activation of 5'-AMP-activated protein kinase increases GLUT-4, hexokinase, and glycogen in muscle. J Appl Physiol (1985) *87*, 1990-1995. 10.1152/jappl.1999.87.5.1990.

Hsieh, A.C., Liu, Y., Edlind, M.P., Ingolia, N.T., Janes, M.R., Sher, A., Shi, E.Y., Stumpf, C.R., Christensen, C., Bonham, M.J., et al. (2012). The translational landscape of mTOR signalling steers cancer initiation and metastasis. Nature *485*, 55-61. 10.1038/nature10912.

Hu, Z., Li, H., Jiang, H., Ren, Y., Yu, X., Qiu, J., Stablewski, A.B., Zhang, B., Buck, M.J., and Feng, J. (2020). Transient inhibition of mTOR in human pluripotent stem cells enables robust formation of mouse-human chimeric embryos. Sci Adv *6*, eaaz0298. 10.1126/sciadv.aaz0298.

Hue, L., and Rider, M.H. (1987). Role of fructose 2,6-bisphosphate in the control of glycolysis in mammalian tissues. Biochem J *245*, 313-324.

Hunter, S.M., Evans, Martin (1999). Non-surgical method for the induction of delayed implantation and recovery of viable blastocysts in rats and mice by the use of tamoxifen and Depo-Provera. In M. Evans, ed. WILEY -LISS.

Hussein, A.M., Wang, Y., Mathieu, J., Margaretha, L., Song, C., Jones, D.C., Cavanaugh, C., Miklas, J.W., Mahen, E., Showalter, M.R., et al. (2020). Metabolic Control over mTOR-Dependent Diapause-like State. Dev Cell *52*, 236-250.e237. 10.1016/j.devcel.2019.12.018.

Inoki, K., Zhu, T., and Guan, K.L. (2003). TSC2 mediates cellular energy response to control cell growth and survival. Cell *115*, 577-590.

Itahana, K., Dimri, G.P., Hara, E., Itahana, Y., Zou, Y., Desprez, P.Y., and Campisi, J. (2002). A role for p53 in maintaining and establishing the quiescence growth arrest in human cells. J Biol Chem *277*, 18206-18214. 10.1074/jbc.M201028200.

Jacob, B., and Osato, M. (2009). Stem cell exhaustion and leukemogenesis. J Cell Biochem *107*, 393-399. 10.1002/jcb.22150.

Jewell, J.L., Kim, Y.C., Russell, R.C., Yu, F.X., Park, H.W., Plouffe, S.W., Tagliabracci, V.S., and Guan, K.L. (2015). Metabolism. Differential regulation of mTORC1 by leucine and glutamine. Science *347*, 194-198. 10.1126/science.1259472.

Johnson, W.E., Li, C., and Rabinovic, A. (2007). Adjusting batch effects in microarray expression data using empirical Bayes methods. Biostatistics *8*, 118-127. 10.1093/biostatistics/kxj037.

Jones, D.C. (2016). Isolator: accurate and stable analysis of isoform-level expression in RNA- Seq experiments. BioRxiv.

Jones, K.M., Sarić, N., Russell, J.P., Andoniadou, C.L., Scambler, P.J., and Basson, M.A. (2015). CHD7 maintains neural stem cell quiescence and prevents premature stem cell depletion in the adult hippocampus. Stem Cells *33*, 196-210. 10.1002/stem.1822.

Kapoor-Vazirani, P., Kagey, J.D., and Vertino, P.M. (2011). SUV420H2-mediated H4K20 trimethylation enforces RNA polymerase II promoter-proximal pausing by blocking hMOF-dependent H4K16 acetylation. Mol Cell Biol *31*, 1594-1609. 10.1128/MCB.00524-10.

Karachentsev, D., Sarma, K., Reinberg, D., and Steward, R. (2005). PR-Set7-dependent methylation of histone H4 Lys 20 functions in repression of gene expression and is essential for mitosis. Genes Dev *19*, 431-435. 10.1101/gad.1263005.

Kho, A.T., Zhao, Q., Cai, Z., Butte, A.J., Kim, J.Y., Pomeroy, S.L., Rowitch, D.H., and Kohane, I.S. (2004). Conserved mechanisms across development and tumorigenesis revealed by a mouse development perspective of human cancers. Genes Dev *18*, 629-640. 10.1101/gad.1182504.

Kim, D., Langmead, B., and Salzberg, S.L. (2015). HISAT: a fast spliced aligner with low memory requirements. Nat Methods *12*, 357-360. 10.1038/nmeth.3317.

Kim, Y.C., and Guan, K.L. (2015). mTOR: a pharmacologic target for autophagy regulation. J Clin Invest *125*, 25-32. 10.1172/JCI73939.

Kind, T., Liu, K.H., Lee, D.Y., DeFelice, B., Meissen, J.K., and Fiehn, O. (2013). LipidBlast in silico tandem mass spectrometry database for lipid identification. Nat Methods *10*, 755-758. 10.1038/nmeth.2551.

Kohn, K.W. (1999). Molecular interaction map of the mammalian cell cycle control and DNA repair systems. Mol Biol Cell *10*, 2703-2734. 10.1091/mbc.10.8.2703.

Kouba, D.J., Nakano, H., Nishiyama, T., Kang, J., Uitto, J., and Mauviel, A. (2001). Tumor necrosis factor-alpha induces distinctive NF-kappa B signaling within human dermal fibroblasts. J Biol Chem *276*, 6214-6224. 10.1074/jbc.M004511200.

Kourmouli, N., Jeppesen, P., Mahadevhaiah, S., Burgoyne, P., Wu, R., Gilbert, D.M., Bongiorni, S., Prantera, G., Fanti, L., Pimpinelli, S., et al. (2004). Heterochromatin and tri-methylated lysine 20 of histone H4 in animals. J Cell Sci *117*, 2491-2501. 10.1242/jcs.01238.

Kreitzer, F.R., Salomonis, N., Sheehan, A., Huang, M., Park, J.S., Spindler, M.J., Lizarraga, P., Weiss, W.A., So, P.L., and Conklin, B.R. (2013). A robust method to derive functional neural crest cells from human pluripotent stem cells. Am J Stem Cells *2*, 119-131.

Kuppusamy, K.T., Jones, D.C., Sperber, H., Madan, A., Fischer, K.A., Rodriguez, M.L., Pabon, L., Zhu, W.Z., Tulloch, N.L., Yang, X., et al. (2015). Let-7 family of microRNA is required for maturation and

adult-like metabolism in stem cell-derived cardiomyocytes. Proc Natl Acad Sci U S A *112*, E2785-2794. 10.1073/pnas.1424042112.

Kurth-Kraczek, E.J., Hirshman, M.F., Goodyear, L.J., and Winder, W.W. (1999). 5' AMP-activated protein kinase activation causes GLUT4 translocation in skeletal muscle. Diabetes *48*, 1667-1671.

Kurtoglu, M., Gao, N., Shang, J., Maher, J.C., Lehrman, M.A., Wangpaichitr, M., Savaraj, N., Lane, A.N., and Lampidis, T.J. (2007). Under normoxia, 2-deoxy-D-glucose elicits cell death in select tumor types not by inhibition of glycolysis but by interfering with N-linked glycosylation. Mol Cancer Ther *6*, 3049-3058. 10.1158/1535-7163.MCT-07-0310.

Lachner, M., Sengupta, R., Schotta, G., and Jenuwein, T. (2004). Trilogies of histone lysine methylation as epigenetic landmarks of the eukaryotic genome. Cold Spring Harb Symp Quant Biol *69*, 209-218. 10.1101/sqb.2004.69.209.

Lam, S.M., Wang, Z., Li, J., Huang, X., and Shui, G. (2017). Sequestration of polyunsaturated fatty acids in membrane phospholipids of Caenorhabditis elegans dauer larva attenuates eicosanoid biosynthesis for prolonged survival. Redox Biol *12*, 967-977. 10.1016/j.redox.2017.05.002.

Lancaster, G.I., Langley, K.G., Berglund, N.A., Kammoun, H.L., Reibe, S., Estevez, E., Weir, J., Mellett, N.A., Pernes, G., Conway, J.R.W., et al. (2018). Evidence that TLR4 Is Not a Receptor for Saturated Fatty Acids but Mediates Lipid-Induced Inflammation by Reprogramming Macrophage Metabolism. Cell Metab *27*, 1096-1110.e1095. 10.1016/j.cmet.2018.03.014.

Lapa, C., Arias-Loza, P., Hayakawa, N., Wakabayashi, H., Werner, R.A., Chen, X., Shinaji, T., Herrmann, K., Pelzer, T., and Higuchi, T. (2017). Whitening and Impaired Glucose Utilization of Brown Adipose Tissue in a Rat Model of Type 2 Diabetes Mellitus. Sci Rep *7*, 16795. 10.1038/s41598-017-17148-w.

Lee, J.E., Oh, H.A., Song, H., Jun, J.H., Roh, C.R., Xie, H., Dey, S.K., and Lim, H.J. (2011). Autophagy regulates embryonic survival during delayed implantation. Endocrinology *152*, 2067-2075. 10.1210/en.2010-1456.

Lee, S.L., Sadovsky, Y., Swirnoff, A.H., Polish, J.A., Goda, P., Gavrilina, G., and Milbrandt, J. (1996). Luteinizing hormone deficiency and female infertility in mice lacking the transcription factor NGFI-A (Egr-1). Science *273*, 1219-1221. 10.1126/science.273.5279.1219.

Lemons, J.M., Feng, X.J., Bennett, B.D., Legesse-Miller, A., Johnson, E.L., Raitman, I., Pollina, E.A., Rabitz, H.A., Rabinowitz, J.D., and Coller, H.A. (2010). Quiescent fibroblasts exhibit high metabolic activity. PLoS Biol *8*, e1000514. 10.1371/journal.pbio.1000514.

Li, B., Castano, A.P., Hudson, T.E., Nowlin, B.T., Lin, S.L., Bonventre, J.V., Swanson, K.D., and Duffield, J.S. (2010). The melanoma-associated transmembrane glycoprotein Gpnmb controls trafficking of cellular debris for degradation and is essential for tissue repair. FASEB J *24*, 4767-4781. 10.1096/fj.10-154757.

Li, H., Wang, J., Xu, H., Xing, R., Pan, Y., Li, W., Cui, J., Zhang, H., and Lu, Y. (2013). Decreased fructose-1,6-bisphosphatase-2 expression promotes glycolysis and growth in gastric cancer cells. Mol Cancer *12*, 110. 10.1186/1476-4598-12-110.

Li, W.Z., Wang, Z.W., Chen, L.L., Xue, H.N., Chen, X., Guo, Z.K., and Zhang, Y. (2015). Hesx1 enhances pluripotency by working downstream of multiple pluripotency-associated signaling pathways. Biochem Biophys Res Commun *464*, 936-942. 10.1016/j.bbrc.2015.07.074.

Liao, J., Karnik, R., Gu, H., Ziller, M.J., Clement, K., Tsankov, A.M., Akopian, V., Gifford, C.A., Donaghey, J., Galonska, C., et al. (2015). Targeted disruption of DNMT1, DNMT3A and DNMT3B in human embryonic stem cells. Nat Genet *47*, 469-478. 10.1038/ng.3258.

Liberzon, A., Birger, C., Thorvaldsdóttir, H., Ghandi, M., Mesirov, J.P., and Tamayo, P. (2015). The Molecular Signatures Database (MSigDB) hallmark gene set collection. Cell Syst *1*, 417-425. 10.1016/j.cels.2015.12.004.

Liu, P., Calvisi, D.F., Kiss, A., Cigliano, A., Schaff, Z., Che, L., Ribback, S., Dombrowski, F., Zhao, D., and Chen, X. (2017). Central role of mTORC1 downstream of YAP/TAZ in hepatoblastoma development. Oncotarget *8*, 73433-73447. 10.18632/oncotarget.20622.

Liu, W.M., Cheng, R.R., Niu, Z.R., Chen, A.C., Ma, M.Y., Li, T., Chiu, P.C., Pang, R.T., Lee, Y.L., Ou, J.P., et al. (2020). Let-7 derived from endometrial extracellular vesicles is an important inducer of embryonic diapause in mice. Sci Adv *6*. 10.1126/sciadv.aaz7070.

Liu, W.M., Pang, R.T., Cheong, A.W., Ng, E.H., Lao, K., Lee, K.F., and Yeung, W.S. (2012). Involvement of microRNA lethal-7a in the regulation of embryo implantation in mice. PLoS One *7*, e37039. 10.1371/journal.pone.0037039.

Lopes, F.L., Desmarais, J.A., and Murphy, B.D. (2004). Embryonic diapause and its regulation. Reproduction *128*, 669-678. 10.1530/rep.1.00444.

Maddocks, O.D., Labuschagne, C.F., Adams, P.D., and Vousden, K.H. (2016). Serine Metabolism Supports the Methionine Cycle and DNA/RNA Methylation through De Novo ATP Synthesis in Cancer Cells. Mol Cell *61*, 210-221. 10.1016/j.molcel.2015.12.014.

Manning, B.D., Tee, A.R., Logsdon, M.N., Blenis, J., and Cantley, L.C. (2002). Identification of the tuberous sclerosis complex-2 tumor suppressor gene product tuberin as a target of the phosphoinositide 3-kinase/akt pathway. Mol Cell *10*, 151-162. 10.1016/s1097-2765(02)00568-3.

Mantalenakis, S.J., and Ketchel, M.M. (1966). Frequency and extent of delayed implantation in lactating rats and mice. J Reprod Fertil *12*, 391-394. 10.1530/jrf.0.0120391.

Martin, P.M., and Sutherland, A.E. (2001). Exogenous amino acids regulate trophectoderm differentiation in the mouse blastocyst through an mTOR-dependent pathway. Dev Biol *240*, 182-193. 10.1006/dbio.2001.0461.

Mathieu, J., Detraux, D., Kuppers, D., Wang, Y., Cavanaugh, C., Sidhu, S., Levy, S., Robitaille, A.M., Ferreccio, A., Bottorff, T., et al. (2019). Folliculin regulates mTORC1/2 and WNT pathways in early human pluripotency. Nat Commun *10*, 632. 10.1038/s41467-018-08020-0.

Mathieu, J., and Ruohola-Baker, H. (2017). Metabolic remodeling during the loss and acquisition of pluripotency. Development *144*, 541-551. 10.1242/dev.128389.

Mathieu, J., Zhou, W., Xing, Y., Sperber, H., Ferreccio, A., Agoston, Z., Kuppusamy, K.T., Moon, R.T., and Ruohola-Baker, H. (2014). Hypoxia-inducible factors have distinct and stage-specific roles during reprogramming of human cells to pluripotency. Cell Stem Cell *14*, 592-605. 10.1016/j.stem.2014.02.012.

Matsuda, N., Sato, S., Shiba, K., Okatsu, K., Saisho, K., Gautier, C.A., Sou, Y.S., Saiki, S., Kawajiri, S., Sato, F., et al. (2010). PINK1 stabilized by mitochondrial depolarization recruits Parkin to damaged mitochondria and activates latent Parkin for mitophagy. J Cell Biol *189*, 211-221. 10.1083/jcb.200910140.

McGivan, J.D., and Pastor-Anglada, M. (1994). Regulatory and molecular aspects of mammalian amino acid transport. Biochem J *299 (Pt 2)*, 321-334.
McLaren, A. (1968). A STUDY OF BLASTOCYSTS DURING DELAY AND SUBSEQUENT IMPLANTATION IN LACTATING MICE. BioScientifica.

Meng, D., Frank, A.R., and Jewell, J.L. (2018). mTOR signaling in stem and progenitor cells. Development *145*. 10.1242/dev.152595.

Menke, T.M., and McLaren, A. (1970). Carbon dioxide production by mouse blastocysts during lactational delay of implantation or after ovariectomy. J Endocrinol *47*, 287-294.

Miklas, J.W., Clark, E., Levy, S., Detraux, D., Leonard, A., Beussman, K., Showalter, M.R., Smith, A.T., Hofsteen, P., Yang, X., et al. (2019). TFPa/HADHA is required for fatty acid beta-oxidation and cardiolipin re-modeling in human cardiomyocytes. Nat Commun *10*, 4671. 10.1038/s41467-019-12482-1.

Moody, J.D., Levy, S., Mathieu, J., Xing, Y., Kim, W., Dong, C., Tempel, W., Robitaille, A.M., Dang, L.T., Ferreccio, A., et al. (2017). First critical repressive H3K27me3 marks in embryonic stem cells identified using designed protein inhibitor. Proc Natl Acad Sci U S A *114*, 10125-10130. 10.1073/pnas.1706907114.

Murphy, B.D. (2012). Embryonic diapause: advances in understanding the enigma of seasonal delayed implantation. Reprod Domest Anim *47 Suppl 6*, 121-124. 10.1111/rda.12046.

Nagy, A., Rossant, J., Nagy, R., Abramow-Newerly, W., and Roder, J.C. (1993). Derivation of completely cell culture-derived mice from early-passage embryonic stem cells. Proc Natl Acad Sci U S A *90*, 8424-8428. 10.1073/pnas.90.18.8424.

Nakanishi, M., Adami, G.R., Robetorye, R.S., Noda, A., Venable, S.F., Dimitrov, D., Pereira-Smith, O.M., and Smith, J.R. (1995). Exit from G0 and entry into the cell cycle of cells expressing p21Sdi1 antisense RNA. Proc Natl Acad Sci U S A *92*, 4352-4356. 10.1073/pnas.92.10.4352.

Narendra, D., Tanaka, A., Suen, D.F., and Youle, R.J. (2008). Parkin is recruited selectively to impaired mitochondria and promotes their autophagy. J Cell Biol *183*, 795-803. 10.1083/jcb.200809125.

Narendra, D.P., Jin, S.M., Tanaka, A., Suen, D.F., Gautier, C.A., Shen, J., Cookson, M.R., and Youle, R.J. (2010). PINK1 is selectively stabilized on impaired mitochondria to activate Parkin. PLoS Biol *8*, e1000298. 10.1371/journal.pbio.1000298.

Nichols, J., Chambers, I., Taga, T., and Smith, A. (2001). Physiological rationale for responsiveness of mouse embryonic stem cells to gp130 cytokines. Development *128*, 2333-2339.

Nichols, J., and Smith, A. (2009). Naive and primed pluripotent states. Cell Stem Cell *4*, 487-492. 10.1016/j.stem.2009.05.015.

Nicklin, P., Bergman, P., Zhang, B., Triantafellow, E., Wang, H., Nyfeler, B., Yang, H., Hild, M., Kung, C., Wilson, C., et al. (2009). Bidirectional transport of amino acids regulates mTOR and autophagy. Cell *136*, 521-534. 10.1016/j.cell.2008.11.044.

Nishioka, K., Rice, J.C., Sarma, K., Erdjument-Bromage, H., Werner, J., Wang, Y., Chuikov, S., Valenzuela, P., Tempst, P., Steward, R., et al. (2002). PR-Set7 is a nucleosome-specific methyltransferase that modifies lysine 20 of histone H4 and is associated with silent chromatin. Mol Cell *9*, 1201-1213. 10.1016/s1097-2765(02)00548-8.

Noda, A., Ning, Y., Venable, S.F., Pereira-Smith, O.M., and Smith, J.R. (1994). Cloning of senescent cell-derived inhibitors of DNA synthesis using an expression screen. Exp Cell Res *211*, 90-98. 10.1006/excr.1994.1063.

Norwitz, E.R., Schust, D.J., and Fisher, S.J. (2001). Implantation and the survival of early pregnancy. N Engl J Med *345*, 1400-1408. 10.1056/NEJMra000763.

Oda, H., Okamoto, I., Murphy, N., Chu, J., Price, S.M., Shen, M.M., Torres-Padilla, M.E., Heard, E., and Reinberg, D. (2009). Monomethylation of histone H4-lysine 20 is involved in chromosome structure and stability and is essential for mouse development. Mol Cell Biol *29*, 2278-2295. 10.1128/MCB.01768-08.

Orford, K.W., and Scadden, D.T. (2008). Deconstructing stem cell self-renewal: genetic insights into cell-cycle regulation. Nat Rev Genet *9*, 115-128. 10.1038/nrg2269.

Owen, T.A., Soprano, D.R., and Soprano, K.J. (1989). Analysis of the growth factor requirements for stimulation of WI-38 cells after extended periods of density-dependent growth arrest. J Cell Physiol *139*, 424-431. 10.1002/jcp.1041390227.

Padgett, J., and Santos, S.D.M. (2020). From clocks to dominoes: lessons on cell cycle remodelling from embryonic stem cells. FEBS Lett. 10.1002/1873-3468.13862.

Paria, B.C., Huet-Hudson, Y.M., and Dey, S.K. (1993). Blastocyst's state of activity determines the "window" of implantation in the receptive mouse uterus. Proc Natl Acad Sci U S A *90*, 10159-10162.

Parker, D.J., Iyer, A., Shah, S., Moran, A., Hjelmeland, A.B., Basu, M.K., Liu, R., and Mitra, K. (2015). A new mitochondrial pool of cyclin E, regulated by Drp1, is linked to cell-density-dependent cell proliferation. J Cell Sci *128*, 4171-4182. 10.1242/jcs.172429.

Pike, I. (1981). Comparative studies of embryo metabolism in early pregnancy.

Pozzi, S., Bowling, S., Apps, J., Brickman, J.M., Rodriguez, T.A., and Martinez-Barbera, J.P. (2019). Genetic Deletion of Hesx1 Promotes Exit from the Pluripotent State and Impairs Developmental Diapause. Stem Cell Reports *13*, 970-979. 10.1016/j.stemcr.2019.10.014.

Ptak, G.E., Modlinski, J.A., and Loi, P. (2013). Embryonic diapause in humans: time to consider? Reprod Biol Endocrinol *11*, 92. 10.1186/1477-7827-11-92.

Ptak, G.E., Tacconi, E., Czernik, M., Toschi, P., Modlinski, J.A., and Loi, P. (2012). Embryonic diapause is conserved across mammals. PLoS One *7*, e33027. 10.1371/journal.pone.0033027.

Qi, J., Yu, J.Y., Shcherbata, H.R., Mathieu, J., Wang, A.J., Seal, S., Zhou, W., Stadler, B.M., Bourgin, D., Wang, L., et al. (2009). microRNAs regulate human embryonic stem cell division. Cell Cycle *8*, 3729-3741. 10.4161/cc.8.22.10033.

Quentien, M.H., Manfroid, I., Moncet, D., Gunz, G., Muller, M., Grino, M., Enjalbert, A., and Pellegrini, I. (2002). Pitx factors are involved in basal and hormone-regulated activity of the human prolactin promoter. J Biol Chem *277*, 44408-44416. 10.1074/jbc.M207824200.

Ralser, M., Wamelink, M.M., Struys, E.A., Joppich, C., Krobitsch, S., Jakobs, C., and Lehrach, H. (2008). A catabolic block does not sufficiently explain how 2-deoxy-D-glucose inhibits cell growth. Proc Natl Acad Sci U S A *105*, 17807-17811. 10.1073/pnas.0803090105.

Rapp, U.R., Ceteci, F., and Schreck, R. (2008). Oncogene-induced plasticity and cancer stem cells. Cell Cycle *7*, 45-51. 10.4161/cc.7.1.5203.

Rehman, S.K., Haynes, J., Collignon, E., Brown, K.R., Wang, Y., Nixon, A.M.L., Bruce, J.P., Wintersinger, J.A., Singh Mer, A., Lo, E.B.L., et al. (2021). Colorectal Cancer Cells Enter a Diapause-like DTP State to Survive Chemotherapy. Cell *184*, 226-242.e221. 10.1016/j.cell.2020.11.018.

Renfree, M.B., and Fenelon, J.C. (2017). The enigma of embryonic diapause. Development *144*, 3199-3210. 10.1242/dev.148213.

Renfree, M.B., and Shaw, G. (2000). Diapause. Annu Rev Physiol *62*, 353-375. 10.1146/annurev.physiol.62.1.353.

Renfree, M.B., and Shaw, G. (2014). Embryo-endometrial interactions during early development after embryonic diapause in the marsupial tammar wallaby. Int J Dev Biol *58*, 175-181. 10.1387/ijdb.140059mr.

Richards, M., Tan, S.P., Tan, J.H., Chan, W.K., and Bongso, A. (2004). The transcriptome profile of human embryonic stem cells as defined by SAGE. Stem Cells *22*, 51-64. 10.1634/stemcells.22-1-51.

Rose-John, S. (2002). GP130 stimulation and the maintenance of stem cells. Trends Biotechnol *20*, 417-419. 10.1016/s0167-7799(02)02056-5.

Sajedi, E., Gaston-Massuet, C., Andoniadou, C.L., Signore, M., Hurd, P.J., Dattani, M., and Martinez-Barbera, J.P. (2008). DNMT1 interacts with the developmental transcriptional repressor HESX1. Biochim Biophys Acta *1783*, 131-143. 10.1016/j.bbamcr.2007.08.010.

Sanders, S.L., Portoso, M., Mata, J., Bähler, J., Allshire, R.C., and Kouzarides, T. (2004). Methylation of histone H4 lysine 20 controls recruitment of Crb2 to sites of DNA damage. Cell *119*, 603-614. 10.1016/j.cell.2004.11.009.

Sang, L., Coller, H.A., and Roberts, J.M. (2008). Control of the reversibility of cellular quiescence by the transcriptional repressor HES1. Science *321*, 1095-1100. 10.1126/science.1155998.

Sanjana, N.E., Shalem, O., and Zhang, F. (2014). Improved vectors and genome-wide libraries for CRISPR screening. Nat Methods *11*, 783-784. 10.1038/nmeth.3047.

Schotta, G., Lachner, M., Sarma, K., Ebert, A., Sengupta, R., Reuter, G., Reinberg, D., and Jenuwein, T. (2004). A silencing pathway to induce H3-K9 and H4-K20 trimethylation at constitutive heterochromatin. Genes Dev *18*, 1251-1262. 10.1101/gad.300704.

Schotta, G., Sengupta, R., Kubicek, S., Malin, S., Kauer, M., Callén, E., Celeste, A., Pagani, M., Opravil, S., De La Rosa-Velazquez, I.A., et al. (2008). A chromatin-wide transition to H4K20 monomethylation impairs genome integrity and programmed DNA rearrangements in the mouse. Genes Dev *22*, 2048-2061. 10.1101/gad.476008.

Schubert, A.F., Gladkova, C., Pardon, E., Wagstaff, J.L., Freund, S.M.V., Steyaert, J., Maslen, S.L., and Komander, D. (2017). Structure of PINK1 in complex with its substrate ubiquitin. Nature *552*, 51-56. 10.1038/nature24645.

Schütze, S., Potthoff, K., Machleidt, T., Berkovic, D., Wiegmann, K., and Krönke, M. (1992). TNF activates NF-kappa B by phosphatidylcholine-specific phospholipase C-induced "acidic" sphingomyelin breakdown. Cell *71*, 765-776.

Scognamiglio, R., Cabezas-Wallscheid, N., Thier, M.C., Altamura, S., Reyes, A., Prendergast, Á., Baumgärtner, D., Carnevalli, L.S., Atzberger, A., Haas, S., et al. (2016). Myc Depletion Induces a Pluripotent Dormant State Mimicking Diapause. Cell *164*, 668-680. 10.1016/j.cell.2015.12.033.

Shahbazi, M.N., Jedrusik, A., Vuoristo, S., Recher, G., Hupalowska, A., Bolton, V., Fogarty, N.N.M., Campbell, A., Devito, L., Ilic, D., et al. (2016). Self-organization of the human embryo in the absence of maternal tissues. Nat Cell Biol *18*, 700-708. 10.1038/ncb3347.

Shalem, O., Sanjana, N.E., Hartenian, E., Shi, X., Scott, D.A., Mikkelson, T., Heckl, D., Ebert, B.L., Root, D.E., Doench, J.G., and Zhang, F. (2014). Genome-scale CRISPR-Cas9 knockout screening in human cells. Science *343*, 84-87. 10.1126/science.1247005.

Shaw, G., and Renfree, M.B. (1986). Uterine and embryonic metabolism after diapause in the tammar wallaby, Macropus eugenii. J Reprod Fertil *76*, 339-347. 10.1530/jrf.0.0760339.

Shaw, R.J., Bardeesy, N., Manning, B.D., Lopez, L., Kosmatka, M., DePinho, R.A., and Cantley, L.C. (2004). The LKB1 tumor suppressor negatively regulates mTOR signaling. Cancer Cell *6*, 91-99. 10.1016/j.ccr.2004.06.007.

Shcherbata, H.R., Hatfield, S., Ward, E.J., Reynolds, S., Fischer, K.A., and Ruohola-Baker, H. (2006). The MicroRNA pathway plays a regulatory role in stem cell division. Cell Cycle *5*, 172-175. 10.4161/cc.5.2.2343.

Shimizu, H., Bolati, D., Adijiang, A., Muteliefu, G., Enomoto, A., Nishijima, F., Dateki, M., and Niwa, T. (2011). NF-κB plays an important role in indoxyl sulfate-induced cellular senescence, fibrotic gene expression, and inhibition of proliferation in proximal tubular cells. Am J Physiol Cell Physiol *301*, C1201-1212. 10.1152/ajpcell.00471.2010.

Shimura, H., Hattori, N., Kubo, S., Mizuno, Y., Asakawa, S., Minoshima, S., Shimizu, N., Iwai, K., Chiba, T., Tanaka, K., and Suzuki, T. (2000). Familial Parkinson disease gene product, parkin, is a ubiquitin-protein ligase. Nat Genet *25*, 302-305. 10.1038/77060.

Shimura, H., Hattori, N., Kubo, S., Yoshikawa, M., Kitada, T., Matsumine, H., Asakawa, S., Minoshima, S., Yamamura, Y., Shimizu, N., and Mizuno, Y. (1999). Immunohistochemical and subcellular localization of Parkin protein: absence of protein in autosomal recessive juvenile parkinsonism patients. Ann Neurol *45*, 668-672. 10.1002/1531-8249(199905)45:5<668::aid-ana19>3.0.co;2-z.

Shiraki, N., Shiraki, Y., Tsuyama, T., Obata, F., Miura, M., Nagae, G., Aburatani, H., Kume, K., Endo, F., and Kume, S. (2014). Methionine metabolism regulates maintenance and differentiation of human pluripotent stem cells. Cell Metab *19*, 780-794. 10.1016/j.cmet.2014.03.017.

Shogren-Knaak, M., Ishii, H., Sun, J.M., Pazin, M.J., Davie, J.R., and Peterson, C.L. (2006). Histone H4-K16 acetylation controls chromatin structure and protein interactions. Science *311*, 844-847. 10.1126/science.1124000.

Soccio, R.E., Li, Z., Chen, E.R., Foong, Y.H., Benson, K.K., Dispirito, J.R., Mullican, S.E., Emmett, M.J., Briggs, E.R., Peed, L.C., et al. (2017). Targeting PPARγ in the epigenome rescues genetic metabolic defects in mice. J Clin Invest *127*, 1451-1462. 10.1172/JCI91211.

Somasundaram, L., Levy, S., Hussein, A.M., Ehnes, D.D., Mathieu, J., and Ruohola-Baker, H. (2020). Epigenetic metabolites license stem cell states. Curr Top Dev Biol *138*, 209-240. 10.1016/bs.ctdb.2020.02.003.

Son, M.J., Rho, S.B., Kim, K., Oh, M., Son, C., Song, S.Y., and Park, K. (2020). Homeoprotein Msx1-PIASy Interaction Inhibits Angiogenesis. Cells *9*. 10.3390/cells9081854.

Sone, M., Morone, N., Nakamura, T., Tanaka, A., Okita, K., Woltjen, K., Nakagawa, M., Heuser, J.E., Yamada, Y., Yamanaka, S., and Yamamoto, T. (2017). Hybrid Cellular Metabolism Coordinated by Zic3 and Esrrb Synergistically Enhances Induction of Naive Pluripotency. Cell Metab *25*, 1103-1117.e1106. 10.1016/j.cmet.2017.04.017.

Sousa, M.I., Correia, B., Rodrigues, A.S., and Ramalho-Santos, J. (2020). Metabolic characterization of a paused-like pluripotent state. Biochim Biophys Acta Gen Subj *1864*, 129612. 10.1016/j.bbagen.2020.129612.

Sperber, H., Mathieu, J., Wang, Y., Ferreccio, A., Hesson, J., Xu, Z., Fischer, K.A., Devi, A., Detraux, D., Gu, H., et al. (2015). The metabolome regulates the epigenetic landscape during naive-to-primed human embryonic stem cell transition. Nat Cell Biol *17*, 1523-1535. 10.1038/ncb3264.

Spurlock, B., Tullet, J., Hartman, J.L., and Mitra, K. (2020). Interplay of mitochondrial fission-fusion with cell cycle regulation: Possible impacts on stem cell and organismal aging. Exp Gerontol *135*, 110919. 10.1016/j.exger.2020.110919.

Staropoli, J.F., McDermott, C., Martinat, C., Schulman, B., Demireva, E., and Abeliovich, A. (2003). Parkin is a component of an SCF-like ubiquitin ligase complex and protects postmitotic neurons from kainate excitotoxicity. Neuron *37*, 735-749. 10.1016/s0896-6273(03)00084-9.

Takashima, Y., Guo, G., Loos, R., Nichols, J., Ficz, G., Krueger, F., Oxley, D., Santos, F., Clarke, J., Mansfield, W., et al. (2014). Resetting transcription factor control circuitry toward ground-state pluripotency in human. Cell *158*, 1254-1269. 10.1016/j.cell.2014.08.029.

Tang, D.G. (2012). Understanding cancer stem cell heterogeneity and plasticity. Cell Res *22*, 457-472. 10.1038/cr.2012.13.

Tao, J., Ma, Y.C., Yang, Z.S., Zou, C.G., and Zhang, K.Q. (2016). Octopamine connects nutrient cues to lipid metabolism upon nutrient deprivation. Sci Adv *2*, e1501372. 10.1126/sciadv.1501372.

Tarín, J.J., and Cano, A. (1999). Do human concepti have the potential to enter into diapause? Hum Reprod *14*, 2434-2436. 10.1093/humrep/14.10.2434.

Tesar, P.J., Chenoweth, J.G., Brook, F.A., Davies, T.J., Evans, E.P., Mack, D.L., Gardner, R.L., and McKay, R.D. (2007). New cell lines from mouse epiblast share defining features with human embryonic stem cells. Nature *448*, 196-199. 10.1038/nature05972.

Theunissen, T.W., Friedli, M., He, Y., Planet, E., O'Neil, R.C., Markoulaki, S., Pontis, J., Wang, H., Iouranova, A., Imbeault, M., et al. (2016). Molecular Criteria for Defining the Naive Human Pluripotent State. Cell Stem Cell *19*, 502-515. 10.1016/j.stem.2016.06.011.

Theunissen, T.W., Powell, B.E., Wang, H., Mitalipova, M., Faddah, D.A., Reddy, J., Fan, Z.P., Maetzel, D., Ganz, K., Shi, L., et al. (2014). Systematic identification of culture conditions for induction and maintenance of naive human pluripotency. Cell Stem Cell *15*, 471-487. 10.1016/j.stem.2014.07.002.

Thomson, J.A., Itskovitz-Eldor, J., Shapiro, S.S., Waknitz, M.A., Swiergiel, J.J., Marshall, V.S., and Jones, J.M. (1998). Embryonic stem cell lines derived from human blastocysts. Science *282*, 1145-1147. 10.1126/science.282.5391.1145.

Towler, M.C., Fogarty, S., Hawley, S.A., Pan, D.A., Martin, D.M., Morrice, N.A., McCarthy, A., Galardo, M.N., Meroni, S.B., Cigorraga, S.B., et al. (2008). A novel short splice variant of the tumour suppressor LKB1 is required for spermiogenesis. Biochem J *416*, 1-14. 10.1042/BJ20081447.

Trapnell, C., Pachter, L., and Salzberg, S.L. (2009). TopHat: discovering splice junctions with RNA-Seq. Bioinformatics *25*, 1105-1111. 10.1093/bioinformatics/btp120.

Tsugawa, H., Cajka, T., Kind, T., Ma, Y., Higgins, B., Ikeda, K., Kanazawa, M., VanderGheynst, J., Fiehn, O., and Arita, M. (2015). MS-DIAL: data-independent MS/MS deconvolution for comprehensive metabolome analysis. Nat Methods *12*, 523-526. 10.1038/nmeth.3393.

Tsuyuki, S., Takabayashi, M., Kawazu, M., Kudo, K., Watanabe, A., Nagata, Y., Kusama, Y., and Yoshida, K. (2014). Detection of WIPI1 mRNA as an indicator of autophagosome formation. Autophagy *10*, 497-513. 10.4161/auto.27419.

Urakami, K., Zangiacomi, V., Yamaguchi, K., and Kusuhara, M. (2013). Impact of 2-deoxy-D-glucose on the target metabolome profile of a human endometrial cancer cell line. Biomed Res *34*, 221-229.

Valamehr, B., Robinson, M., Abujarour, R., Rezner, B., Vranceanu, F., Le, T., Medcalf, A., Lee, T.T., Fitch, M., Robbins, D., and Flynn, P. (2014). Platform for induction and maintenance of transgene-free hiPSCs resembling ground state pluripotent stem cells. Stem Cell Reports *2*, 366-381. 10.1016/j.stemcr.2014.01.014.

Valente, E.M., Abou-Sleiman, P.M., Caputo, V., Muqit, M.M., Harvey, K., Gispert, S., Ali, Z., Del Turco, D., Bentivoglio, A.R., Healy, D.G., et al. (2004). Hereditary early-onset Parkinson's disease caused by mutations in PINK1. Science *304*, 1158-1160. 10.1126/science.1096284.

Van Blerkom, J., Chavez, D.J., and Bell, H. (1978). Molecular and cellular aspects of facultative delayed implantation in the mouse. Ciba Found Symp, 141-172.

van Velthoven, C.T.J., and Rando, T.A. (2019). Stem Cell Quiescence: Dynamism, Restraint, and Cellular Idling. Cell Stem Cell *24*, 213-225. 10.1016/j.stem.2019.01.001.

Van Winkle, L.J., Tesch, J.K., Shah, A., and Campione, A.L. (2006). System B0,+ amino acid transport regulates the penetration stage of blastocyst implantation with possible long-term developmental consequences through adulthood. Hum Reprod Update *12*, 145-157. 10.1093/humupd/dmi044.

Varum, S., Rodrigues, A.S., Moura, M.B., Momcilovic, O., Easley, C.A., Ramalho-Santos, J., Van Houten, B., and Schatten, G. (2011). Energy metabolism in human pluripotent stem cells and their differentiated counterparts. PLoS One *6*, e20914. 10.1371/journal.pone.0020914.

Veeriah, S., Taylor, B.S., Meng, S., Fang, F., Yilmaz, E., Vivanco, I., Janakiraman, M., Schultz, N., Hanrahan, A.J., Pao, W., et al. (2010). Somatic mutations of the Parkinson's disease-associated gene PARK2 in glioblastoma and other human malignancies. Nat Genet *42*, 77-82. 10.1038/ng.491.

Vermeulen, M., Eberl, H.C., Matarese, F., Marks, H., Denissov, S., Butter, F., Lee, K.K., Olsen, J.V., Hyman, A.A., Stunnenberg, H.G., and Mann, M. (2010). Quantitative interaction proteomics and genome-wide profiling of epigenetic histone marks and their readers. Cell *142*, 967-980. 10.1016/j.cell.2010.08.020.

Vives-Bauza, C., Zhou, C., Huang, Y., Cui, M., de Vries, R.L., Kim, J., May, J., Tocilescu, M.A., Liu, W., Ko, H.S., et al. (2010). PINK1-dependent recruitment of Parkin to mitochondria in mitophagy. Proc Natl Acad Sci U S A *107*, 378-383. 10.1073/pnas.0911187107.

Vuong, B., Hogan-Cann, A.D., Alano, C.C., Stevenson, M., Chan, W.Y., Anderson, C.M., Swanson, R.A., and Kauppinen, T.M. (2015). NF-κB transcriptional activation by TNFα requires phospholipase C, extracellular signal-regulated kinase 2 and poly(ADP-ribose) polymerase-1. J Neuroinflammation *12*, 229. 10.1186/s12974-015-0448-8.

Wang, B., Rong, X., Palladino, E.N.D., Wang, J., Fogelman, A.M., Martín, M.G., Alrefai, W.A., Ford, D.A., and Tontonoz, P. (2018). Phospholipid Remodeling and Cholesterol Availability Regulate Intestinal Stemness and Tumorigenesis. Cell Stem Cell *22*, 206-220.e204. 10.1016/j.stem.2017.12.017.

Wang, Y., Hussein, A.M., Somasundaram, L., Sankar, R., Detraux, D., Mathieu, J., and Ruohola-Baker, H. (2019). microRNAs Regulating Human and Mouse Naïve Pluripotency. Int J Mol Sci *20*. 10.3390/ijms20235864.

Ware, C.B. (2017). Concise Review: Lessons from Naïve Human Pluripotent Cells. Stem Cells *35*, 35-41. 10.1002/stem.2507.

Ware, C.B., Nelson, A.M., Mecham, B., Hesson, J., Zhou, W., Jonlin, E.C., Jimenez-Caliani, A.J., Deng, X., Cavanaugh, C., Cook, S., et al. (2014). Derivation of naive human embryonic stem cells. Proc Natl Acad Sci U S A *111*, 4484-4489. 10.1073/pnas.1319738111.

Webley, K., Bond, J.A., Jones, C.J., Blaydes, J.P., Craig, A., Hupp, T., and Wynford-Thomas, D. (2000). Posttranslational modifications of p53 in replicative senescence overlapping but distinct from those induced by DNA damage. Mol Cell Biol *20*, 2803-2808. 10.1128/mcb.20.8.2803-2808.2000.

Weinberger, L., Ayyash, M., Novershtern, N., and Hanna, J.H. (2016). Dynamic stem cell states: naive to primed pluripotency in rodents and humans. Nat Rev Mol Cell Biol *17*, 155-169. 10.1038/nrm.2015.28.

Weissman, I.L. (2000). Stem cells: units of development, units of regeneration, and units in evolution. Cell *100*, 157-168. 10.1016/s0092-8674(00)81692-x.

Wolfson, R.L., Chantranupong, L., Saxton, R.A., Shen, K., Scaria, S.M., Cantor, J.R., and Sabatini, D.M. (2016). Sestrin2 is a leucine sensor for the mTORC1 pathway. Science *351*, 43-48. 10.1126/science.aab2674.

Wu, J., Okamura, D., Li, M., Suzuki, K., Luo, C., Ma, L., He, Y., Li, Z., Benner, C., Tamura, I., et al. (2015). An alternative pluripotent state confers interspecies chimaeric competency. Nature *521*, 316-321. 10.1038/nature14413.

Wu, J., Yamauchi, T., and Izpisua Belmonte, J.C. (2016). An overview of mammalian pluripotency. Development *143*, 1644-1648. 10.1242/dev.132928.

Wu, M., Neilson, A., Swift, A.L., Moran, R., Tamagnine, J., Parslow, D., Armistead, S., Lemire, K., Orrell, J., Teich, J., et al. (2007). Multiparameter metabolic analysis reveals a close link between attenuated mitochondrial bioenergetic function and enhanced glycolysis dependency in human tumor cells. Am J Physiol Cell Physiol *292*, C125-136. 10.1152/ajpcell.00247.2006.

Wu, Y., Shi, W., Tang, T., Wang, Y., Yin, X., Chen, Y., Zhang, Y., Xing, Y., Shen, Y., Xia, T., et al. (2019). miR-29a contributes to breast cancer cells epithelial-mesenchymal transition, migration, and invasion via down-regulating histone H4K20 trimethylation through directly targeting SUV420H2. Cell Death Dis *10*, 176. 10.1038/s41419-019-1437-0.

Yanez, I., and O'Farrell, M. (1989). Variation in the length of the lag phase following serum restimulation of mouse 3T3 cells. Cell Biol Int Rep *13*, 453-462. 10.1016/0309-1651(89)90140-9.

Yang, X., Haghiac, M., Glazebrook, P., Minium, J., Catalano, P.M., and Hauguel-de Mouzon, S. (2015). Saturated fatty acids enhance TLR4 immune pathways in human trophoblasts. Hum Reprod *30*, 2152-2159. 10.1093/humrep/dev173.

Yavari, A., Stocker, C.J., Ghaffari, S., Wargent, E.T., Steeples, V., Czibik, G., Pinter, K., Bellahcene, M., Woods, A., Martínez de Morentin, P.B., et al. (2016). Chronic Activation of γ2 AMPK Induces Obesity and Reduces β Cell Function. Cell Metab *23*, 821-836. 10.1016/j.cmet.2016.04.003.

Yokoyama, Y., Matsumoto, A., Hieda, M., Shinchi, Y., Ogihara, E., Hamada, M., Nishioka, Y., Kimura, H., Yoshidome, K., Tsujimoto, M., and Matsuura, N. (2014). Loss of histone H4K20 trimethylation predicts poor prognosis in breast cancer and is associated with invasive activity. Breast Cancer Res *16*, R66. 10.1186/bcr3681.

Yoshinaga, K. (2013). A sequence of events in the uterus prior to implantation in the mouse. J Assist Reprod Genet *30*, 1017-1022. 10.1007/s10815-013-0093-z.

Yoshinaga, K., and Adams, C.E. (1966). Delayed implantation in the spayed, progesterone treated adult mouse. J Reprod Fertil *12*, 593-595.

Zamorano, J., Rivas, M.D., Garcia-Trinidad, A., Qu, C.K., and Keegan, A.D. (2003). Phosphatidylcholine-specific phospholipase C activity is necessary for the activation of STAT6. J Immunol *171*, 4203-4209.

Zhan, Z., Song, L., Zhang, W., Gu, H., Cheng, H., Zhang, Y., Yang, Y., Ji, G., Feng, H., Cheng, T., and Li, Y. (2019). Absence of cyclin-dependent kinase inhibitor p27 or p18 increases efficiency of iPSC generation without induction of iPSC genomic instability. Cell Death Dis *10*, 271. 10.1038/s41419-019-1502-8.

Zhang, Z., Albers, T., Fiumera, H.L., Gameiro, A., and Grewer, C. (2009). A conserved Na(+) binding site of the sodium-coupled neutral amino acid transporter 2 (SNAT2). J Biol Chem *284*, 25314-25323. 10.1074/jbc.M109.038422.

Zhang, Z., Gameiro, A., and Grewer, C. (2008). Highly conserved asparagine 82 controls the interaction of Na+ with the sodium-coupled neutral amino acid transporter SNAT2. J Biol Chem *283*, 12284-12292. 10.1074/jbc.M706774200.

Zheng, D., MacLean, P.S., Pohnert, S.C., Knight, J.B., Olson, A.L., Winder, W.W., and Dohm, G.L. (2001). Regulation of muscle GLUT-4 transcription by AMP-activated protein kinase. J Appl Physiol (1985) *91*, 1073-1083. 10.1152/jappl.2001.91.3.1073.

Zhou, W., Choi, M., Margineantu, D., Margaretha, L., Hesson, J., Cavanaugh, C., Blau, C.A., Horwitz, M.S., Hockenbery, D., Ware, C., and Ruohola-Baker, H. (2012). HIF1α induced switch from bivalent to exclusively glycolytic metabolism during ESC-to-EpiSC/hESC transition. EMBO J *31*, 2103-2116. 10.1038/emboj.2012.71.

Zoncu, R., Bar-Peled, L., Efeyan, A., Wang, S., Sancak, Y., and Sabatini, D.M. (2011). mTORC1 senses lysosomal amino acids through an inside-out mechanism that requires the vacuolar H(+)-ATPase. Science *334*, 678-683. 10.1126/science.1207056.